ABSTRACT

SIMULATION OF CREEP IN NICKEL BASED SINGLE CRYSTAL SUPERALLOYS

by

Yunhong Pang

Nickel based single crystal Superalloys are finding wide spread use in high temperature gas turbines and other similar applications because of their superior high-temperature strength and creep properties as compared to the other materials. This is due to two factors: solid solution and precipitation strengthening of the gamma (γ) and gamma prime (γ') phases, and the elimination of grain boundaries. Creep of Nickel based single crystal Superalloys are caused by two primary mechanisms, dislocation creep and diffusion creep. Several factors that affect the creep life of Nickel based single crystal Superalloys are the specific microstructure, stress, temperature and rafting. Also, the creep behavior is highly anisotropic, with the degree of anisotropy varying with temperature.

This research is focused on developing a continuum model to simulate the creep response of Nickel based single crystal Superalloys that includes the influence of microstructure, anisotropy and recognizes the fact that these materials are inelastic and dissipate energy. A framework, built on the idea of evolving of natural configurations, utilizing the maximization of the rate of dissipation, has been used to formulate the model. The specific model is constructed by specifying forms of the stored energy and the rate of dissipation. The reduced energy-dissipation equation is used to obtain the constitutive relations for the stress and the maximization of the rate of the dissipation is

used to obtain equations for the evolution of the underlying natural configurations through a rate equation for the inelastic strain.

The material constants for the model are obtained by comparing predictions of the model with experimental data. Solving the required boundary value problem is complicated due to the anisotropic material behavior. Two coordinate systems need to be introduced to solve the problem, since all the constitutive equations are developed in the crystal coordinate system while the stress and strain are usually measured in the specimen coordinate system. Transformation from the crystal coordinate system and specimen coordinate system is required. This is being done by introducing two 4^{th} order tensors

The main material parameters required to solve the equations are the components of the viscosity tensor, k . A parametric study is required to decide the viscosity tensor k , for a FCC material k has three independent components. We determine functional forms for these three components as a function of inelastic strain, temperature and stress. The specific forms are different for the low and high temperature regimes, because the underlying creep mechanisms are different. Simulation results, creep curves and strain vs. strain rate curve, clearly indicate the difference between the low and high temperature regimes. The parameters chosen fit the experimental data adequately.

This model was implemented into a Finite Element software ABAQUS by using a User-Defined Material Subroutine, UMAT. The Finite Element simulation results also showed a reasonable fit with the experimental data.

SIMULATION OF CREEP IN NICKEL BASED SINGLE CRYSTAL SUPERALLOYS

by
Yunhong Pang

A Dissertation
Submitted to the Faculty of
New Jersey Institute of Technology
in Partial Fulfillment of the Requirements for the Degree of
Doctor of Philosophy in Mechanical Engineering

Department of Mechanical Engineering

May 2005

APPROVAL PAGE

SIMULATION OF CREEP IN NICKEL BASED SINGLE CRYSTAL SUPERALLOYS

Yunhong Pang

Dr. I. Joga Rao, Dissertation Advisor — Date
Assistant Professor of Mechanical Engineering, NJIT

Dr. Rong-Yaw Chen, Committee Member — Date
Professor of Mechanical Engineering, NJIT

Dr. Ernest S. Geskin, Committee Member — Date
Professor of Mechanical, NJIT

Dr. Kwabena A.Narh, Committee Member — Date
Associate Professor Mechanical Engineering, NJIT

Dr. Michael Booty, Committee Member — Date
Associate Professor, Mathematical Sciences, NJIT

BIOGRAPHICAL SKETCH

Author: Yunhong Pang

Degree: Doctor of Philosophy

Date: May 2005

Undergraduate and Graduate Education:

- Doctor of Philosophy in Mechanical Engineering, 2005
  New Jersey Institute of Technology, Newark, NJ
- Master of Engineering in Material Science and Engineering,
  Northwestern Polytechnical University, Xi'an, P. R. China, 1992
- Bachelor of Science in Material Science and Engineering,
  Northwestern Polytechnical University, Xi'an, P. R. China, 1987

Major: Mechanical Engineering

Publications and Presentations:

Yunhong Pang, Suigeng Du, -"*3D FEM Analysis on the Process and Physical Parameter Fields During Linear Friction Welding of Renè95 and DD3*", submitted to Modeling and Simulation of Material Science and Engineering, Dec, 2004

Suigeng Du, **Yunhong Pang**, "*Forming Mechanism of Carbide Band in Friction Welding Joint of Superalloy and Steel*", submitted to Modeling and Simulation of Material Science and Engineering, Sept. 2004

To my beloved
daughter, husband, parents and sisters
for their love, encouragement, and unceasing support

ACKNOWLEDGMENT

I would like to express my deepest appreciation to Dr. I. Joga Rao, who not only served as my research supervisor, providing valuable and countless resources, but also constantly gave me support, encouragement, and reassurance. Special thanks are given to Dr. Rong-Yaw Chen, Dr. Ernest S. Geskin, Dr. Kwabena A. Narh and Dr. Michael Booty for actively participating in my committee, and for giving many helpful suggestions and corrections

I am grateful to the department of Mechanical Engineering from NJIT for the financial support. Many of my fellow graduate students in the Mechanical Engineering are deserving of recognition for their support.

A penultimate thank-you goes to my wonderful parents, Zhenbang Pang and Chunying Chen and my sister Diana Pang. For always being there when I needed them most, they deserve far more credit than I can ever give them.

My final, and most heartfelt, acknowledgment must go to my husband, Yu Zhou and my daughter, Nancy Zhou. Their support, encouragement, and companionship have turned my journey through graduate school into a pleasure. For all that, and for being everything I am not, they have my everlasting love.

TABLE OF CONTENTS

TABLE OF CONTENTS
(Continued)

Chapter **Page**

TABLE OF CONTENTS
(Continued)

Chapter **Page**

TABLE OF CONTENTS
(Continued)

Chapter **Page**

LIST OF TABLES

LIST OF FIGURES

LIST OF FIGURES
(Continued)

Figure **Page**

LIST OF FIGURES
(Continued)

Figure **Page**

LIST OF SYMBOLS

A	Driving force (Pa)
$\boldsymbol{A_t}$, $\boldsymbol{B_t}$	Transformation matrix
$\boldsymbol{B}$	Left Cauchy-Green stretch tensor
$\boldsymbol{b}$	Body force per unite mass in Euler coordinate system
a, b, c	Components of elastic constant (N/m^2)
$\boldsymbol{C}$	Right Cauchy-Green stretch tensor
$\boldsymbol{D}$, $\boldsymbol{D_{in}}$,	Symmetric part of velocity gradient $\boldsymbol{L}$ and $\boldsymbol{L_{in}}$
$\boldsymbol{E}$, $\boldsymbol{e}$	Cauchy and Green Strain
$\boldsymbol{E_{in}}$, $\boldsymbol{E_e}$/$\boldsymbol{e_{in}}$,$\boldsymbol{e_e}$	Inelastic and Elastic Cauchy/Green strain
$\boldsymbol{F}$	Deformation gradient
$\boldsymbol{F_{in}}$, $\boldsymbol{F_e}$	Inelastic and elastic deformation gradient
$\boldsymbol{G}$	Transformation tensor from elastic to inelastic
$\boldsymbol{I}$	Second order identity tensor
J	Determinat of deformation gradient
i, j, k	Directional viscosity component
$\boldsymbol{K}$	Isotropic viscosity tensor
$\boldsymbol{L}$	Velocity gradient
$\boldsymbol{L_{in}}$,	Inelastic part of velocity gradient
$\boldsymbol{n}$	Normal direction of the surface
$\boldsymbol{P}$	First Piolar stress
$\boldsymbol{q}$	Heat flux vector

$\boldsymbol{R}$	Proper orthogonal tensor
S	Entropy
$\boldsymbol{S}$	Second Piolar stress
t	Time
$\boldsymbol{t}$	Surface traction per unit area
$\boldsymbol{T}$	Stress in Lagrangian coordinate system
$\boldsymbol{u}$	Displacement vector
$\boldsymbol{U}$	Positive defined symmetric tensor
$\boldsymbol{v}$	Velocity vector
$\boldsymbol{V}$	Positive defined symmetric tensor
$\boldsymbol{W}$, $\boldsymbol{W_{in}}$	Skew symmetric part of $\boldsymbol{L}$ and $\boldsymbol{L}_{\text{in}}$
$\boldsymbol{x}$, $\boldsymbol{X}$	Position vector in Eulerian and Lagrangian coordinate systems
x, y, z	Euler coordinate system
X,Y,Z	Lagrangian coordinate system
χ	Mapping function
$\boldsymbol{\varepsilon}$, $\boldsymbol{\varepsilon_{in}}$	Linearized strain and linearized inelastic strain tensor
$\bar{\varepsilon}$	Nominal strain strength
θ	Temperature
ρ	Material density
ξ	Dissipation
Ψ	Helmholtz potential

ψ_{in} , ψ_e	Inelastic and elastic potential
μ	Shear viscosity
$\otimes$	Dyad of two tensor
$\boldsymbol{II}$	4^{th} order identity tensor
$\mathbb{k}$	Directional viscosity tensor
$\mathbb{C}$	Elastic constant tensor
$\alpha_1 \sim \alpha_4$	Material constants
$\beta_1 \sim \beta_2$	Material constants
$\gamma_1 \sim \gamma_4$	Material constants
η	Specific entropy

CHAPTER 1

INTRODUCTION TO CREEP AND NICKEL BASED SINGLE CRYSTAL SUPERALLOYS

1.1 Introduction to Creep

Creep is a very common damage phenomenon observed in materials subject to stress at high temperatures. It can take place in metals and alloys, ceramics, polymers, mantle, soil, ice, et al. Creep effects under mechanical stress are observed in most solid materials. They occur in glass which may be considered more or less as liquids with very high viscosity. In concrete, creep effects had already been observed (Reiner, 1960). In organic material such as polymers, creep has been studied extensively (Tobolsky, 1960). In all these cases creep is of a linear visco-elastic nature. For metal, the physical mechanism is obviously quite different from that in solids, and non-linear behavior is predominant. In this dissertation the attention is mainly paid to the creep of metals and alloys.

Creep is defined as time-dependent strain occurring under a stress which is lower than the yield point (Powell, 1986). The effect of creep is a permanent, irreversible deformation. Excessive temperature is the cause of high creep deformation (Pratt & Whitney Aircraft, 1974). In metals and ceramics, creep becomes noticeable when the temperature reaches about one-third to one-half of the melting temperature. In polymers, creep becomes noticeable when the temperature approaches the glass-transition temperature (which is near room temperature for many polymers).

The continuous process can be represented by the deformation curve as shown in Figure 1.1. Three stages observed are, primary creep, steady state creep and tertiary creep. Primary creep is usually interpreted as an adaptation stage, secondary creep as the useful life period, while tertiary creep is the precursor to final failure. The part of the curve which is of interest to designers is the steady state creep since the component will spend the largest portion of its life in this region. Meanwhile, the deformation rates are different at three stages. At primary stage strain rate decreases with time; at steady-state stage the strain rate is almost a constant; and at tertiary stage the creep rate increases fast with time till the material ruptures.

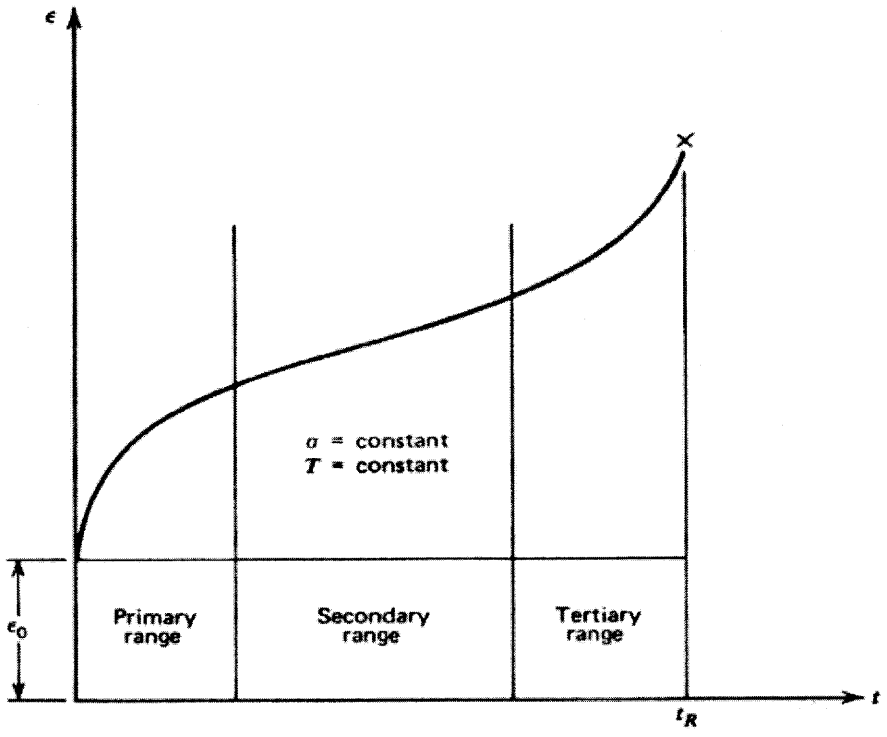

Figure 1.1 Typical creep curve.

The knowledge of the creep rate allows estimation of how much time is needed until a component reaches a certain deformation and becomes incompatible with the geometry of the system it is part of. A jet engine is a good example. The gap between the tip of the rotating blades and the engine casing has to be very small in order to maximize the engine efficiency so that the amount of gas that flows through the engine without acting on the blades is kept as small as possible. However, if a blade elongates too much as a result of creep, it ends up scraping against the inner wall of the casing causing serious damage. If, however, the creep rate of the material is known along with the lifetime already spent by the blades, they can be replaced before the irreparable damage happens.

1.2 Nickel Based Single Crystal Superalloys and Its Creep Property

Creep is undesirable in practice because it results in the change of geometry of components and eventually in their failure. For turbine and blade which work at a complex condition and creep is one of the most important potential damage, extending creep life for these components becomes critical.

To increase maximum speed and improve efficiency (lower fuel costs) the operating temperature should be increased continuously. The temperature at the turbine entry can exceed its melting point. At such high temperatures, creep and creep rapture appear to be critical factors which affect the performance of the whole turbine or engine. The development of Nickel based single crystal Superalloys is to meet the requirement of the high temperature working condition in the turbines.

1.2.1 Nickel Based Single Crystal Superalloy

Development of nickel based single crystal Superalloys originated in 1930 in the United States. The whole process mainly includes specific choices for the alloying components and a change in the method.

Through these studies, the modern Ni-based Superalloys contain more than 10 alloy additions (plus impurities) for getting solid solution strengthening (Co, Cr, Fe, Mo, W, Ta, Re), grain boundary strengthening with carbides (W, Ta, Ti, Mo, Nb, Hf, Cr) and other precipitates (e.g. carbonitrides), γ' formers Al, Ti, improving oxidation resistance (Al, Cr, Y, La, Ce), improving hot corrosion resistance (Cr, Co, Si, La, Th) and gaining boundary refiners (B, C, Zr, Hf). The following is the nominal composition of CMSX-4; a third generation nickel based single crystal Superalloy (Table 1.1).

Table 1.1 Nominal Composition of CMSX-4, γ and γ' Phase

Alloy (Weight-%)	Ni	Al	Ti	Cr	Co	Mo	Ta	W	Re
CMSX-4	61.3	5.6	1.0	6.5	10.0	0.6	6.0	6.0	3.0

Figure 1.2 is a typical microstructure of a nickel based single crystal Superalloy. The main characteristic is that the two phases, gama (γ) and gama prime (γ') are coherent with each other.

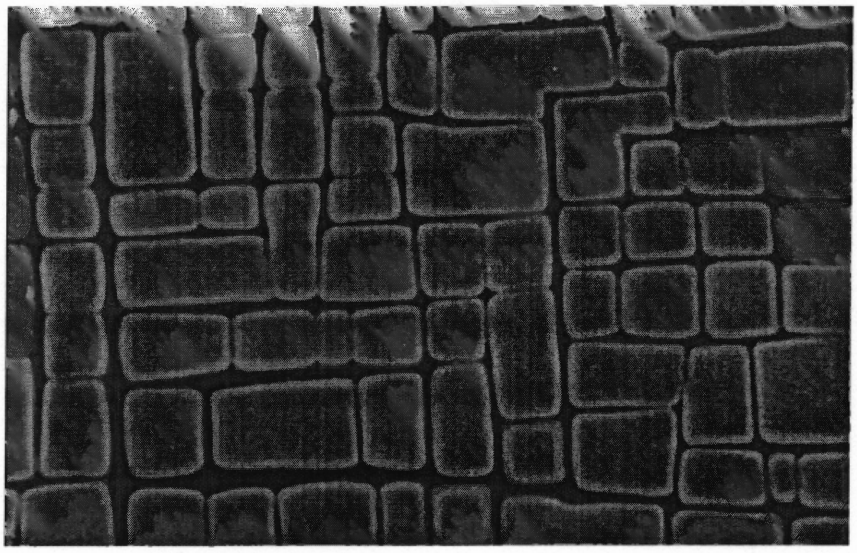

Figurer 1.2 Typical microstructure of a nickel based single crystal Superalloy (ONERA, 1996-2004).

Unlike the polycrystalline alloys, which are manufactured by conventional casting methods, and have microstructures containing multiple grains and grain boundaries that can coordinate the deformation, single crystal Superalloys are manufactured by a special installation, which is similar to the directional solidification casting. This method uses an investment mould located on a water-cooled copper chill. After metal is cast, heat is removed from the chill, resulting in directional solidification. Since solidification rates are different for different crystal directions thus resulting in one direction grains that grow faster than other directions, thus grains with this orientation are favored.

Figure 1.3 is a comparison of the creep life for different casting methods. It is clear that single crystal has the longest creep life while conventional casting has the shortest one. Single crystal nickel based Superalloy has three times the creep life of directional solidification Superalloys.

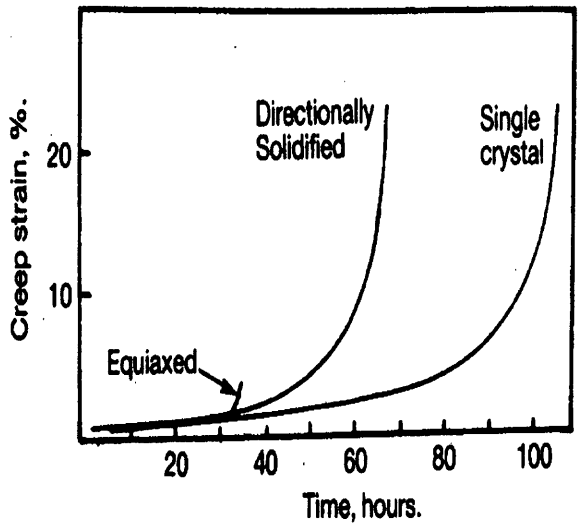

Figurer 1.3 Creep behaviors vs. processing techniques.

1.2.2 Creep Property of Nickel Based Single Crystal Superalloys

The most valuable mechanical property of nickel-based Superalloys is their excellent creep resistance. This property makes Superalloys the choice in high-temperature, high-fatigue environments where excellent structural integrity is required. This creep resistance is due to two factors: solid solution and precipitation strengthening of the gamma and gamma prime phases, and manipulation of grain size and shape.

There are many factors that affect the creep behavior in Nickel based single crystal Superalloys, such as volume fraction and size of γ' (Fleischer, 1963; Mkamaraj, 2003; Caron et al. 1988), crystal orientation (Kear and Piearcey, 1967; Leverant et al. 1971, 1973; Oblak and Rand, 1974; Mackay and Maier, 1982; Leverant et al. 1970; Lukas et al. 1996; Caron,1988; Sass et al. 1996, 1998; Lukas, Cadek, et al. 1996), temperature/stress (J. Svoboda, P. Lukas, 1997; Mkamaraj, 2003; Sass, Glarzel, et al. 1996; Sass, Feller-Kniepmeier, 1998; Kolbe, Dlouhy, et al. 1998; Mayr, Eggeler, et al.

1995) and the effects of interaction among them (Mkamaraj, 2003), including rafting, a directional γ' coarsening. An outline of the effect factors is given in the following.

1.2.2.1 Orientation Dependence. Kear and Piearcy (1967) were the first to study the creep behavior of single crystals at various orientations. They found that the substantial improvement in creep life of single crystals over conventional cast or directional solidified alloys occurs between 750°C and 850°C for crystals with orientation near [001] and [111]. Conversely, very short lives were exhibited by crystals orientated near [001].

The anisotropic creep behavior has been extensively studied for several nickel based single crystal Superalloys, such as MAR-M20 (Kear and Piearcey, 1967; Leverant et al. 1971, 1973; Oblak and Rand, 1974), Mar-M247 (Mackay and Maier, 1982; Leverant et al. 1970), CMSX-4 (Lukas et al. 1996). In general, the functional dependence of the creep behavior was found to be the same at their test condition (Figure 1.4 and 1.5), although contradictory results were also obtained by Caron (1988).

The research carried out on CMSX-4 (Sass et al. 1996, 1998) focused on whether [001] or [111] crystal orientation is stronger in uniaxial tensile creep. But so far there is no engineering application of Superalloy single crystals which is used in any orientation other than <001> (Lukas, Cadek, et al. 1996).

Creep behavior anisotropy is mainly restricted to primary creep (Sass, Glarzel, et al. 1996; Sass, Feller-Kniepmeier, 1998). The pronounced creep anisotropy can be attributed to the superposition of coherency and external stress, leading to different microstructure configurations.

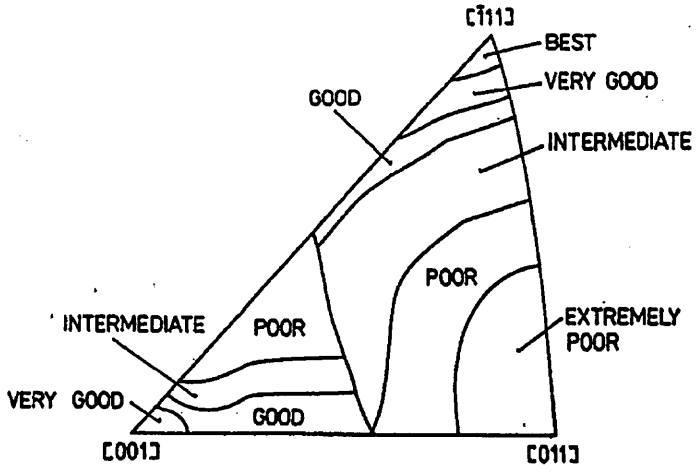

Figurer 1.4 Regimes of stress rupture lives for MAR-M247 and Mar-M200 single crystals at about 760°C.

1.2.2.2 Temperature and Stress Dependence. Stress level and temperature are two very important factors that affect the creep properties. Figure 1.6 is a typical curve of creep changing with temperature for Nickel based single crystal Superalloys. Stress has the same influence with temperature (Honeycombe, 1984).

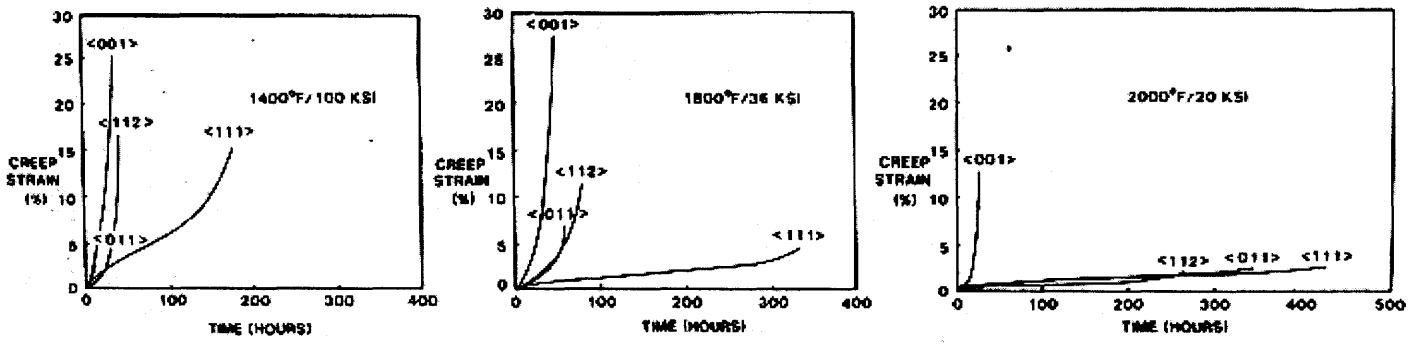

Figurer 1.5 Change in creep properties with orientation (Chest, 1987).

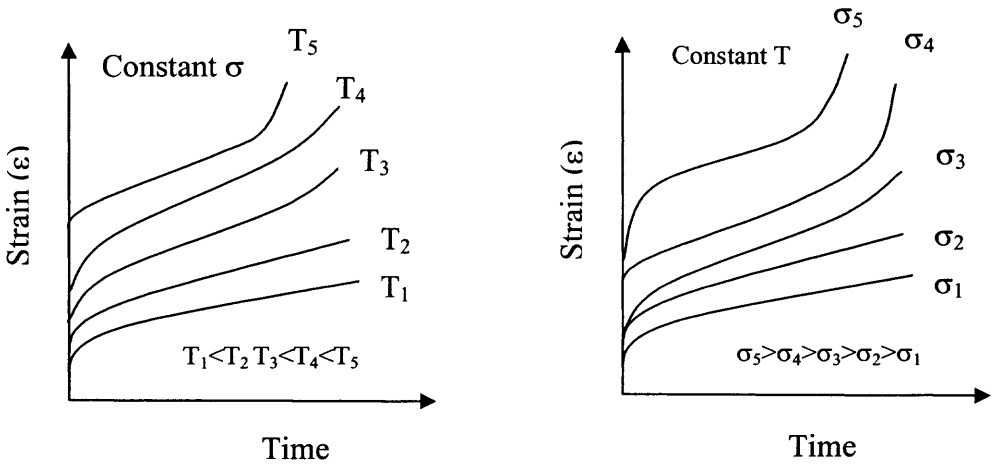

Figurer 1.6 Change of creep curve with temperature and stress.

For the convenience of study, the regime selected is a combination of temperature/stress level, high stress/low temperature creep and low stress/high temperature creep. For Nickel single crystal Superalloy CMSX-4, the stress/temperature ranges are defined as (J. Svoboda, P. Lukas, 1997):

Low temperature: 700~850°C, high stress: 600~800MPa

High temperature: 900~1100°C, low stress: 100~300MPa.

Temperature is a critical factor for creep. It not only affects the creep life but also the anisotropic property. Studies showed (Sass, Glarzel, et al. 1996; Sass, Feller-Kniepmeier, 1998) that the creep strength of tested samples is highly anisotropic at lower temperature, while at high temperature (980°C), the creep anisotropy is clearly reduced, and the misorientation dependence of creep deformation is also less pronounced. The reason is due to the increase of the active slip systems at high temperature (Kolbe, Dlouhy, et al. 1998; Mayr, Eggeler, et al. 1995).

1.2.2.3 Other Factors Dependence. Orientation and stress/temperatures are important factors which affect the material creep life. These can be regarded as working condition or external factors. There are still other factors, internal (inherited from the alloy manufacture) and external, such as γ′ volume and size, lattice misfit, rafting etc., which can also control the creep property.

γ′ volume and size: Two phases are included in the Nickel based single crystal Superalloys, γ and γ'. γ is the matrix and is a soft phase while γ' is the precipitate and is a hard phase. The creep strength of Nickel based Superalloys depends strongly on the volume fraction of γ'. A series of studies on creep property dependence on γ' volume fraction (from 0 to 100%) indicated that the longest creep life occurred at volume fraction of proximately 60% (Fleischer, 1963). In practice, most of the Nickel based single crystal Superalloys have the γ volume fraction around 60%, for example, Rene N4 65%, PWA1480 55-60%, SRR99 60% and Mar-M200 60%. For the second or third generation Nickel based single crystal Superalloys, the peak value can reach 68–70 vol.% (Mkamaraj, 2003). But the reason for the existence of the peak value is not very clear, so far.

Caron's (Caron, et al. 1988) study showed that the size of γ' precipitates also affects the creep life at different degree at different crystal orientations. The creep life of <111> oriented crystals is highly dependent on the size of the γ' precipitates, while the <001> oriented crystal depends weakly on the size of γ' precipitates.

Misfit The γ phase forms the matrix in which the γ′ precipitates. Since both phases have a cubic lattice with similar lattice parameters, the γ′ precipitates in a cube-cube orientation relationship with the γ. This means that its cell edges are exactly parallel

to corresponding edges of the γ phase. Furthermore, because their lattice parameters are similar, the γ' is coherent with the γ when the precipitate size is small. However, if the lattice parameters are not the same, there can be a misfit between them.

The small misfit between the γ and γ' lattices is important for two reasons. Firstly, when combined with the cube-cube orientation relationship, it ensures a low γ/γ' interfacial energy. The ordinary mechanism of precipitate coarsening is driven entirely by the minimization of total interfacial energy. A coherent or semi-coherent interface therefore makes the microstructure stable, a property which is useful for elevated temperature applications.

The magnitude and sign of the misfit also influences the development of microstructure under the influence of a stress at elevated temperatures. The misfit is said to be positive when the γ' has a larger lattice parameter than γ. The misfit can be controlled by altering the chemical composition, particularly the aluminum to titanium ratio. A negative misfit stimulates the formation of rafts of γ', essentially layers of the phase in a direction normal to the applied stress. Rafting of γ' helps minimize creep since dislocations find it difficult to traverse the precipitate rafts.

Rafting refers to directional γ' coarsening. It usually occurs at high temperature. Recent research results show that rafting can also affect the creep life (Mkamaraj, 2003). At 950°C for all stress level specimens SRR99 single crystal exhibits longer creep life than that of the pre-rafted specimens. However, at elevated temperature, 1050°C, the pre-rafted specimens tested at high stress level exhibit shorter creep lives but the situation changes when the stress level is below 150 MPa, a pre-rafting improves the creep strength under given temperature and stress.

Many factors affect the creep life of nickel based single crystal Superalloy as stated above. Some are determined by the microstructure while others are affected by the creep condition. For a certain alloy the stress, temperature and orientation are significant factors. Thus in this dissertation attention is mainly paid to stress and orientation at an isothermal condition.

1.3 Outline of the Dissertation

Some machine components are subject to stresses during lengthy time of use. For example, rotary components of jet engines, such as blades and disks, experience stresses due to centrifugal force. In addition, the hot combustion gases that flow through a jet engine cause the temperature to be very high. In fact, in some cases it may reach levels as high as 80% of the melting temperature of the material the engine components are made of. The data from creep tests on many different materials, which are collected in databases, along with the exact knowledge of the service stress and temperature conditions help designers in the choice of the suitable materials for a given component and in the prediction of its lifetime under those conditions.

In order to predict the creep life and guide the practice, a new model is developed in this dissertation to simulate the creep life of nickel based single crystal Superalloys, considering both the creep mechanisms and anisotropic material property. Further this model is implemented into commercial finite element software, ABAQUS, by using a user defined material subroutine, UMAT, to test the correctness of the model.

This dissertation is composed of eight chapters. Chapter 1 is the introduction of nickel single crystal and its creep property. Present models of creep in Nickel based

single crystal Superalloys and motivation of this dissertation is given in the second Chapter.

Chapter 3 to Chapter 7 focus on the development of the constitutive equations, including an introduction to the preliminary information in Chapter 3; an introduction of development of the constitutive equation along with the basic conservation laws in Chapter 4. Parametric study and numerical results are presented in Chapter 6. The finite element implementation of UMAT to ABAQUS and finite analysis results are presented in Chapter7. Chapter 8 is a summary and conclusion of this dissertation.

CHAPTER 2

MODELS OF CREEP FOR NICKEL BASED SINGLE CRYSTAL SUPERALLOYS

Accurate modeling of deformation occurring under complex working conditions has been highlighted as a requirement for optimizing the efficiency in design of components with respect to both preventing failure and avoiding over-design.

In recent years the reduction in cost and increase in computational speed of digital computers has led to an increasing number of engineers relying more heavily on numerical analyses. This, in turn, has fueled a steady increase in the level of sophistication in the mathematical models developed. Consequently, the engineer is not constrained only to exact or analytical solutions.

The accuracy of creep deformation and simulation of creep deformation in Nickel based single crystal Superalloy depends not only on the material components, but also on the choice of the constitutive models and their numerical implementations into finite element programs. Among these factors, the material constitutive equations play important roles in describing the mechanical behavior of creep because it is essential to obtain the accurate stress distribution in a creep part in order to correctly predict the creep life.

Over the past 30 years, two categories of constitutive model have been developed for single crystal Nickel based Superalloys (Choi and Krempl, 1989; Jordan and walker, 1992; Nouaihas, 1990; Stouffer et al. 1990; Li and Smith 1998). These two

categories are usually classified as crystallographic modeling and phenomenological modeling, and are based on different theories.

2.1 Crystallographic Model

Modeling creep behavior of Nickel based single crystal Superalloys started with crystallographic (Stouffer et al. 1990; Meric et al. 1991; Jordan and Walker, 1992; Li and Smith, 1995a) models. These models are based on the micro aspect of the material plastic deformation, which is determined by slip and a slip plane. This concept came from the single crystal framework established by Pierce et al. (1982, 1983) and Asaro (1983). It is used to describe large deformation, rate dependent, and single crystal plasticity. It is assumed that the overall behavior of single crystal under a given loading condition is controlled by the deformation characteristics of a certain number of active slip systems.

In the context of a single crystal, plasticity is described by continuum shear flows $\dot{\gamma}_\alpha$, which occur along the various slip systems, α, of the crystal. The kinematics of single crystal deformation is described by configuration changes. The initial unreformed, stress free lattice represents the reference configuration. Slip system, α, is defined by the orthogonal pair of unit vectors $(\mathbf{s}_\alpha, \mathbf{n}_\alpha)$, where $\mathbf{s}_\alpha$ is parallel to the α slip plane and is the direction in which slip takes place. $\mathbf{n}_\alpha$ is normal to the α slip plane in the reference configuration. Plastic deformation involves shear flows along the various slip systems of the crystal to reach an intermediate configuration. The spatial velocity gradient of this plastic shear flow is the sum of the slip taking place on a number of the slip systems and is given by

$$\mathbf{L}_p = \sum_{\alpha} \dot{\gamma}_{\alpha} \mathbf{s}_{\alpha} \mathbf{n}_{\alpha} \tag{2.1}$$

where $\boldsymbol{L}_p$ is the velocity gradient, the sum α is over all the slip systems, and $\dot{\gamma}$ is the slip system shear rate.

For Nickel based single crystal Superalloys, 18 slip systems are generally considered in a full crystallographic model (Figure 2.1).

The yield criteria for the cubic and octahedral slip systems are given by the Chaboche isotropic mode (Chaboche, 1989) as:

$$\begin{aligned} f_c^s &= \left|\tau_c^s - x_c^s\right| - k_c - r_c^s \le 0, \text{ (s=1,2,3, ...,18)} \\ f_o^s &= \left|\tau_o^s - x_o^s\right| - k_o - r_o^s \le 0, \text{ (s=1,2,3, ...,12)} \end{aligned} \tag{2.2}$$

where τ_c^s and τ_o^s are the Resolved Shear Stress (RSS) for cubic and octahedral slip systems. x^s and r^s are the kinematics hardening and isotropic hardening variables, for each slip plane respectively, and k_c and k_o are the initial critical resolved shear stresses (CRSS) for the cubic and octahedral slip systems respectively.

In a typical crystallographic model the constitutive equations are established at two levels, macroscopic and microscopic.

At the microscopic level, a unified model is adopted where the total strain rate decomposes into elastic and inelastic strain rate,

$$\dot{\boldsymbol{\varepsilon}}^T = \dot{\boldsymbol{\varepsilon}}^e + \dot{\boldsymbol{\varepsilon}}^{in} \tag{2.3}$$

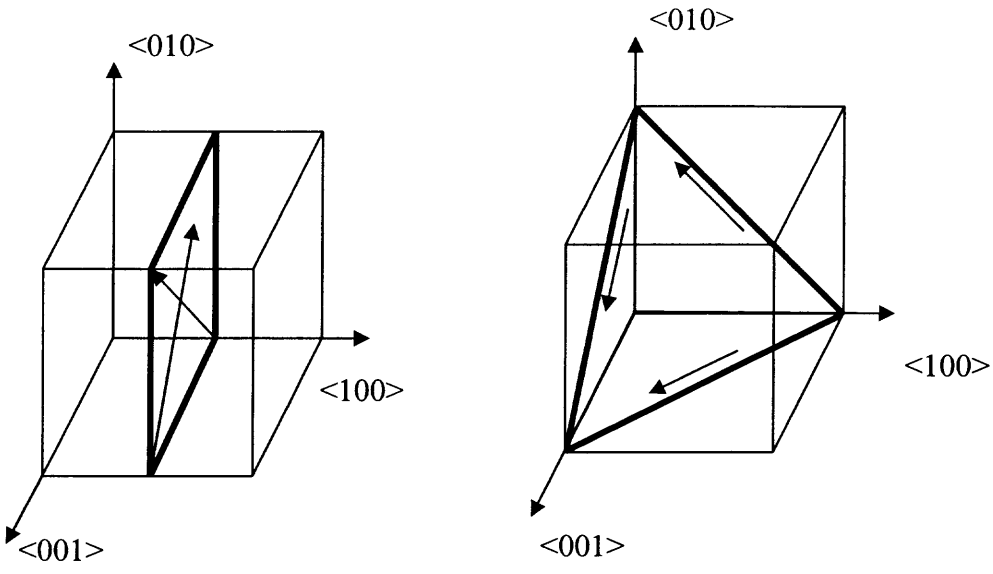

(a) Cubic slip system

(b) Octahedral slip system

Figure 2.1 Slip planes and slip directions for the FCC crystal (Stouffer, 1996) (a). Cubic slip systems [110] {100}: three slip planes {100}; two directions [110] in each plane; total six cubic slip system. (b). octahedral slip systems [110] {111}: four slip planes {111}; three directions [110] in each plane; total 12 octahedral slip systems.

The elastic strain rate at the macroscopic level is

$$\dot{\boldsymbol{\varepsilon}}^{e} = \mathbf{S}\dot{\boldsymbol{\sigma}}^{e} \tag{2.4}$$

where $\boldsymbol{S}$ is a 4^{th} order tensor called elastic compliance matrix of the single crystal Superalloy. For a time-dependent inelastic deformation, the overall inelastic strain is the sum of the inelastic shear strains on a number of active slip systems.

At any loading condition, a transformation for stress from global coordinate system to local coordinate system must be done so that the connection between the macroscopic stress and microscopic RSS (Resolved Shear Stress) can be built up. The relationship can be expressed by Schmid's law (Schmid and Siebel, 1931),

$$\tau^s = \sigma^*_{ij} m^\alpha_{ij} \tag{2.5}$$

with

$$m^\alpha_{ij} = \frac{1}{2}(n^\alpha_i s^\alpha_j + n^\alpha_j s^\alpha_i), \text{ (i, j=1, 2, 3; } \alpha\text{=1, 2, 3,..., 18)} \tag{2.6}$$

where n^α_i and s^α_j are the slip plane normal and slip plane direction vectors, respectively, for each α slip system. The matrix m^α_{ij} is related to the 18 slip systems of Nickel single crystal Superalloys.

By using the Chaboche (1989) model at the microscopic level, the equations describing the relationship between the inelastic shear strain rate and the resolved shear stress are given for cubic and octahedral slip systems respectively.

Then summation of the strain rate $\dot{\gamma}^\alpha$ for each slip system to get the overall macroscopic viscoplastic strain rate $\dot{\varepsilon}^*$ in the local coordinate system is given as:

$$\dot{\varepsilon}^{*in}_{ij} = \sum_{\alpha}^{18} m^\alpha_{ij} \dot{\gamma}^\alpha_c + \sum_{\alpha}^{12} m^\alpha_{ij} \dot{\gamma}^\alpha_o \tag{2.7}$$

The final step is another transformation from local coordinate system to global coordinate system for strain rate $\dot{\varepsilon}_{ij}$.

In constitutive equations development from the crystallographic model, there are a total of 14 material constants, 7 constants for octahedral slip system and 7 constants for cubic slip system that need to be determined.

2.2 Phenomenological Model

Unlike the crystallographic model, phenomenological models are based on the modified isotropic theory that was originally proposed for polycrystalline materials. A number of studies including those of Choi and Krempl (1989), Nouailhas (1990), and Li (1993) have been carried out using this approach.

The model considered here is a generalization of a unified model initially proposed by Chobache (1989) for isotropic materials. In the generalized form, the anisotropic characteristics of single crystal Superalloys are taken into account, by introducing a number of anisotropic material parameters.

The phenomenological models also decompose the total strain rate as elastic strain rate and inelastic strain rate. The elastic strain rate is calculated by using the same equations as used in the crystallographic models.

The significant difference between phenomenological model and crystallographic model is that the phenomenological models are based on the basic mathematical formulation of anisotropic viscoplastic model that is developed in the material principal axis for a cubic single crystal. Both the yield function and yield criteria in this model, for example, Chobache's (1989) model, are modified by introducing a 4^{th} order material

anisotropy tensor M_{ijkl}, to describe the initial anisotropy and the possibility of deformation induced material anisotropy. They can be described using the following equation:

$$f = \sqrt{\frac{3}{2}(\sigma_{ij}^{*'} - X_{ij}^{*'})M_{ijkl}(\sigma_{kl}^{*'} - X_{kl}^{*'})} - R - k \leq 0 \tag{2.8}$$

where $\sigma_{ij}^{*'}$ and $X_{ij}^{*'}$ are the deviatoric component of stress and back stress tensors, respectively.

The viscoplastic potential, Ω, is the same as is proposed in Chobache's (1989) model,

$$\Omega = \frac{K}{n+1}\left\langle \frac{f}{K} \right\rangle^{n+1} \tag{2.9}$$

where n and K are similar to viscosity and are strongly dependent on temperature. The bracket $< >$ is defined as: $< u >= \begin{cases} u & \text{if } u>0 \\ 0 & \text{if } u\leq 0 \end{cases}$.

The inelastic strain rate is then obtained as:

$$\begin{aligned} \dot{\varepsilon}_{ij}^{*'} &= \frac{\partial \Omega}{\partial \sigma_{ij}^{*}} \\ &= \frac{3}{2}\left\langle \frac{f}{K} \right\rangle^{n+1} \times \frac{M_{ijkl}(\sigma_{kl}^{*'} - X_{kl}^{*'})}{\sqrt{\frac{3}{2}(\sigma_{mn}^{*'} - X_{mn}^{*'})M_{mnuv}(\sigma_{uv}^{*'} - X_{uv}^{*'})}} \end{aligned} \tag{2.10}$$

The evolution equations for isotropic and kinematics hardenings are, respectively, given by:

$$\begin{aligned} \dot{R} &= b(W-R)\dot{p}^* \\ \dot{X}_{ij}^* &= \frac{3}{2} N_{ijkl}\dot{\varepsilon}_{kl}^{*in} - Q_{ijkl}X_{kl}^*\dot{p}^* \end{aligned} \tag{2.11}$$

with

$$\dot{p}^* = \sqrt{\frac{3}{2}\dot{\varepsilon}_{ij}^{*in}M_{ijkl}^{-1}\dot{\varepsilon}_{ikl}^{*in}} = \left\langle \frac{f}{K} \right\rangle^n \tag{2.12}$$

where b and W are two material constants used to describe deformation induced isotropic material hardening; N_{ijkl} and Q_{ijkl} are two tensors used to introduce the anisotropic hardening induced by microstructural anisotropic; $\dot{p}^*$ is the total accumulated inelastic strain rate.

In this model the transformation of stress from global (specimen) to local (crystallographic) coordinate system and strain from local (crystallographic) to global (specimen) coordinate system are required as in the crystallographic model. There are also at least 11 material constants that need to be determined.

The model which should be mentioned here is that developed by Bertram and his co-workers' (Bertram. A, et al., 1994). They proposed a viscoelastic model to simulate the creep property of poly- and single-crystalline nickel based Superalloys. This model is developed for the monotonous uniaxial creep behavior under tensile loading at [001] direction and generalized to a 3-D model by directly substituting the scalars to the matrices in the equation. Then the final constitutive equation includes 17 material constants, which depends solely on stress.

This is an alternative approach for modeling the creep behavior of nickel based single crystal Superalloys. It is simple and in certain degree it can capture the creep behavior well. On the other hand, like the model mentioned above it also includes many parameters.

2.4 Objectives of Research

From the above discussion it is clear that there is a significant difference between these two models. First is the definition of the yield criterion. The crystallographic model uses a multicriteria approach, for which the resolved shear stress on each slip system τ^{α} is computed from the stress tensor and the orientation tensor **m** of the slip system. It assumes that the only mechanism of plastic deformation is crystallographic slip, i.e., other mechanisms are ignored. The inelastic strain rate is the result of the contribution of inelastic shear on each slip system. The fundamental requirement in the application of the crystallographic model is the identification of active slip systems in the single crystal under a given loading condition.

The way in which the anisotropic response is handled is also different. The phenomenological model accounts for the anisotropic characteristic by introducing a 4^{th} order tensor **M** (equation 2.9). For the crystallographic model, since the model was developed on the crystal coordinate system, anisotropy is considered directly in the model through the active slip systems.

Third is the hardening equation. The kinematics hardening equation introduced from isotropic material models is modified by two additional anisotropic tensors **N** and **Q**

(equation 2.10) in the phenomenological model, while in the crystallographic model this is done by using two scalar variables for each slip systems.

Although major differences between these two models exist there are also many common features between them. For example, the general procedure used to develop the constitutive model is very similar; both models are modified from the isotropic plastic material models thus the yield criteria and yield function are important factors for them. Also both models consider hardening (kinematics and isotropic) and hence require complex equations to model the anisotropic behavior. And finally, both models have a large number of material constants that need to be determined from creep test conducted on actual specimens under different conditions.

All of the above models do not consider the thermodynamic nature of the creep behavior.

Objectives for this study enumerated below are motivated by the need to develop a general model to predict creep life at the primary and secondary creep for Nickel based single crystal Superalloy components at different temperatures by the use of available data and finite element modeling. This model was developed on the basis of the multiple-natural configurations framework and the viscoelastic concept. The simulation work includes the following tasks:

1. *Develop a new creep model for Nickel based single crystal superalloys by using multiple natural configurations, second law of thermodynamics and related theories.*

2. *Since the creep of Nickel based single crystal is highly anisotropic, material symmetry will be taken into account.*

3. *Determine the material parameters for this model and validate the model developed against experimental data available in literature.*

4. *Use finite element theory to implement this model into the commercial code of ABAQUS program by writing the material subroutine UMAT.*

2.5 Conclusions

So far two different approaches have been used in modeling the creep deformation of nickel based single crystal superalloys, which are based either on crystallographic model or phenomenological model. In the crystallographic model, the creep deformation is described by continuum shear flow along various slip system. The total creep strain is then calculated by summing the discrete dislocation slips that take place on specific lattice planes and along particular crystallographic directions. This method is powerful because the creep evolution can be accounted for by each slip systems. However, it requires a huge amount of computation time to simulate any particular creep deformation. Meanwhile a large number of parameters and constants are needed to be determined in these models.

The second approach is classical plasticity phenomenological model. Plastic flow occurs when a yield criterion is satisfied. Creep model for nickel based single crystal superalloys is introduced by using several 4^{th} order tensors to account for the anisotropic material property. Compared with the crystallographic model, this approach has a simpler mathematic form and thus it is more feasible for finite element programming.

The model developed in this dissertation, though uses continuum theory, is based on a new framework, multiple natural configuration framework which will simplify the development of constitutive equations and thus lead to a simplification of the implementation.

CHAPTER 3

PRELIMINARY

Matter is formed of molecules which in turn consist of atoms and subatomic particles. Thus matter is not continuous. However, there are many aspects of everyday experience regarding the behavior of materials, such as the amount of lengthening of a steel bar under the action of given forces, the rate of discharge of water in a pipe under a given pressure difference or the drag force experienced by a body moving in air *etc.*, all these phenomena can be described and predicted with theories that pay no attention to the molecular structure of materials. The theory which describes relationships between gross phenomena, neglecting the structure of materials on a smaller scale, is known as the continuum theory. The continuum theory regards matter as infinitely divisible. Thus, within the theory, one accepts the idea of an infinitesimal volume of material referred to as a particle in the continuum, and in every neighborhood of a particle there are always infinitely many particles present. Thus the concept of a material continuum as a mathematical idealization of the real world is applicable to problems in which the fine structure of the matter can be ignored. When the consideration of fine structure is important, we should use principles of particle physics, statistical mechanics or a theory of micropolar continuum.

Mechanics studies the motion of matter and the forces required to cause its motion. Mechanics is based on the concepts of time, space, force, energy and matter. Knowledge of mechanics is needed for the study of all branches of physics, chemistry, biology and engineering.

3.1 Kinematics

From the view point of continuum mechanics, a body is a set whose elements can be put into objective correspondence with the position of a region A of a Euclidean space. As a continuum body *B* moves in the three-dimensional Euclidean space from one instant of time to another it occupies a continuous sequence of geometrical regions. The regions that are occupied by the continuum body at a given time t are known as the *configurations* of *B* at time t. The continuum body *B* may have infinitely many configurations in space, Such as *reference configuration*, *current configuration*, etc. A region at initial time t=0 is referred to as initial configuration. The configuration of body *B* at time t is called current (deformed) configuration.

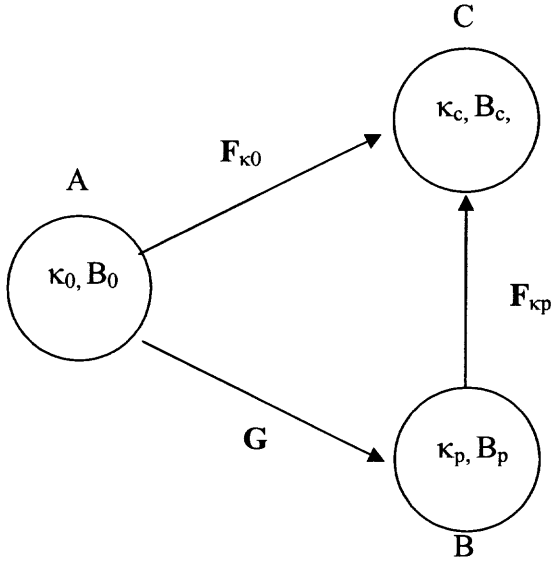

Figure 3.1 Schematic representation of the evolution of natural configurations

In the schematic plotting (Figure 3.1) κ_0 is the reference configuration, κ_p is the stress free configuration and κ_t is the current configuration. Usually the initial configuration is regarded to be coincident with the reference configuration.

3.1.1 Motion

As stated above, let κ_0 (initial configuration) be the reference configuration. Pick a particle at **X** which belongs to κ_0 and point **x** which belongs to κ_c (current configuration). The particle changes its position due to the movement and this can be expressed as

$$\mathbf{x}=\chi(\mathbf{X},t) \tag{3.1}$$

The function χ in equation (3.1) assigns to each point belonging to κ_0 at t_0 a position at time t in configuration κ_c. The vector field χ, which specifies the place **x** of **X** for all fixed t, is called the *motion* of body B.

Two descriptions can be used to describe the motion, *material (or referential) description* and *Eulerian (spatial) description*. The material description is a characterization of the motion (or any other quantity) with respect to the material coordinates (X_1, X_2, X_3) and time t. At this description the attention is paid to a particle and its movement. Traditionally the material description is often referred to as the *Lagrangian description (or Lagrangian form)*. On the other hand, the Eulerian description is a characterization of the motion (or any other quantity) with respect to the spatial coordinates (x_1, x_2, x_3) and time t. In the spatial description the attention is paid to

a point in the space and the changes at that point with time. Both of these two descriptions will be used in this research.

3.1.2 Displacement

In Lagrangian description, the *displacement field* $\boldsymbol{u}$ *(X, t), Velocity field* $\boldsymbol{v}$ *(X, t),* and *Deformation gradient* $\boldsymbol{F}$ *(X, t),* can be written as follows, respectively,

$$\boldsymbol{u(X,t) = \chi(X,t) - X} \tag{3.2}$$

$$\boldsymbol{v}(X,t) = \frac{\partial \boldsymbol{\chi}(X,t)}{\partial t} \tag{3.3}$$

$$\boldsymbol{F}(X, t) = \frac{\partial \boldsymbol{\chi}(X,t)}{\partial \boldsymbol{x}} \tag{3.4}$$

The deformation gradient, $\boldsymbol{F}$, is a positive definite second order tensor and gives information on how the body is deformed locally. Since the motion is invertible, so is $\boldsymbol{F}$.

3.1.3 Polar Decomposition

The polar decomposition theorem of Cauchy (Halmos, 1958), states that a non-singular matrix equals an orthogonal matrix either pre or post multiplied by a positive definite symmetric matrix. If we apply this theorem to the deformation gradient $\boldsymbol{F}$, we get

$$\begin{aligned} \boldsymbol{F} &= \boldsymbol{RU} \quad \text{(a)} \\ \boldsymbol{F} &= \boldsymbol{VR} \quad \text{(b)} \end{aligned} \tag{3.5}$$

in which $\boldsymbol{R}$ is a proper orthogonal matrix and $\boldsymbol{U}$ and $\boldsymbol{V}$ are positive definite symmetric matrices. Note that the decomposition (equation (3.5)) of $\boldsymbol{F}$ is unique in that $\boldsymbol{R}$, $\boldsymbol{U}$ and $\boldsymbol{V}$ are uniquely determined by $\boldsymbol{F}$.

The physical meaning of this equation is that every deformation can be decomposed locally as a rotation followed by a pure stretch or a pure stretch followed by a rotation.

To combine deformation gradient with displacement vector, a second-order tensor, displacement tensor is defined in the material description as follows:

$$\nabla \boldsymbol{u} := \frac{\partial \boldsymbol{u}(\boldsymbol{X},t)}{\partial \boldsymbol{X}} = \boldsymbol{F}(\boldsymbol{X},t) - \boldsymbol{I} \tag{3.6}$$

In the spatial description the displacement and its gradient are defined in the following forms

$$\boldsymbol{u}(\boldsymbol{x},t) = \boldsymbol{x} - \boldsymbol{X}(\boldsymbol{x},t) \tag{3.7}$$

$$grad\boldsymbol{u} := \frac{\partial \boldsymbol{u}(\boldsymbol{x},t)}{\partial \boldsymbol{x}} = \boldsymbol{I} - \boldsymbol{F}^{-1}(\boldsymbol{x},t) \tag{3.8}$$

The relation between these two descriptions of displacement tensors can be deduced from equation (3.6) and (3.8):

$$grad\boldsymbol{u} = \nabla \boldsymbol{u}\boldsymbol{F}^{-1} \tag{3.9}$$

The tensors

$$\begin{aligned} \boldsymbol{C} &:= \boldsymbol{F}^T\boldsymbol{F} = \boldsymbol{U}^2 \qquad \text{(a)} \\ \boldsymbol{B} &:= \boldsymbol{F}\boldsymbol{F}^T = \boldsymbol{V}^2 \qquad \text{(b)} \end{aligned} \tag{3.10}$$

are the right and left Cauchy-Green stretch tensors respectively. The Cauchy-Green tensors contain information about the deformation of the body and the measures of strain are usually defined in terms of either $\boldsymbol{C}$ or $\boldsymbol{B}$. The Green-St.Venant or Lagrangian strain is defined as:

$$\boldsymbol{E} := \frac{\boldsymbol{C} - \boldsymbol{I}}{2} \tag{3.11}$$

and the Almansi-Hamel or Eulerian strain is defined as:

$$\boldsymbol{e} := \frac{\boldsymbol{I} - \boldsymbol{B}}{2} \tag{3.12}$$

I denotes the identity tensor.

The velocity gradient is given by:

$$\boldsymbol{L} = grad\boldsymbol{v} := \frac{\partial \boldsymbol{v}}{\partial \boldsymbol{x}} = \dot{\boldsymbol{F}}\boldsymbol{F}^{-1} \tag{3.13}$$

In general $\boldsymbol{L}$ is a non-symmetric second-order tensor. $\dot{\boldsymbol{F}}$ is the material time derivative of $\boldsymbol{F}$.

Now we are going to define $\boldsymbol{G}$. Similarly, let κ_p be the natural configuration (stress-free state) associated with the current configuration, κ_c, of the body. For a homogeneous deformation, $\boldsymbol{F}_e$ denotes the deformation gradient between these two configurations. In general, $\boldsymbol{F}_e$ may not be the gradient of a mapping (Rajapopal, 1998). Thus the evolution of the configuration $\boldsymbol{G}$, is defined through

$$\boldsymbol{G} = \boldsymbol{F}_{\kappa_0 \to \kappa_p} = \boldsymbol{F}_e^{-1} \boldsymbol{F}_{\kappa_0 \to \kappa_c} \tag{3.14}$$

and inelastic velocity gradient defined as

$$\boldsymbol{L}_{in} = \dot{\boldsymbol{G}} \boldsymbol{G}^{-1} \tag{3.15}$$

where the dot signifies the usual material time derivative. Each fixed $\boldsymbol{G}$ corresponds to an elastic regime.

3.2 Stress Measures

In physics, stress is the internal distribution of forces within a body that balances and reacts with the loads applied to it. When a deformable continuum body, which occupies an arbitrary region of physical space with surface at a certain time, subjects arbitrary force acting on parts or the whole of the boundary surface, the continuum body will deform from its reference configuration to a new configuration. During this period there is also a stress exerted on the continuum body. For the solid continuum body, it is more convenient to use the reference configuration or intermediate configuration to define the

stress tensor so that it can be easily used in the constitutive equations. There is a necessity to introduce the other expressions of stress.

Two kinds of measures can be used to calculate the stresses based on the different configurations. The stress defined in the current configuration is called Cauchy stress tensor and usually expressed as $\boldsymbol{T}$. The Cauchy stress tensor is symmetric and always can be resolved into the sum of two symmetric tensors:

- A mean or hydrostatic tensor, involving only pure tension and compression; and
- A shear stress tensor, involving only stress

$$\begin{aligned} \boldsymbol{T}_v &= tr(\boldsymbol{T})\boldsymbol{I} \\ \boldsymbol{T}_d &= \boldsymbol{T} - \frac{1}{3}\boldsymbol{T}_v \end{aligned} \tag{3.16}$$

where $\boldsymbol{T}_v$ is the hydrostatic stress tensor, $\boldsymbol{T}_d$ is the deviatoric stress tensor, $\boldsymbol{I}$ is the 2nd order identity tensor and $tr(\cdot)$ the trace of $(\cdot)$.

The stress defined in the reference configuration is called first Piola-Kirchoff stress and is expressed by the symbol $\boldsymbol{P}$. The relationship is usually represented by equation:

$$\boldsymbol{P} = J\boldsymbol{T}\boldsymbol{F}^{-T} \tag{3.17}$$

where J is the determinate of deformation gradient F and the subscript (–T) represents the inverse transpose. If the material is incompressible then J=1.

It can be shown easily that the first Piola-Kirchoff stress in equation (3.17) is not a symmetric tensor which usually has 9 independent components. In order to overcome this drawback of the first Piola-Kirchoff stress another stress measure is introduced, which is the second Piola-Kirchoff stress, $\boldsymbol{S}$, and is defined as:

$$\boldsymbol{S} = J\boldsymbol{F}^{-1}\boldsymbol{T}\boldsymbol{F}^{-T} \tag{3.18}$$

Second Piola-Kirchoff stress S is a symmetric tensor and this makes the computation and the formulation of the constitutive equation easier.

CHAPTER 4

CONSTITUTIVE LAWS AND MODEL DEVELOPMENT

There are two important types of laws in continuum mechanics: conservation laws and constitutive laws. The first kind concerns the universal or general principles that govern the motion of bodies under applied external forces regardless of the material properties of the body. In other words, any material undergoing elastic and inelastic deformation must obey these principles whenever it moves and deforms under the applied load. There are five such universal principles, balance of mass, balance of linear momentum, balance of angular momentum, balance of energy and Clausium-Duhem inequality.

The second kind of law relates the stress and strain and/or strain rate that characterize the behavior of a material under an application of load. These are called constitutive equations and they vary for different materials. They can even differ for the same material in different regimes of deformation. For example, the response during elastic deformation and the inelastic deformation will be different.

Constitutive equations serve to describe the material properties of the medium when it is subject to external forces considering both basic balance laws and the equations that take into account material characteristics. Constitutive equations are usually constructed from some basic axioms. The resulting equations have unknown material parameters which can be determined from experimental investigations.

4.1 Conservation Laws

Since the general balance laws also govern the creep deformation which is the main topic of this dissertation and since some theories and concepts which were presented and discussed in this dissertation were developed using thermodynamics, the general balance laws is briefly discussed in this chapter. Detailed mathematics of the treatment can be found in advanced continuum mechanics books, such as Truesdell and Noll (1965).

4.1.1 Balance of Mass, Linear Momentum and Angular Momentum

For the convenience of research the balance principles should be mentioned here. The fundamental balance laws, i.e. conservation of mass, the momentum balance principles and balance of energy, are valid in all branches of continuum mechanics. They are applicable to any particular material and must be satisfied for all times.

Conservation of Mass

The balance of mass law states the phenomenon that the mass of a moving body remains constant regardless of what kind of motion it undergoes. In the current configuration the conservation of mass is:

$$\frac{d\rho}{dt} + div(\rho \boldsymbol{v}) = 0 \tag{4.1}$$

For the incompressible material, the density of the material is a constant and thus equation (4.1) reduces to

$$div(\boldsymbol{v}) = 0 \tag{4.2}$$

According to the definition of the velocity gradient $\boldsymbol{L}$, equation (3.13), this can be written as:

$$tr(\boldsymbol{D}) = 0 \tag{4.3}$$

where $\boldsymbol{D}$ which is introduced later in equation (5.7), is the symmetric part of $\boldsymbol{L}$. This kind of deformation is called an isochoric motion (or a volume preserving motion)

In the reference configuration the conservation of mass can be expressed as:

$$\rho_0 = \rho \det(\boldsymbol{F}) \tag{4.4}$$

Simplification of the conservation of mass in the Lagrangian form for an incompressible continuum body is:

$$\det(\boldsymbol{F}) = 1 \tag{4.5}$$

Conservation of Momentum

The conservation of momentum law is in fact the generalization of Newton's second law of motion for continuum mechanics. It provides that the internal action among particles of a continuum can be represented by internal tractions and that these tractions follow the same laws as the external forces. It can be expressed as an equation in the current configuration,

$$div(\boldsymbol{T}^T) + \rho \boldsymbol{b} = \rho \frac{d\boldsymbol{v}}{dt} \tag{4.6}$$

Where $\boldsymbol{T}$ is the Cauchy stress tensor, ρ is material density, $\boldsymbol{b}$ is body force per mass, $\boldsymbol{v}$ is the velocity and t is the time. This is also known as Cauchy's equation of motion.

In terms of the first or second Piola-Kirchoff stress $\boldsymbol{P}$ or $\boldsymbol{S}$, the conservation of momentum can be written in the reference configuration as:

$$Div(\boldsymbol{P}^T) + \rho_0 \boldsymbol{b} = \rho_0 \frac{d\boldsymbol{v}}{dt} \quad \text{or} \quad Div(\boldsymbol{S}\boldsymbol{F}^T) + \rho_0 \boldsymbol{b} = \rho_0 \frac{d\boldsymbol{v}}{dt} \tag{4.7}$$

where operator *Div* refers to the divergence taken with respect to the reference configuration.

In the case that the body couples and distributed couples over any boundary surfaces are absent, which is called the nonpolar case, the conservation of angular momentum can be written as:

$$\boldsymbol{T} = \boldsymbol{T}^T \tag{4.8}$$

This indicates that Cauchy stress tensor $\boldsymbol{T}$ is symmetric. In this dissertation only nonpolar case is studied. Thus the Cauchy stress tensor is always symmetric in this work. The results for the first Piola and second Piola stress tensors reduce to:

$$\boldsymbol{P}\boldsymbol{F}^{\mathrm{T}} = \boldsymbol{F}\boldsymbol{P} \quad \text{and} \quad \boldsymbol{S}^{\mathrm{T}} = \boldsymbol{S} \tag{4.9}$$

4.1.2 Thermodynamics

Conservation of energy states the nature of the fact that the change of the total energy in a continuum body should be equal to the heat input rate Q_{heat} and the power P_{force} exerted by the external forces, including the body and the surface forces.

$$Q_{heat} = -\int_{\partial\Omega} \boldsymbol{q}\cdot\boldsymbol{n}dS + \int_{\Omega}\rho r dV \tag{4.10}$$

$$P_{force} = \int_{\partial\Omega} \boldsymbol{t}\cdot\boldsymbol{v}dS + \int_{\Omega}\rho\boldsymbol{b}\cdot\boldsymbol{v}dV \tag{4.11}$$

where $\boldsymbol{q}$ is the heat flux vector, $\boldsymbol{n}$ is the normal direction of the surface, r is the strength of the distributed internal heat source, $\boldsymbol{t}$ and $\boldsymbol{b}$ are external surface tractions per unit area and body force per unit mass, respectively; $\boldsymbol{v}$ is the velocity, dS and dV are unit area and unit volume, respectively.

Using $t_i = T_{ji}n_j$, transpose theorem, $\int_{\partial\Omega}\boldsymbol{T}^T\boldsymbol{n}\,dS = \int_{\Omega} div\boldsymbol{T}\,dV$, and definition of velocity gradient $\boldsymbol{L}$, equation (4.11) can be simplified and rearranged as:

$$P_{force} = \int_{\Omega}\boldsymbol{T}\cdot\boldsymbol{L}dV + \frac{d}{dt}\int_{\Omega}\frac{1}{2}\rho\boldsymbol{b}\cdot\boldsymbol{v}dV \tag{4.12}$$

where $\boldsymbol{T}\cdot\boldsymbol{L} = \boldsymbol{T}\cdot\boldsymbol{D}$ is a scalar and called stress power. The energy equation for a continuum can be shown to be:

$$\rho\dot{\varepsilon} = \boldsymbol{T}\cdot\boldsymbol{L} - div\boldsymbol{q} + \rho r \tag{4.13}$$

where ε is the specific internal energy.

4.1.3 Entropy and Second Law of Thermodynamics

Second law of thermodynamics: Second law of thermodynamics is proposed by Kelvin. It states: *It is impossible to devise energy which, working in a cycle, shall produce no effect other than extract of heat from a reservoir and the performance of an equivalent amount of mechanical work.* Clausius-Duhem inequality is the consequence of this statement.

For a closed-cycle system, during a heat transfer process from heat source q at temperature θ, the following equation holds

$$\oint \frac{dq}{\theta} \le 0 \tag{4.14}$$

If the cycle is reversible then the equality sign will be held.

Now we introduce the entropy S as a state variable directly from equation 4.14:

$$S_B - S_A = (\int_A^B \frac{dq}{\theta})_{rev} \tag{4.15}$$

where the process that leads from A to B is reversible. If the process is irreversible, then from equation (4.14), we have:

$$S_B - S_A = (\int_A^B \frac{dq}{\theta})_{irrev} \tag{4.16}$$

In general,

$$S_B - S_A \geq \int_A^B \frac{dq}{\theta} \tag{4.17}$$

Equation (4.17) can be rewritten in the following form:

$$\theta \dot{S} - Q \geq 0 \tag{4.18}$$

where Q is the heat transfer in the system and can be defined as:

$$Q = -\int_{\partial\Omega} \boldsymbol{q} \cdot \boldsymbol{n} dS + \int_{\Omega} \rho r dV \tag{4.19}$$

where r is the radiant heating and $\boldsymbol{q}$ is the heat flux through the surface of Ω.

Next, assuming that

$$S = \int_{\Omega} \rho \eta dV \tag{4.20}$$

Now we can obtain a local form for equation (4.18). Substituting equation (4.19) and equation (4.20) into equation (4.18), using conservation of mass and assuming the regularity of the integrands, it follows,

$$0 \leq \rho \eta \dot{\theta} - \frac{\boldsymbol{q} \cdot grad\theta}{\theta} + div\boldsymbol{q} - \rho r =: \xi \tag{4.21}$$

Substituting equation of equation (4.13) into equation (4.21), it yields,

$$\xi = \boldsymbol{T} \cdot \boldsymbol{L} - \rho\dot{\varepsilon} - \rho\eta\dot{\theta} - \frac{\boldsymbol{q} \cdot \operatorname{grad}\theta}{\theta} \geq 0 \tag{4.22}$$

which is known as Clausius-Duhem inequality. It is customary to introduce the specific Helmholtz potential ψ as

$$\psi = \varepsilon - \theta\eta \tag{4.23}$$

then the Clausius-Duhem inequality becomes:

$$\xi = \boldsymbol{T} \cdot \boldsymbol{L} - \rho(\dot{\psi} - \eta\dot{\theta}) - \frac{\boldsymbol{q} \cdot \operatorname{grad}\theta}{\theta} \geq 0 \tag{4.24}$$

where ξ is a measure of energy dissipation

$\boldsymbol{T}$ and $\boldsymbol{L}$ represent the stress/velocity gradient tensors, respectively

ρ is material density

ε is internal energy

ψ is the Helmholtz potential

η is the specific entropy

$\boldsymbol{q}$ is the heat flux vector (positive outwards)

θ is the absolute temperature

The dissipation can be further split into two parts,

$$\xi = \xi_{mech} + \xi_{heat} \tag{4.25}$$

where

$$\begin{aligned} \xi_{mech} &= \boldsymbol{T} \cdot \boldsymbol{L} - \rho\dot{\psi} - \rho\eta\dot{\theta} \\ \xi_{heat} &= \frac{\boldsymbol{q} \cdot \operatorname{grad}\theta}{\theta} \end{aligned} \tag{4.26}$$

are the rate of mechanical dissipation and the rate of dissipation due to heat conduction.

For an isothermal process, i.e., θ=constant, thus $\xi_{heat} = 0$ and the mechanical dissipation reduces to

$$\xi_{mech} = \boldsymbol{T} \cdot \boldsymbol{L} - \rho\dot{\psi} \tag{4.27}$$

The physical meaning of equation (4.27) is that part of the external power supply that cannot be covered as work, is dissipated into thermal energy.

The stored energy of material is commonly assumed as

$$\psi = \psi(\boldsymbol{F}_e, \boldsymbol{G}) \tag{4.28}$$

And the standard formula for Cauchy-stress, ***T***, is given by:

$$\boldsymbol{T} = 2\rho\boldsymbol{F}_e \frac{\partial\psi}{\partial\boldsymbol{C}} \boldsymbol{F}_e^T \tag{4.29}$$

Using the chain rule for $\dot{\psi}$, and substituting equation (4.29) into equation (4.27), the following equation is obtained,

$$\xi_{mech} = (\boldsymbol{T}\boldsymbol{F}_e^{-T} - 2\rho \boldsymbol{F}_e \frac{\partial \psi}{\partial \boldsymbol{C}_e}) \cdot \dot{\boldsymbol{F}}_e + (\boldsymbol{F}_e^T \boldsymbol{T} \boldsymbol{F}_e^{-T} - \rho \frac{\partial \psi}{\partial \boldsymbol{G}} \boldsymbol{G}^T) \cdot \boldsymbol{L}_{in} \geq 0 \qquad (4.30)$$

4.2 Principle of Constitutive Theories

The balance laws introduced in section 4.1 are the fundamental equations common to all material bodies. However, these laws are insufficient to fully characterize the behavior of material bodies because physical experience has shown, in general, that two bodies of exactly the same size and shape will not have the same behavior when they are subject to exactly the same outside general condition, say, external supplies and boundary conditions. For example, aluminums and rubber with the same diameter and length will have different elongation when subject to the same force.

The basic equations describe the physical effects created by external forces acting upon solids and fluids. In addition to the basic equations that are applicable to all continua, there are equations which are constructed to take into account material characteristics. These equations are called constitutive equations. The validation of a constitutive equation can be verified by experimenting on the results it predicts. On the other hand, experiments in some degree also depend on the constitutive functions. In other words, experiments alone can't totally determine the correctness of the constitutive equation. Therefore, generally, in search of the correct formulation of a constitutive equation, some universal requirement should be imposed on the proposed constitutive models. These include material frame invariance which deals with the transformation properties of constitutive equations; material symmetry which characterizes the specific

symmetric properties of material particles; and thermodynamic consideration which governs thermodynamic aspects of material bodies.

For example, in the study of solids the constitutive equations for a linear elastic material are a set of relations between stress and strain. In the study of fluids, the constitutive equations consist of a set of relations between stress and rate of strain.

The resulting equations have unknown material parameters which can be determined by experimental investigations.

4.2.1 Material Frame Invariance

As it is known, the natures laws preserve at any time, any place and do not depend on the frame or observers. Constitutive theories that reflect the physical phenomenon should also keep the mathematical presentations independent of the observers. This property is called material frame-indifference (invariance), a basic axiom for development of the constitutive equations. The principal of frame-indifference requires constitutive equations to be invariant under changes of frames that preserve the essential structure of space and time. If this principle is violated, the constitutive equations are affected and meaningless results are obtained.

A constitutive equation includes several parts: basic fields, $\rho(\mathbf{X},t)$, $\chi(\mathbf{X},t)$, $\theta(\mathbf{X},t)$; other fields quantities, $\boldsymbol{T}(\boldsymbol{X},t)$, $\boldsymbol{q}(\boldsymbol{X},t)$, $\varepsilon(\boldsymbol{X},t)$; and external supplies, $\boldsymbol{b}(\boldsymbol{X},t)$, $r(\boldsymbol{X},t)$, where ρ, χ, θ, $\boldsymbol{T}$, $\boldsymbol{q}$, ε, $\boldsymbol{b}$ and r are material density, the motion function, temperature, stress tensor, heat flux, internal energy, body force and the energy supply respectively. Usually it is assumed that material properties are independent of external supplies, while the field quantities, stress, heat flux, and the internal energy

will depend not only on the behavior of the body but also depend on the kind of material that constitutes the body, which are referred to as constitutive equations.

According to material invariance, the response of a material is the same to any pair of equivalent observer. In the mathematical terms, material response is described by constitutive equations and an observer is identical with a frame that signifies a system of measure position in the Euclidean space together with a means of measuring time.

An observer is characterized mathematically as a frame and is therefore equipped to measure positions by distance and time. Different observers may obtain different value of distance and time even by using the same unit for distance and time. But the distance and time elapse should be the same between any two events under observation. Let π and π^* denote two frames which originate at different point O and O^* with different points $\mathbf{x}$, $\mathbf{x}^*$ and time t, t^*, then the above expression can be mathematically interpreted as:

$$\begin{aligned} |\boldsymbol{x}_1 - \boldsymbol{x}_0| &= |\boldsymbol{x}_1^* - \boldsymbol{x}_0^*| \\ |t_1 - t_0| &= |t_1^* - t_0^*| \end{aligned} \tag{4.31}$$

where $\mathbf{x}_0$, t_0 are the initial position and time, $\mathbf{x}_1$ and t_1 are the current position and time. Plain letters represent the position and time at frame one while the letters with * represent the position and time for frame two. These two frames satisfy the invariant condition if and only if position and time satisfy the equation:

$$\mathbf{x}^* = \mathbf{c}(t) + \mathbf{Q}(t)\mathbf{x}, \quad t^* = t + \alpha \tag{4.32}$$

where x^* and x are related by the Euclidean transformation, a one to one mapping as shown in equation (4.31), where Q(t) is an orthogonal tensor, with the property $Q^{-1}(t) = Q^T(t)$. To maintain the orientation, Q is assumed to be proper orthogonal, $\det Q(t) = 1$.

More specifically, the fields of scalar ϕ, vector **u** and tensor A are said to be frame invariants relative to any change of frame given by a Euclidean transformation in equation (4.32), and can be represented by the following equations,

$$\begin{aligned} \mathrm{A}^*(\mathbf{x}^*, t^*) &= \mathbf{Q}(t)\mathbf{A}(\mathbf{x}, t)\mathbf{Q}^T(t) \\ \mathbf{u}^*(\mathbf{x}^*, t^*) &= \mathbf{Q}(t)\mathbf{u}(\mathbf{x}, t) \\ \phi^*(\mathbf{x}^*, t^*) &= \phi(\mathbf{x}, t) \end{aligned} \tag{4.33}$$

For any constitutive quantity $\mathfrak{M}$, its constitutive relation can be expressed as:

$$\mathfrak{M}_\pi(X, t:\pi) = \mathbb{Z}_\pi(\rho^t(X,t),\ \chi^t(X,t),\ \theta^t(X,t), X, t) \tag{4.34}$$

where π is a frame of reference, $\mathfrak{M}_\pi(X, t:\pi)$ is the value of the constitutive function at the position of X and time t in the frame π. Generally, the constitutive function depends on the frame as shown in equation (4.31).

Since any intrinsic property of materials should be independent of frame or observer, it is required that the constitutive quantity $\mathfrak{M}$ must be independent of the frame, that is

$$\mathfrak{M}_\pi(\cdot) = \mathfrak{M}_{\pi^*}(\cdot) \tag{4.35}$$

for any frame π and π^*.

The principle of material frame-indifference can restrict the response of elastic materials. This can be seen from the following derivation. The constitutive equation for an elastic material can be presented in the Cauchy stress tenors $\boldsymbol{T}$ as

$$\boldsymbol{T} = \boldsymbol{g}(\boldsymbol{F}) \tag{4.36}$$

where **g,** the response function**,** is a symmetric tensor-valued function. When an alternative reference configuration is picked, the stress then can be written as

$$\boldsymbol{T}^* = \boldsymbol{g}^*(\boldsymbol{F}^*) \tag{4.37}$$

From the theory of principle of material frame-indifference the stress at these two configurations should be identical,

$$\boldsymbol{T}^*=\boldsymbol{Q}\boldsymbol{T}\boldsymbol{Q}^T \tag{4.38}$$

Since $\boldsymbol{F}^*=\boldsymbol{Q}\boldsymbol{F}$ holds true

$$\boldsymbol{g}(\boldsymbol{Q}\boldsymbol{F}) = \boldsymbol{Q}\boldsymbol{g}(\boldsymbol{F})\boldsymbol{Q}^T \tag{4.39}$$

In other words, the Cauchy stress for elastic material is compatible with the principle of material invariance if and only if the above condition (equation 4.39) holds.

4.2.2 Material Symmetry and Anisotropy

Suppose an elastic body is subject to a given deformation in relation to a specified reference configuration, if the elastic body changes to another reference configuration while still maintaining the same deformation, the stress produced at a fixed point will be different. However, for most elastic materials, the stress exhibits material symmetry in the sense that particular changes of reference configuration keep the stress at the fixed point arising from an arbitrary deformation invariant. The larger the collection of such transformations the greater the degree of symmetry possessed by the material.

The mathematical representation of the material symmetry arises from the effect of change of reference configuration on deformation gradient. Two deformation gradients $\boldsymbol{F}$ and $\boldsymbol{F}^*$ relate to an arbitrary pair of configurations π_r (reference configuration) and $\boldsymbol{\pi}_r^*$ (current configuration). In the rectangular Cartesian systems $(\boldsymbol{O}, \boldsymbol{E})$, $(\boldsymbol{O}^*, \boldsymbol{E}^*)$ and $(\boldsymbol{o}, \boldsymbol{e})$ of the referential and spatial coordinates, $\boldsymbol{F}$ and $\boldsymbol{F}^*$ are given by

$$\boldsymbol{F} = \frac{\partial \boldsymbol{x}_p}{\partial \boldsymbol{X}_\pi} \boldsymbol{e}_p \otimes \boldsymbol{E}_\pi \quad and \quad \boldsymbol{F}^* = \frac{\partial \boldsymbol{x}_p}{\partial \boldsymbol{X}_\pi^*} \boldsymbol{e}_p \otimes \boldsymbol{E}_\pi^* \tag{4.40}$$

Using the chain rule for partial differentiation and the orthonormality of the basis $\boldsymbol{E}^*$, we have

$$\boldsymbol{F} = \frac{\partial \boldsymbol{x}_p}{\partial \boldsymbol{X}_g^*} \frac{\partial \boldsymbol{X}_g^*}{\partial \boldsymbol{X}_\pi} \boldsymbol{e}_p \otimes \boldsymbol{E}_\pi = (\frac{\partial \boldsymbol{x}_p}{\partial \boldsymbol{X}_g^*} \boldsymbol{e}_p \otimes \boldsymbol{E}_g^*)(\frac{\partial \boldsymbol{X}_g^*}{\partial \boldsymbol{X}_\pi} \boldsymbol{E}_g^* \otimes \boldsymbol{E}_\pi) = \boldsymbol{F}^* \boldsymbol{G} \tag{4.41}$$

$\boldsymbol{G}$ being the deformation gradient associated with the mapping $\boldsymbol{\pi}_r \rightarrow \boldsymbol{\pi}_r^*$

From equation (4.41) we can conclude that the stress response of an elastic material does not discriminate between the reference configurations π_r and π_r^*.

Since an arbitrary invertible tensor can be expressed as a product of a unimodular tensor (Mrisky, 1995) (i.e. a tensor whose determinant is ± 1) and a spherical tensor (i.e. scalar multiple of the identity tensor), it suffices to consider changes of reference configuration for which the associated deformation gradient is a member of the unimodular group U. The set of all unimodular tensors **H** satisfying equation

$$\mathbf{g}(\mathbf{AH}) = \mathbf{g}(\mathbf{A}) \tag{4.42}$$

is called the isotropy group.

Further, if the elastic material possessed a reference configuration in relation to which the isotropic group contains the full orthogonal group $\boldsymbol{O}$ (i.e. the set of all orthogonal tensors) it is called isotropic material. For an isotropic elastic material the stress response is not affected by the change of the reference configuration and the material does not exhibit the preferred directions.

On the other hand, if the orthogonal tensor is only part of the orthogonal group $\boldsymbol{O}$, this kind of material is called an anisotropic material. Therefore this kind of material does have preferred directions. Nickel based single crystal Superalloys are an example of an anisotropic material.

4.3 The Nature of Anisotropy in Nickel Based Single Crystal Superalloys

Anisotropy is a very common phenomenon in nature. It can be observed in wood, concrete, metals and alloys, etc. At the macroscopic level, anisotropy is displayed by the

fact that the material properties are not the same in different directions. From the microscopic point of view, anisotropy originates from the crystal structure inherent to the metal and alloy.

It is well known that a crystal is made of atoms in a regular array according to some rules. For a cubic crystal, for example, the atom numbers along the three axes may not be the same; the density of atoms along the diagonal of the plane may or may not be the same. This results in the different crystal structure such as face centered cubic crystal structure and body centered cubic crystal structure. At the same time, for a certain crystal structure the different atom density also leads to different material properties at different crystal orientations. For an anisotropic material, the Young's modulus is greater in the higher atom density direction and less in the lower atom density orientation. The difference between maximum and minimum Young's could be as much as 4 times.

It seems that anisotropy should be observed in all the metals and alloys due to the reasons stated above. This is true for a single crystal. But engineering materials, generally, are polycrystalline. Because the Young's modulus is determined by bond strength among the atoms, thus grain size and grain boundary have no significant effect on the Young's modulus. Since polycrystalline has a large quantity of the atoms at random orientations, although every grain has different Young's modulus at different orientations, from the macroscopic point of view the young's modulus is still isotropic.

The exact nature of this anisotropy depends upon both alloy composition and process history (e.g. casting, rolling, extrusion, annealing, etc). During these procedures, metals and alloys usually flow along the orientation with higher Young's modulus, thus resulting in textured structures. With the increase of the plastic deformation, the slip directions of every grain rotate to the main deformation direction. As a result all the

grains, which originally had different orientations, now have the same orientation, resulting in a textured microstructure in the polycrystalline material. When the textured structure reaches 80-90%, the anisotropic property will be seen in the polycrystalline material. This anisotropic behavior can be harmful or beneficial. For example, cold forming anisotropic material can result in ears; but it can also be beneficial, for example, to obtain a high property along a certain orientation such as in a nickel based single crystal Superalloy.

Anisotropy of nickel based single crystal Superalloy originates from the casting methods.

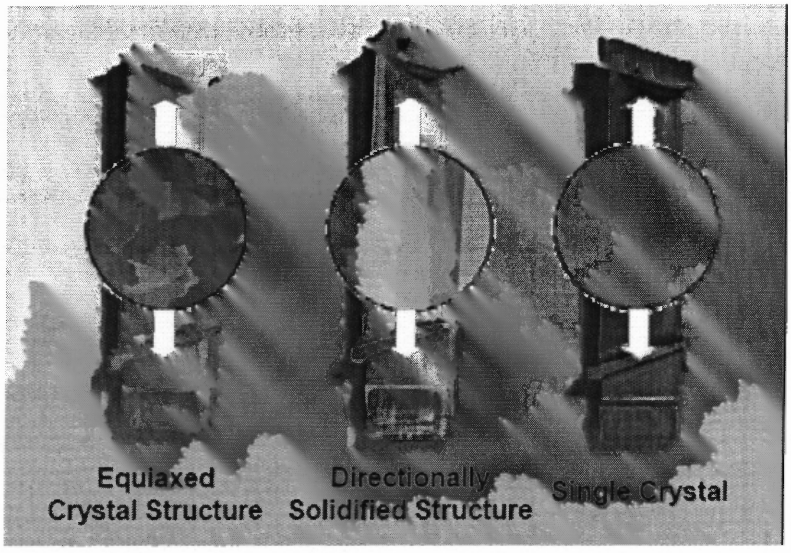

Figure 4.1 Casting methods and their corresponding microstructures (Betteridge, 1982).

Figure 4.1 (Betteridge, 1982) shows the three typical microstructures inherited from the corresponding casting methods: conventional casting, directional solidification casting and the single crystal method. The most significant difference among these is: the equiaxed structure has grain boundaries and the grains are of similar size; it is a

typical polycrystalline material and the material properties are isotropic; directionally solidified (DS) casting eliminates the transverse grain boundaries thus it has a texture structure. This material structure displays anisotropic material properties. Single crystal (SG) method eliminates all the grain boundaries, i.e. the cast object is totally a single crystal. The material is significantly anisotropic.

CHAPTER 5

CREEP DEFORMATION AND THE THEORY OF MATERIALS POSSESSING MULTIPLE NATURAL CONFIGURATIONS

As it is well known, there are basically two kinds of deformation solids usually undergo, one is the elastic deformation in which upon unloading the material can recover its original shape; and the other, inelastic deformation, refers to the deformation which upon unloading the material does not recover its original shape. For an inelastic deformation there are stresses and strains left in the material body.

Inelastic deformation includes time-independent and time-dependent deformations. Time-independent inelastic deformation has been widely studied and lots of successful theories have been developed. However, it is not the topic of this dissertation, although there are some similarities between plastic deformation and creep. Here, the main attention will be paid to creep deformation.

Creep usually denotes a slow viscous flow of solid under macroscopically non-zero stress, via dislocation motion (glide or climb) and atomic diffusion (through lattice or along grain boundary). The mechanism of creep depends on material composition, microstructural features, temperature and stress. For Nickel single crystal Superalloy orientation is also a significant factor.

Multiple natural configurations were first recognized by Eckart (1948), developed by Rajagopal and Wineman (1980), Rajagopal and Srinivasa (1998, I and II). The central tenet of the theory is that plastic materials, unlike elastic bodies, possess multiple stress-free (or natural) configurations and that these configurations, evolving gradually with the deformation, play a fundamental role in the mechanical behavior of material.

In this chapter an introduction of creep mechanisms and multiple natural configurations is given. Based on these theories, a constitutive model for creep is developed by using the framework of multiple natural configurations for nickel based single crystal Superalloys. The techniques related to the development of the model are also introduced.

5.1 Mechanisms Underlying Creep Behavior

Creep is the time-dependent elongation for a material under constant load/stress. It is a common phenomenon for engineering applications where products undergo specific loadings and the product's service life is a major concern. Therefore, it is critical to understand the origin of creep deformation and to be able to predict the long time creep behavior for a given material under consideration.

5.1.1 Polycrystalline Materials

Crystals are solids in which the constituent atoms, molecule, or ions are packed in a regular order with repeating patterns extending in the three spatial dimensions. This is the main difference between a crystalline and non-crystalline solid. Due to the different arrays in space, three typical microstructures of crystals exist in metals: face centered cubic (F.C.C), body centered cubic (B. C. C) and hexagonal close-packed (H.C.P). In real crystals, defects, or irregularities exist, including dot defect such as vacancies, interstitials and impurity atoms (substitutional and interstitial); line defects such as dislocations; and face defects such as grain boundaries, phase boundaries, and twins. These defects play a very important role in plastic and creep deformation and also critically determine many of the electrical and mechanical properties of real materials. In particular, dislocations in

the crystal allow shear at a much lower stress than what is needed for a perfect crystal structure. Movement of these defects is the origin of the creep deformation.

There are four different mechanisms that control creep in polycrystalline material, depending on the applied stress and on the temperature at which the test is performed. These involve dislocations motion and diffusion of vacancies and interstitials. The dependent mechanisms of deformations involve the motion through the grains or around the grain boundaries of lattice defects such as vacancies or dislocations for polycrystalline materials.

A dislocation is a line discontinuity in the regular crystal structure. There are two basic types: edge dislocation and skew dislocation. These two types of dislocations have different shapes and will be activated under different conditions. When dislocations move along a certain crystal direction, slip/glide takes place. The accumulation of the dislocations slip/glide will result in the macroscopic inelastic deformation.

Dislocations exist in all the metals and alloys. The only difference is the dislocation density, dislocation lines per square meter. Even in a well annealed crystalline metal the dislocation density can still reach 10^8 (m^{-2}). In a single crystal, the dislocation density is no less than 10^7-10^8. Normally in metals and alloys the dislocation density is about 10^{10}-10^{12}. It can reach as high as 10^{15}-10^{16} for metals that have been heavily cold worked. It is clear that dislocation density changes with the material deformation. Dislocation line has a strain energy associated with it.

The mechanisms involved in the creep deformation include the following: **Dislocation glide**, which is determined by dislocations moving conservatively along their glide planes. It occurs if the stress is high enough for the dislocations to overcome obstacles in the lattice; **Dislocation creep**, which is the movement of dislocations outside

their glide plane and is assisted by diffusion of vacancies. It occurs only at relatively high temperatures, i.e. when the influence of diffusion becomes significant. **Diffusion creep**, which occurs at relatively low stress. The deformation of the material is due to the flow of atoms and vacancies that cause them to rearrange themselves along the direction of load. At lower temperatures the diffusion occurs mainly along easier paths, such as grain boundaries (Coble creep), whereas at high temperatures, atoms and vacancies diffuse across the bulk of the material (Nabarro-Herring creep); **Grain boundary sliding** is also an important mechanism. In order to maintain continuity within the creeping material, the grains must rearrange themselves and they can do so only by sliding along each other. Moreover, grain boundary sliding is important as; in the third part of the creep experiment it determines the onset of fracture.

As stated above, creep deformation is very complicated. It can involve one or more mechanisms acting simultaneously, and there seems no way to distinguish which mechanism operates and which does not. From experiments, Ashby and his coworkers summarized a schematic plot (Figure 5.1) to describe the active mechanism at a given stress and temperature. For a specific material the plot is different, since every material is different from others in composition, microstructure, etc.

5.1.2 Single Crystal Materials

Nickel based single crystals have a special microstructure as stated in Chapter 1. The whole component only has one grain thus there is no grain boundary in it. This will eliminate grain boundary glide creep mechanism mentioned in subsection 5.1.1 for polycrystalline materials. In nickel based single crystal Superalloys only dislocation creep/glide and diffusion creep exist.

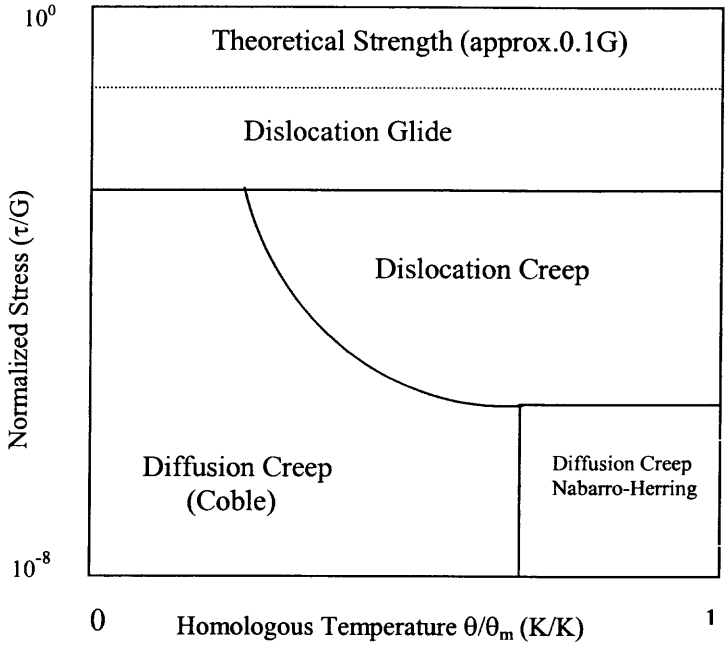

Figure 5.1 Schematic plot of the mechanism of creep deformation (After Ashby etc.1978).

Diffusion creep is caused by the point defects flow through a crystal or around the grain boundaries in a polycrystalline and no dislocation movement is involved. Two different types of diffusion creep are listed here, Nabarro-Herring creep and Coble creeps. In the former type of creep the diffusion path is through the bulk grains while in the latter the path goes through the grain boundaries which dominate at low stress and low temperature. Since the special single crystal manufacturing method results in a large decrease of the point defects, diffusion creep is less important than dislocation creep compared with polycrystalline materials.

Dislocation creep, as it is called, is caused by the movement of dislocations. The movement of dislocations can induce inelastic deformation, such as viscoelastic deformation, viscoplastic deformation and plastic deformation. The difference between

plastic deformation and viscoelastic/viscoplastic deformation is that plastic deformation is time independent.

5.1.3 Description of Creep from a Microscopic and Macroscopic Point of View

As in polycrystalline materials, creep of Nickel based single crystal Superalloys has three stages, namely, primary creep, secondary creep and tertiary creep. During the primary creep, the strain is produced when the load is applied at high temperature. With the elapse of time, the strain increases. When the strain rate achieves a constant value, this stage is called secondary creep. Under this loading condition, the specimens elongate with time. As time goes on, at some point necking occurs. Afterwards, the strain rate increases rapidly and so does the elongation. The specimen fractures and this is known as tertiary creep.

These macroscopic processes reflect the microstructural changes taking place in the materials. For a Nickel based single crystal Superalloy, at high temperature regime, during primary creep, the change focuses mainly on the cubic γ' phase evolution which is the directional coarsening called rafting. Arrell and Valle's (1994) and Buffiere and Ignat (1995) pointed out that the mechanism of rafting is similar to the flow of matter, and the driving force of the rafting process is the elastic strain energy. In the meantime, the diffusion and redistribution of alloying elements in the γ' phase take place.

Unlike the creep mechanism in the primary creep in which the restriction of the dislocation allows motion only along the matrix channel, during steady state creep, the dislocation can move in both γ' phase and γ phase. During the tertiary creep, voids expansion and crack formation are the main changes that take place.

The strain developed in the process can be divided into elastic and inelastic strain. Elastic strains are instantaneous and are reversible by the application of a reverse stress comparable in magnitude to the original forward stress. However, during primary creep, although the external shape of the specimen has been restored, its internal structure has been irreversiblely altered. From a metallurgical point of view, the material is made of atoms which are joined by atomic bonds to their neighbors. Elastic strain distorts the bonds without breaking them. But inelastic strain is usually produced by the motion of the dislocation and thus will break bonds and form new bonds.

To activate the movement of dislocations activation energy is required, which is dissipated as the dislocations cross barriers. The energy is supplied by the thermal motion of the atoms. The dislocation motion leads to a permanent inelastic deformation.

The occurrence of accelerated creep is due to the development of cavities in the material. The formation of such cavities is the most common example of what is known as creep damage. The cavities act as stress concentration sites and also cause a decrease in the load-bearing cross-section.

No matter how complicated a deformation can be at the microstructural level, from the macroscopic point of view, the energy can only be stored or dissipated. In other words, energy can be converted from one form to another.

Dissipation is a key factor in distinguishing an inelastic deformation from an elastic deformation. The role of dissipation in an inelastic material can be described by the Clausium-Duhem inequality, also well known as the second law of thermodynamics.

Decomposing equation (4.24) into two parts (see Trusedell and Noll, 1965),

$$\xi = \xi_I + \xi_c \tag{5.1}$$

where

$$\xi_l := \boldsymbol{T} \cdot \boldsymbol{L} - \rho(\dot{\psi} - \eta\theta) \qquad \text{(a)}$$
$$\xi_c := -\frac{\boldsymbol{q} \cdot grad\theta}{\theta} \qquad \text{(b)} \qquad (5.2)$$

The above ξ_l and ξ_c represent the local dissipation and the dissipation by conduction.

It can be seen apparently that if both ξ_l and ξ_c equal to zero, there is no dissipation taking place and the process is regarded as a purely elastic process. If both ξ_l and ξ_c equal nonzero, the process includes local dissipation and thermal dissipation and this is an inelastic process. In between, if $\xi_l = 0$ while $\xi_c > 0$ then the process is thermoelastic.

In this study the process considered is isothermal which leads to $\xi_c=0$. In order to calculate ξ_l, from equation (5.2a), a suitable stored energy ψ should be defined and this will be done in the subsection 5.3.1.

5.2 The Role of Multiple Natural Configurations in the Model

A natural configuration of a body is defined as a stress-free configuration that the body will return to upon unloading at any given time of the loading program. For an elastic material, there is only one single natural configuration (modulus rotations), which is often identified as the reference configuration of the material. On the other hand, an inelastic material can have many such stress-free configurations.

5.2.1 Theory of Multiple Natural Configurations

Natural configuration was first recognized by Eckart (1948), who did not acknowledge the importance of this concept in formulating constitutive theories. Rajagopal and his co-workers have systematically exploited this idea and developed a thermodynamic framework for the bodies that possess multiple natural configurations. One of the principle virtues of this framework is that it is a general framework and can be applied to study many different phenomena, such as: multi-network polymers' response (Rajagopal and Wineman, 1992; Wineman and Rajagopal, 1990), traditional plastic response (Rajagopal and Srinivasa, 1998, I and II), twinning (Rajagopal and Srinivasa, 1995 and 1997 also), solid-to-solid phase transition (Rajagopal and Srinivasa, 1999), viscoelastic response Rajagopal and Srinivasa (2000), anisotropic response of liquids (Rajagopal and Srinivasa, 2001), crystallization of polymers (Rao and Rajagopal, 1999, 2001,2002), and growth and adaptation of biological material (Rao *et al.* 2003). A brief review of this theory is presented here.

As stated in Chapter 3, a body can occupy multiple natural configurations. For metals which have multiple natural configurations, the physical meaning of it can be expressed clearly as follows.

The deformation of metals and alloys can be distinguished as elastic and inelastic deformation. During the elastic deformation the crystal lattice can be stretched and rotated. This kind of deformation can result in the change of the crystal lattice and can be totally removed after unloading, while for the inelastic deformation, the mechanism is the sliding of the dislocation along slip system and it does not change the crystal lattice.

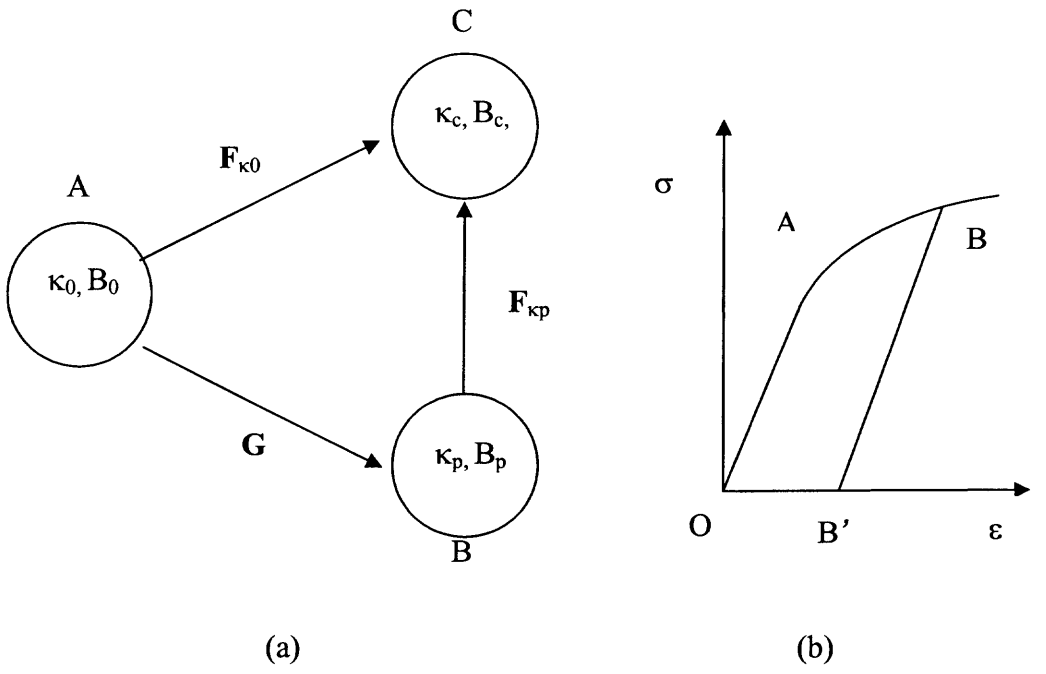

Figure 5.2 Schematic plot of multiple natural configurations.

Figure 5.2 is a Schematic plot of multiple natural configurations. κ_0, κ_c and κ_p are reference, current and natural configuration, respectively (Figure 5.2a). Figure 5.2b is the corresponding deformation interpretation.

For an elastic deformation, once a configuration $\boldsymbol{\kappa}_0$ is chosen, the stress depends only on the deformation $\boldsymbol{\chi}_{\kappa 0}$ for $\boldsymbol{\kappa}_0$. For a simple "elastic material" (Noll, 1957), the Cauchy stress $\boldsymbol{T}$ at $\boldsymbol{x}$ depends upon $\boldsymbol{\chi}_{\kappa}$ only through the deformation gradient $\boldsymbol{F}_{\kappa 0}$ at $\boldsymbol{x}$ and of the form

$$\underset{\sim}{\boldsymbol{T}} = \hat{\boldsymbol{T}}_{\kappa 0}(\boldsymbol{F}_{\kappa 0}) \tag{5.3}$$

where

$$\boldsymbol{F}_{\kappa 0} := \frac{\partial(\chi_{\kappa 0})}{\partial \boldsymbol{X}} \tag{5.4}$$

5.2.2 Nature of the Velocity Gradient G in the Model

Now it is time to define $\boldsymbol{G}$. Let $\boldsymbol{\kappa}_{p(t)}$ be the natural configuration (stress-free state) associated with the current natural configuration $\boldsymbol{\kappa}_{c(t)}$ of the body. For a homogeneous deformation $\boldsymbol{F}_e$ denotes the deformation gradient between these two configurations. In general $\boldsymbol{F}_e$ may not be the gradient of a mapping (Rajapopal, 1998), thus the evolution of the natural configuration $\boldsymbol{G}$, is defined through:

$$\boldsymbol{G} = \boldsymbol{F}_{\kappa_0 \to \kappa_{p(t)}} = \boldsymbol{F}_e^{-1} \boldsymbol{F}_{\kappa_0 \to \kappa_{c(t)}} \tag{5.5}$$

and inelastic velocity gradient is defined as

$$\boldsymbol{L}_{in} = \dot{\boldsymbol{G}} \boldsymbol{G}^{-1} \tag{5.6}$$

where the dot signifies the usual material time derivative

The tensor $\boldsymbol{G}$ captures the evolution of the natural configuration during the inelastic deformation. Form the microscopic point of view; it describes the actual slipping process in an averaged manner.

Inelastic deformation is characterized by changing natural configurations of material. These natural configurations can be identified with the stress-free state of a body but are not limited to these states. The kinematics associated with inelastic material behavior is strongly linked to the fact that the materials possess multiple natural configurations. For example, at the level of dislocation movement, each slipped configuration can be regarded as a natural configuration of the body as shown in Figure 5.3.

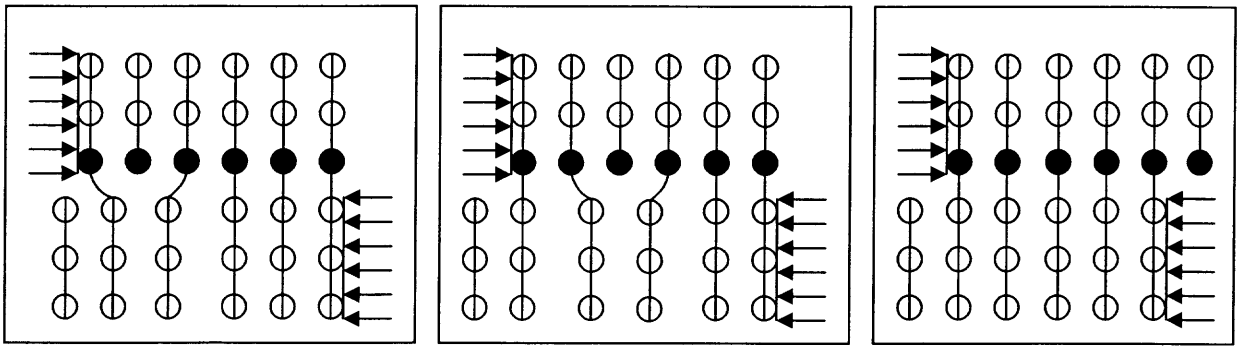

Figure 5.3 Schematic plot of slip deformation (a) an unslipped lattice; (b) a middle phase of slip; (c) a slipped lattice.

Decomposing $\boldsymbol{L}$ and $\boldsymbol{L}_{in}$ into a symmetric part yields the following two equations:

$$\boldsymbol{D} = \frac{1}{2}(\boldsymbol{L} + \boldsymbol{L}^T) \quad and \quad \boldsymbol{D}_{in} = \frac{1}{2}(\boldsymbol{L}_{in} + \boldsymbol{L}_{in}^T) \tag{5.7}$$

The skew part of $\boldsymbol{L}$ and $\boldsymbol{L}_{in}$ are also given, respectively, by the following two equations:

$$\boldsymbol{W} = \frac{1}{2}(\boldsymbol{L} - \boldsymbol{L}^T) \quad and \quad \boldsymbol{W}_{in} = \frac{1}{2}(\boldsymbol{L}_{in} - \boldsymbol{L}_{in}^T) \tag{5.8}$$

5.3 Thermodynamic Sets of Constitutive Equations

In order to complete the development of the constitutive equations, some quantities should be defined corresponding to the creep deformation of Nickel based single crystal Superalloys. In the following subsections, these quantities, such as Helmholtz potential, dissipation functions and driving force are given.

5.3.1 Helmholtz Potential

Helmholtz potential per unit mass ψ was defined in Chapter 4. In order to describe the constitutive equation for a material, a specific form of Helmholtz potential should be assumed.

It is assumed that Helmholtz potential can be split into the following two parts:

$$\psi = \psi_e + \psi_{in} \tag{5.9}$$

where

$$\psi_e = \psi_{\kappa p}(\boldsymbol{F}_{\kappa p}) \tag{5.10}$$

is related to the elastic stored energy and

$$\psi_{in} = \boldsymbol{F}_{\tau=0}^{\infty}[\boldsymbol{G}(t-\tau)] \tag{5.11}$$

is related to the inelastic stored energy. A specific ψ_e is given later in this section.

In the thermodynamic regime incorporating thermal variables, Helmholtz potential rather than strain energy is used to express the internal energy change. For the elastic potential, it is usually assumed that the Helmholtz potential is solely a function of deformation gradient as shown in equation (5.10).

In order to illustrate ψ a deformation which will store energy is assumed. The stored energy ψ ($\boldsymbol{F}$) generated by the motion $\boldsymbol{x} = \boldsymbol{\chi}(\boldsymbol{X},t)$ is assumed to be objective which means, after a translation and rotation of the material in space, the amount of energy stored is unchanged. Hence, the strain energy ψ ($\boldsymbol{F}$) must equal to the strain energy $\psi(\boldsymbol{F}^*)$ generated by a second motion $\boldsymbol{x}^* = \boldsymbol{\chi}^*(\boldsymbol{X},t^*)$. By using the transformation rule for the deformation gradient of superposed rigid-body motion

$$\boldsymbol{F}^* = \frac{\partial \boldsymbol{x}^*}{\partial \boldsymbol{X}} = Q\frac{\partial \boldsymbol{x}}{\partial \boldsymbol{X}} = \boldsymbol{QF} \tag{5.12}$$

The strain energy must obey the following restriction which is required by invariance under superimposed rigid body motion:

$$\psi(\boldsymbol{F}) = \psi(\boldsymbol{F}^*) = \psi(\boldsymbol{QF}) \tag{5.13}$$

for all tensors $\boldsymbol{F}$, with det $\boldsymbol{F}$>0, and for all orthogonal tensors $\boldsymbol{Q}$.

A special proper orthogonal rotation tensor $\boldsymbol{R}^{\mathrm{T}}$ is selected to obtain the equivalent formulation of equation (5.13). By using right Polar decomposition, equation (3.5a), it is found that $\psi(\boldsymbol{F}) = \psi(\boldsymbol{R}^T\boldsymbol{F}) = \psi(\boldsymbol{R}^{\mathrm{T}}\boldsymbol{RU})$. That is

$$\psi(\boldsymbol{F}) = \psi(\boldsymbol{U}) \tag{5.14}$$

And this holds for arbitrary $\boldsymbol{F}$. Clearly, ψ is independent of rotation part of $\boldsymbol{F}$. Equation (5.14) also specifies the necessary and sufficient condition for the strain energy to be objective during superimposed rigid-body motions.

Using equations (3.10a) and (3.11) further, ψ can be represented as a function of $\boldsymbol{C}_e$ or $\boldsymbol{E}_e$, respectively,

$$\psi(\boldsymbol{F}) = \psi(\boldsymbol{C}) = \psi(\boldsymbol{E}_e) \tag{5.15}$$

For an elastic deformation it is reasonable to assume that the elastic stored energy has the following form:

$$\psi_e = \frac{1}{2\rho} \boldsymbol{E}_e \cdot \mathbb{C} \boldsymbol{E}_e \tag{5.16}$$

where $\boldsymbol{E}_e$ is the elastic strain, $\mathbb{C}$ is a fourth order tensor called elastic tensor and has the following form as in equation (5.17). For an isotropic material $\mathbb{C}$ contains only two independent components, for example, Young's modulus and Poison's ratio.

$$\mathbb{C} = \begin{bmatrix} a & b & b & 0 & 0 & 0 \\ b & a & b & 0 & 0 & 0 \\ b & b & a & 0 & 0 & 0 \\ 0 & 0 & 0 & c & 0 & 0 \\ 0 & 0 & 0 & 0 & c & 0 \\ 0 & 0 & 0 & 0 & 0 & c \end{bmatrix} \tag{5.17}$$

5.3.2 Driving Force for Time-dependent Inelastic Deformation in Nickel Based Single Crystal Superalloy

Since one is looking for forms that are sufficient to satisfy equation (4.30) it seems reasonable to assume that the stress is in the form of equation (4.29). Now the driving force $\boldsymbol{A}$ can be defined as

$$\boldsymbol{A} = [\boldsymbol{F}_e^T \boldsymbol{T} \boldsymbol{F}_e^{-T} - \rho \frac{\partial \psi}{\partial \boldsymbol{G}} \boldsymbol{G}^T] \tag{5.18}$$

As stated before, the driving force $\boldsymbol{A}$ comes from both elastic and inelastic parts. Usually the stored energy can be divided into two parts, elastic stored energy and inelastic stored energy, which is some function of $\boldsymbol{G}$. $\boldsymbol{G}$ is related to the inelastic deformation through equations such as the dislocation density and the inelastic path length (Mollica, et al 2001). Such kind of consideration makes the model and simulation more complex. Here we take a simpler approach is taken, and the inelastic stored energy is assumed to be independent of inelastic deformation gradient, i. e.,

$$\psi_{in} = \psi_{in}(\boldsymbol{G}) = C \tag{5.19}$$

Then

$$\frac{\partial \psi_{in}}{\partial \boldsymbol{G}} = 0 \tag{5.20}$$

This assumption is based on the following thought. This constitutive model is developed for the primary and secondary creep stage. The creep strain is limited.

This results in $\rho\frac{\partial \psi}{\partial \boldsymbol{G}}\boldsymbol{G}^{T}=0$. As a result, the driving force equation (5.18) is simplified to:

$$\boldsymbol{A}=\boldsymbol{F}_{\mathrm{e}}^{\mathrm{T}}\boldsymbol{T}\boldsymbol{F}_{\mathrm{e}}^{-\mathrm{T}} \tag{5.21}$$

5.3.3 Nature of Dissipation

Substituting equation (5.16) into equation (4.30), the mechanical dissipation equation can be simplified as

$$\xi_{mech}=\boldsymbol{A}\cdot\boldsymbol{L}_{in} \tag{5.22}$$

$\boldsymbol{A}$ and $\boldsymbol{L}_{\mathrm{in}}$ can be decomposed into symmetric and skew-symmetric parts $\boldsymbol{A}_{\mathrm{sym}}$, $\boldsymbol{A}_{\mathrm{skew}}$ and $\boldsymbol{D}_{\mathrm{in}}$, $\boldsymbol{W}_{\mathrm{in}}$. These are substituted into equation (5.22) and which is then rewritten as follow,

$$\xi_1=\boldsymbol{A}_{sym}\cdot\boldsymbol{D}_{in},\ \xi_2=\boldsymbol{A}_{skew}\cdot\boldsymbol{W}_{in} \tag{5.23}$$

The dissipation equation (4.30) can be further decomposed as

$$\xi_{mech}=\xi_1(\theta,\boldsymbol{D}_{in})+\xi_2(\theta,\boldsymbol{W}_{in}) \tag{5.24}$$

Choosing a specific dissipation form for creep as

$$\begin{aligned}\xi_1&=\boldsymbol{D}_{in}\cdot\mathbb{k}\boldsymbol{D}_{in} &&\text{(a)}\\ \xi_2&=-\mu\boldsymbol{W}_{in}\cdot\boldsymbol{W}_{in} &&\text{(b)}\end{aligned} \tag{5.25}$$

where μ is an undetermined constant for the model. $\mathbb{k}$ is a fourth-order tensor that is a function of temperature and the driving force, which is called the directional viscosity tensor, used to describe the anisotropic material property and deformation.

It is noted that the requirement that the rate of dissipation be positive is automatically satisfied by the rate of dissipation chosen (5.25a).

Maximizing the rate of dissipations ξ_1 and ξ_2 subject to the constraints tr $(\boldsymbol{D}_{in})$ =0 and the relationship with $\boldsymbol{A}_{sys}$ and $\boldsymbol{A}_{skew}$, we get the evolution equation for $\boldsymbol{D}_{in}$ and $\boldsymbol{W}_{in}$:

$$\boldsymbol{D}_{in} = \mathbb{k}^{-1}\left(\boldsymbol{A}_{sys} - \frac{tr(\mathbb{k}^{-1}\boldsymbol{A}_{sys})}{tr(\mathbb{k}^{-1}\boldsymbol{I})}\boldsymbol{I}\right) \quad \text{(a)}$$

$$\boldsymbol{W}_{in} = \frac{\boldsymbol{A}_{skew}}{\mu} \quad \text{(b)} \qquad (5.26)$$

The value of the viscosity tensor $\mathbb{k}$ is based on comparison with experimental data. $\mathbb{k}$ is assumed to be a positive definite tensor, which can be either isotropic or anisotropic. For a totally anisotropic material $\mathbb{k}$ will have 36 material parameters. Due to the FCC microstructure property of Nickel single crystal Superalloys, the total number of material parameters reduces to 3. $\mathbb{k}$ for the anisotropic material has the following structure:

$$\mathbb{k} = \begin{bmatrix} i & j & j & 0 & 0 & 0 \\ j & i & j & 0 & 0 & 0 \\ j & j & i & 0 & 0 & 0 \\ 0 & 0 & 0 & k & 0 & 0 \\ 0 & 0 & 0 & 0 & k & 0 \\ 0 & 0 & 0 & 0 & 0 & k \end{bmatrix} \qquad (5.27)$$

The form of these coefficients *i, j, k*, are functions of stress, inelastic strain and temperature, and can be expressed as the follows:

$$\mathbb{k}(i,j,k) = \mathbb{k}(\boldsymbol{T}, \boldsymbol{E}_{in}, \theta) \tag{5.28}$$

i.e., the viscosity tensor depends on stress ($\boldsymbol{T}$), inelastic strain ($\boldsymbol{E}_{in}$) and temperature θ. In chapter 6 further details are given to its structure and expression.

5.4 Boundary Value Problems under Consideration

As a starting point, the developed constitutive model is used to study the creep deformation of a cylindrical bar of CMSX-4 Nickel single crystal Superalloy loaded in uniaxial tension along an arbitrary orientation <l, m, n> (Figure 5.3)

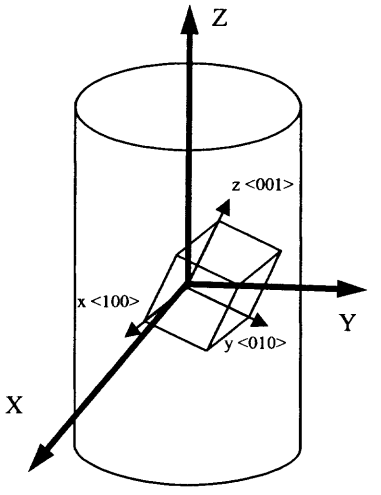

Figure 5.4 Coordinate system for stress and strain transformation.

Assuming the following deformation for the specimen:

$$\begin{aligned} x(t) &= \alpha(t)X \\ y(t) &= \beta(t)Y \\ z(t) &= \gamma(t)Z \end{aligned} \tag{5.29}$$

The deformation gradient associated with the motion is given by

$$\boldsymbol{F} = diag(\alpha(t), \beta(t), \gamma(t)) \tag{5.30}$$

It is further assumed that the creep deformation takes place at a constant stress, which, at global coordinate system, is described as:

$$\boldsymbol{T} = \mathrm{diag}(0, 0, T_{zz}) \tag{5.31}$$

As stated before, since the constitutive equations were derived in the local coordinate system, this stress should be transformed into the local coordinate system using

$$\boldsymbol{T}_c = \boldsymbol{A}_t \boldsymbol{T}_g \tag{5.32}$$

Then the elastic strain at local coordinate system can be calculated by using Hooke's law.

$$\varepsilon_c = \mathbb{C}^{-1} \boldsymbol{A}_t^{-1} \boldsymbol{T}_c \tag{5.33}$$

Finally transformation the strain to the global coordinate system again by using

$$\varepsilon_g = \boldsymbol{B}_t^{-1} \varepsilon_g = \boldsymbol{B}_t^{-1} \mathbb{C}^{-1} \boldsymbol{A}_t^{-1} \boldsymbol{T}_c \tag{5.34}$$

where A_t and B_t are transformation tensors, details of which are presented in Appendix A.

Based on the calculated elastic strain ε_e, the elastic deformation gradient can then be obtained as

$$F_e = \varepsilon_e + I \tag{5.35}$$

Knowing F_e and stress, the driving force can be calculated by using equation (5.18). Further D_{in} is calculated by using equation (5.26a), noting to solve the equation for D_{in}, the viscosity tensor $\mathbb{k}$ is needed to be prescribed. $\mathbb{k}$ is the directional viscosity during the creep deformation of Nickel based single crystal Superalloys.

$$D_{in} = \mathbb{k}^{-1}\left(A_{sys} - \frac{tr(\mathbb{k}^{-1}A_{sys})}{tr(\mathbb{k}^{-1}I)}I\right) \tag{5.36}$$

Since

$$L = \dot{F}F^{-1} \tag{5.37}$$

and

$$F = F_e G \tag{5.38}$$

an equation for L can be obtained by substituting F_e into L and simplifying to get

$$L = \dot{F}_e F_e^{-1} + F_e L_{in} F_e^{-1} \tag{5.39}$$

For the deformation described in this dissertation, $\boldsymbol{F}$ is a diagonal tensor. As a result $\boldsymbol{L}$ and $\boldsymbol{L}_{\text{in}}$ are also diagonal tensors. Thus the follow equation (5.40) is obtained

$$\boldsymbol{L}_{in} = \boldsymbol{D}_{in} \tag{5.40}$$

5.5 Conclusions

Creep is a complicated process. From the microscopic point of view, it is the diffusion of the vacancy/impurity and the movement of the dislocations. As there are no grain boundaries in nickel based single crystal Superalloy, diffusion is harder to take place. The principal mechanism can be regarded as movement of the dislocations. The theory of multiple natural configurations has been used successfully to describe a diverse class of material behavior. This framework uses the thermodynamic quantities, such as stored energy and dissipation, to describe the creep deformation. The connection between the macroscopic quantities and microscopic mechanism is developed by using the multiple natural configurations framework for the creep deformation of Nickel based single crystal Superalloys.

CHAPTER 6

PARAMETERIC STUDY

6.1 Introduction

An elastic solid and a viscous fluid are two extreme cases for ideal mechanics models. For an elastic solid, its natural configuration is its stress free state, i.e., $(\boldsymbol{T}=0, \boldsymbol{E}=0)$ and the relation between stress and strain are one to one. Also, for an elastic material, on unloading the material recovers its original shape and there is no energy dissipation. When loaded the material deforms and the external force does work during the deformation. This work is then stored in the material as the strain energy. When unloaded, the elastic material releases the stored strain energy by doing work on the surroundings. The amount of energy stored by the material and the amount released are identical. On the other hand for a viscous fluid, its current configuration is its natural configuration. It doesn't have the ability to recover the deformation and it dissipates energy.

A viscoelastic material is, as the name suggests, one which shows a combination of viscous and elastic effects, the relationship between stress and strain depends on time. All materials exhibit some degree of viscoelastic response. In common metals such as steel or aluminum, as well as in quartz, at room temperature and at small strain, the behavior does not deviate much from linear elasticity. Synthetic polymers, wood, and human tissue as well as metals at high temperature display significant viscoelastic effects. Viscoelasticity in metals is of interest in the context of fundamental understanding of microscopic processes and in the context of current or potential applications. Substantial

viscoelastic response in metals is commonly but not exclusively associated with high homologous temperature, $TH=\theta/\theta_{melting}=0.5$, with θ is the absolute temperature. Viscoelasticity considers in addition a dissipative phenomenon due to ''internal friction,'' such as between molecules in polymers or between cells in wood. The viscous term leads to energy dissipation and the elastic term to energy storage. Rate effects are very important for these materials.

It is generally agreed that the high-temperature background, which refers to the rapid increase in the damping of metals when the temperature is above about half of the homologous temperature is caused by a combination of thermally activated dislocation mechanisms.

Creep usually denotes a slow viscous flow of a solid under macroscopically non-zero stress, via atomic diffusion (through lattice or along grain boundary) and dislocation motion (glide or climb). The mechanism of creep depends on the composition of the material, its microstructural features, temperature and stress. For anisotropic materials the influence of material orientation is also significant. In this dissertation only the macroscopic factors will be considered, which are stress and orientation under isothermal conditions.

In Chapters 4 and 5 the constitutive equations were derived and the related techniques were also described. As it was stated, the creep deformation is highly dependent on the viscosity tensor $\mathbb{k}$, which is a fourth order tensor and can be expressed as functions of the components i, j and k. But no detailed information was given. In section 6.2 the explicit expression of i, j and k is derived and thus completing the formulation of the viscosity tensor $\mathbb{k}$. In section 6.3, the focus is on the relation between directional viscosity and strain strength. The relation between strain strength and strain

rate is given in the section 6.4. The relation of strain and strain rate is described in subsection 6.5. Section 6.6 contains the simulation and predication of the creep process.

6.2 The Directional Viscosity Tensor

Viscosity is the resistance a material has to change in form. This property can be thought of as an internal friction. As stated before, in linear viscoelasticity viscosity is a constant while in the nonlinear behavior it depends on the mechanism of the deformation and can be regarded as a function of activation volume, stress, strain, strain rate, time, temperature, material nature etc., factors that affects the creep life for a specific material under working condition. In a three dimensional case the viscosity can be expressed as a tensor.

6.2.1 Relationship between Viscous Stress and Strain/Strain Rate

In the theory of continuum mechanics, Malvern (1964) studied the viscosity of the isotropic viscous material behavior. The relationship between stress and strain rate is expressed as

$$\boldsymbol{T} = \mathbb{k}\boldsymbol{D} \tag{6.1}$$

where $\boldsymbol{T}$ is the viscous stress tensor, $\boldsymbol{D}$ is the strain rate tensor, $\mathbb{k}$ is the 4^{th} order viscosity tensor.

For an isotropic material the viscosity tensor can be presented as

$$\mathbb{k} = (k - 2\mu/3)\boldsymbol{II} + \mu(\boldsymbol{I} \otimes \boldsymbol{I}) \tag{6.2}$$

where k and μ are bulk and shear viscosity, respectively, and $\boldsymbol{II}$ and $\boldsymbol{I} \otimes \boldsymbol{I}$ are unit tensor for 2nd and 4th order tensors, respectively, $\otimes$ is the dyad of two tensors. Equation (6.2) is the standard Navier-Stokes equation.

The total stress and strain rate can be decomposed into a spherical stress $\boldsymbol{T}^{\mathrm{M}}$ and a deviatoric stress $\boldsymbol{T}^{\mathrm{D}}$.

$$\begin{aligned} \boldsymbol{T} &= T^{\mathrm{M}}\boldsymbol{I} + \boldsymbol{T}^{D} \\ \boldsymbol{D} &= D^{M}\boldsymbol{I} + \boldsymbol{D}^{D} \end{aligned} \tag{6.3}$$

where $T^{\mathrm{M}} = (tr(\boldsymbol{T})/3)$ and $D^{\mathrm{M}} = (tr(\boldsymbol{D})/3)$.

Substituting equation (6.2) into equation (6.1) and using equation (6.3), the following equations are obtained,

$$\begin{aligned} T^{M}\boldsymbol{I} &= k\boldsymbol{D}^{M}\boldsymbol{I} \\ \boldsymbol{T}^{D} &= 2\mu\boldsymbol{D}^{D} \end{aligned} \tag{6.4}$$

Alternatively, bulk viscosity is a function of the first stress and strain rate invariants, shear viscosity is a function of the second invariant of the stress and strain rate.

Li and his coworkers (1999) further proposed that both bulk and shear viscosities can be the functions of stress and strain invariant J_{T} and J_{E}. It is assumed that the variables in the viscous parameters can be independent from each other, and are able to be expressed by the product of two independent functions.

$$
\begin{aligned}
k &= k_0 (J_{T1})^{u_1} k_1 (N)^{u_2} k_2 (J_{E1})^{u_3} \\
\mu &= \mu_0 (J_{T1})^{v_1} \mu_1 (N)^{v_2} \mu_2 (J_{E2}^D)^{v_3}
\end{aligned}
\tag{6.5}
$$

where J_{T1} is the first invariant of stress, J_{E1} and J_{E2}^D are the first strain invariant and second deviatoric strain invariant, N is the repetition number of cyclic load, u_i (i=0,…,3) and v_i (i=0,…,3) are the power order for different terms, respectively.

Bertram and Olschewski (1996) present a one dimensional nonlinear rheological model based on a four-parameter Burgers model. In this model, the viscosity was regarded as a function of the stress. Although the creep behavior is strongly non-linear, the viscosity was still regarded as a constant during the deformation process. Based on the one dimensional model the authors further generalized it to a three dimensional model. Qi and Bertram (2000) developed a viscoplasticity damage model for single crystal Superalloy SRR99 at temperature of 760°C. In this model 5 material tensors need to be determined, all of them are dependent on the viscosity, which is a function of stress invariants, $\Delta_1, \Delta_2, \Delta_3$ and Δ_4 defined as follows:

$$
\begin{aligned}
\Delta_1 &= \sqrt{T_{11}T_{22} + T_{22}T_{33} + T_{33}T_{11}} \\
\Delta_2 &= T_{12}^2 + T_{23}^2 + T_{31}^2 \\
\Delta_3 &= T_{11}T_{22}T_{33} \\
\Delta_4 &= T_{11}(T_{12}^2 + T_{13}^2) + T_{22}(T_{23}^2 + T_{21}^2) + T_{33}(T_{31}^2 + T_{32}^2)
\end{aligned}
\tag{6.6}
$$

6.2.2 Interpretation of the Directional Viscosity Tensor

6.2.2.1 Directional Viscosity at High Temperatures. As stated in section 6.2.1, viscosity for creep in different materials can be regarded as a function of stress and/or strain invariants depending on the material and the nature of deformation. In creep deformation of single crystal Superalloy CMSX-4, the directional viscosity is defined as a function depending on both first stress invariant and nominal strain strength $\bar{\varepsilon}$, which is defined as,

$$\varepsilon_r = \frac{\sqrt{6}}{4}\bar{\varepsilon} \tag{6.7}$$

where $\bar{\varepsilon}$ is called the shear strain strength and defined as (Kachanov, 1971),

$$\bar{\varepsilon} = 2\sqrt{\left|\boldsymbol{E}_{II}^{d}\right|} \tag{6.8}$$

The physical meaning of $\bar{\varepsilon}$ is the following: it is a quantity that represents of the distortion in shape of an element of the medium. $\boldsymbol{E}_{II}^{d}$ is the second invariant of the strain deviator and is defined as

$$\begin{aligned} \boldsymbol{E}_{II}^{d} &= \frac{1}{2}((trace(\boldsymbol{E}))^2 - trace(\boldsymbol{E}^2)) - \boldsymbol{E}_v \boldsymbol{I} \\ \boldsymbol{E}_v &= \frac{1}{3} trace(\boldsymbol{E}) \end{aligned} \tag{6.9}$$

With these models as a background in this work, the expression of directional viscosity of creep in Nickel based single crystal Superalloy is defined as, $\mathbb{k} = \mathbb{k}(\boldsymbol{T}_I, \boldsymbol{E}_{II}^d)$. The specific form chosen for the directional viscosity components is,

$$\begin{aligned} i &= i_1(\boldsymbol{T}_I) i_2(\boldsymbol{E}_{II}^d) \\ j &= j_1(\boldsymbol{T}_I) j_2(\boldsymbol{E}_{II}^d) \\ k &= k_1(\boldsymbol{T}_I) k_2(\boldsymbol{E}_{II}^d) \end{aligned} \tag{6.10}$$

where $i_1 \sim i_2$, $j_1 \sim j_2$, $k_1 \sim k_2$ are material constants to be determined.

In the study of anisotropic nickel based single crystal Superalloys, the viscous components *i, j* and *k* are independent with each other, and this nature is decided by the FCC crystal structure. The final expression chosen for *i, j, k* are as follows:

$$\begin{aligned} i &= \alpha_1 (tr\boldsymbol{T})^{\alpha_2} \varepsilon_r + (\alpha_3 tr(\boldsymbol{T}) + \alpha_4) \\ j &= \beta_1 (tr\boldsymbol{T})^{\beta_2} \varepsilon_r + (\beta_3 tr(\boldsymbol{T}) + \beta_4) \\ k &= \gamma_1 (tr\boldsymbol{T})^{\gamma_2} \varepsilon_r + (\gamma_3 tr(\boldsymbol{T}) + \gamma_4) \end{aligned} \tag{6.11}$$

where $\alpha_1 \sim \alpha_4$, $\beta_1 \sim \beta_4$ and $\gamma_1 \sim \gamma_4$ are material constants and can be obtained by calibrating with experimental data results. Figure 6.1 shows the curve fitting results at 950°C at different orientations and stress levels.

6.2.2.2 Directional Viscosity at Low Temperature. From above discussion it is clear that at a temperature of 950°C, the parameters *i, j* and *k* depend upon the stress level at any orientation. At <001> orientation, directional viscosity depends only on i and j, and i/j changes with both temperature and stress.

The situation changes significantly when study the creep at low temperature and high stress level. The curve of strain vs. time is totally different from that at high temperature. The parameters can no longer be described using equation (6.11), and the relations between i, j with ε_r are no longer linear. The new relationship is now expressed in equation (6.12):

$$\begin{aligned} i &= i_1 \exp(i_2 \varepsilon_r)^{i_3} + i_4 \varepsilon_r \\ j &= j_1 \exp(j_2 \varepsilon_r)^{j_3} + j_4 \varepsilon_r \\ k &= k_1 \exp(k_2 \varepsilon_r)^{j_3} + k_4 \varepsilon_r \end{aligned} \tag{6.12}$$

Where $i_1 \sim i_4$, $j_1 \sim j_4$, $k_1 \sim k_4$ are material constants to be determined.

The following are the fitting curves obtained by using equation (6.11) for high temperature (Figure 6.1 and Figure 6.2) and equation (6.12) for low temperature (Figure 6.3). It can be seen that the simulation results match well with the available experimental data at 950°C (Duncan et al. 2001), 982°C and 1000°C (Henderson, et al. 1997), and 750°C (Svoboda, et al. 1998).

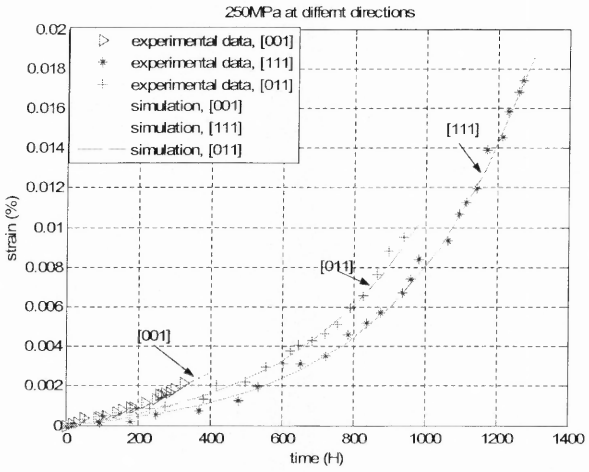

(a)

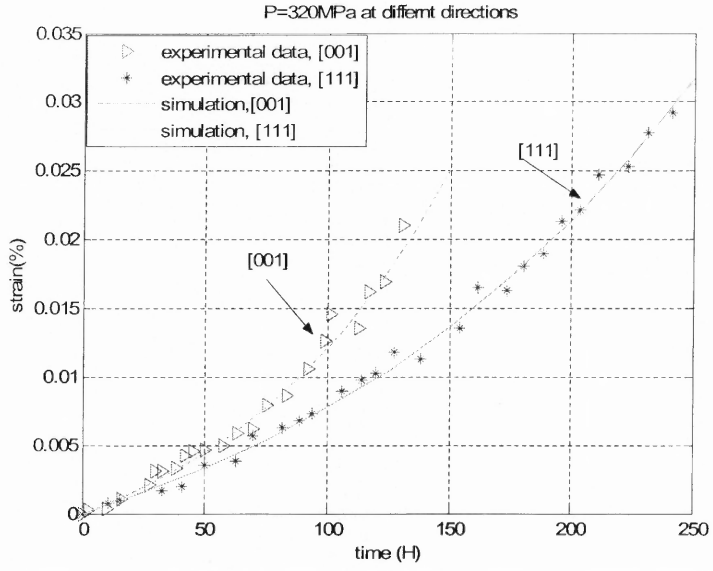

(b)

Figure 6.1 Simulation results (a) 950°C different directions at 250Mpa; (b) 950°C different directions at 320MPa (Experimental data from Duncan et al. 2001).

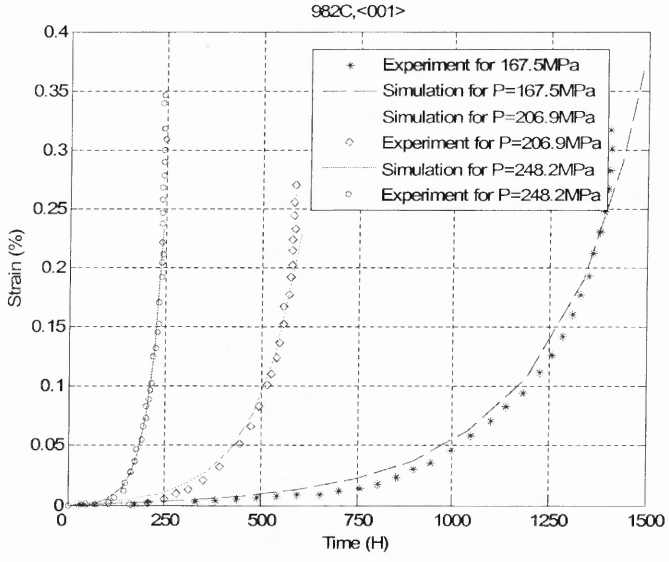

(a)

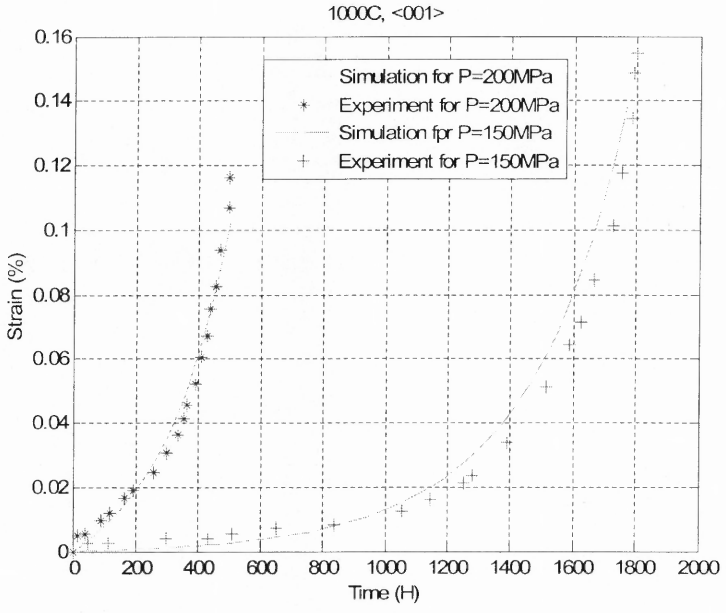

(b)

Figure 6.2 Simulation results (a) 982°C (b) 1000°C at <001> directions at different load Conditions (Experimental data from Henderson, et al. 1997).

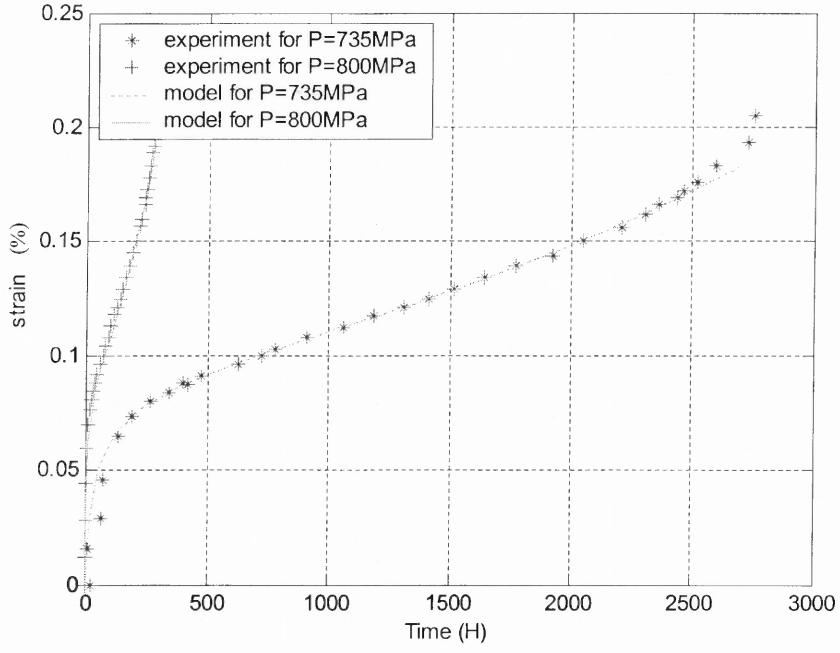

Figure 6.3 Strain changes with time for CMSX-4 at 750°C (Experimental data from Svoboda, et al. 1998).

6.3 Relation of Directional Viscosity on Strain Strength

Relation of directional viscosity with strain strength is discussed in this section and the discussion is based on different directions and temperatures.

6.3.1 At <001> Orientation at Different Temperatures

Study of the directional viscosity in the <001> orientation at different temperature is described in this subsection.

6.3.1.1 High Temperature. At the <001> direction and high temperatures, 950°C and 1000°C, it is clear that viscosity components i, j and k increase with strain strength linearly (Figure 6.4a and Figure 6.5a). At the same time, component i and j seems insensitive to the stress while component k does show a dependence, with an increase in the stress, k increases.

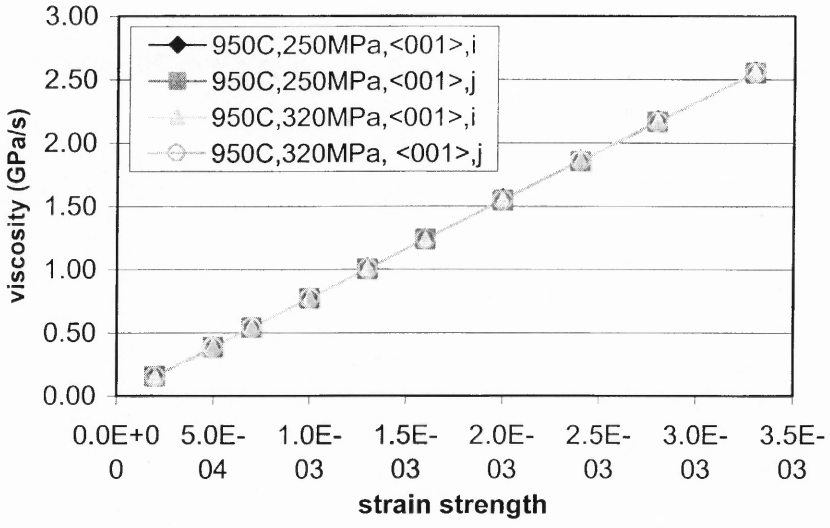

(a)

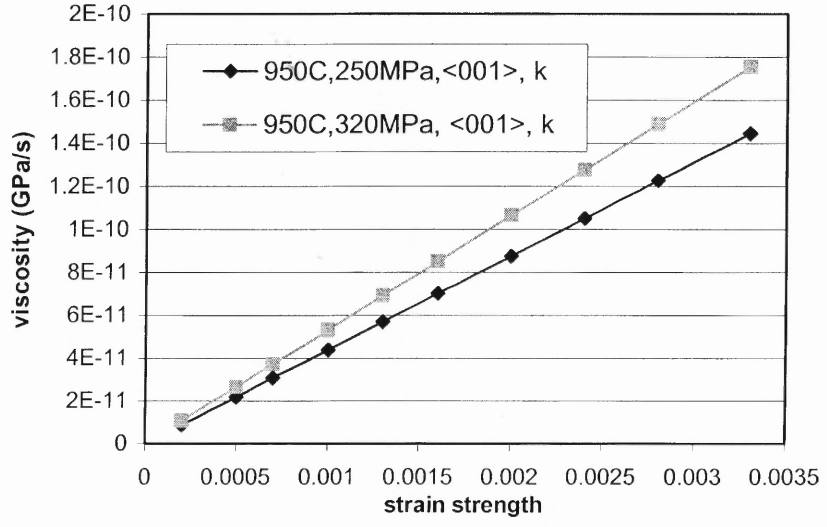

(b)

Figure 6.4 Directional viscosity versus strain strength at 950°C, <001> direction (a) viscosity component i and j (b) viscosity component k.

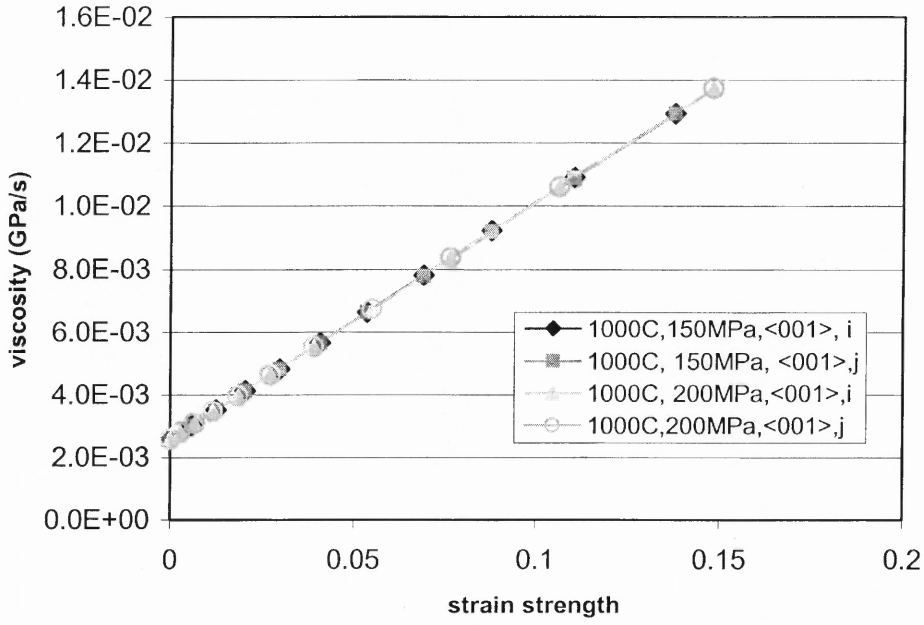

(a)

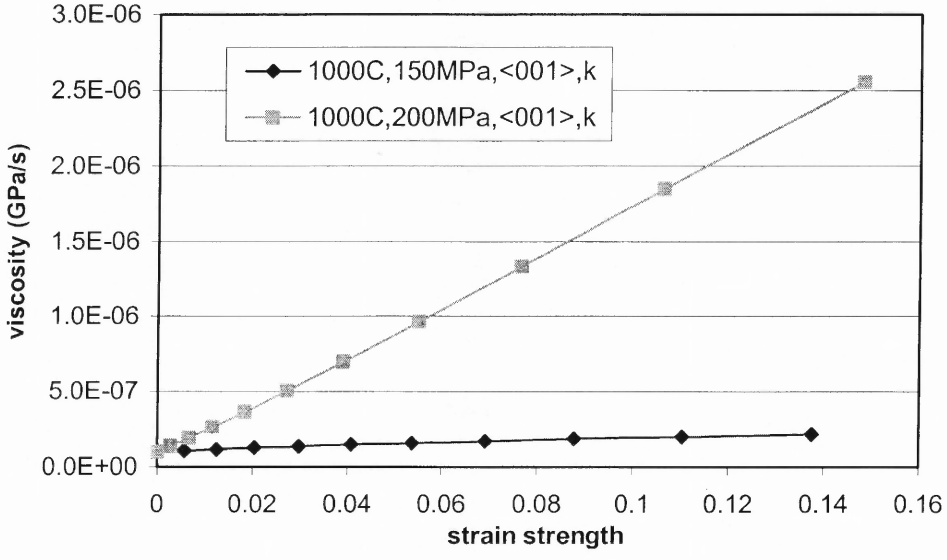

(b)

Figure 6.5 Directional viscosity versus strain strength at 1000°C (a) viscosity component i and j (b) viscosity component k.

6.3.1.2 At Low Temperature and High Stress. At the low temperature of 750°C, the relationship of directional viscosity with strain strength is plotted in the following figures (Figure 6.6).

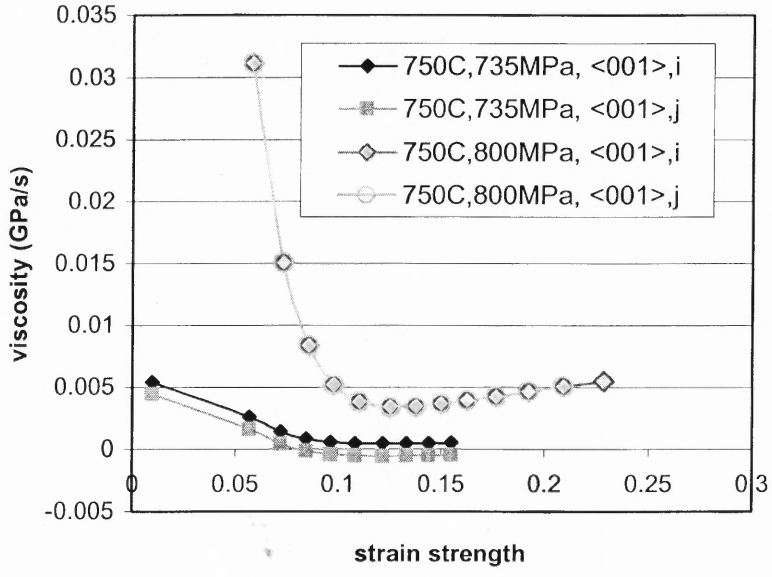

(a)

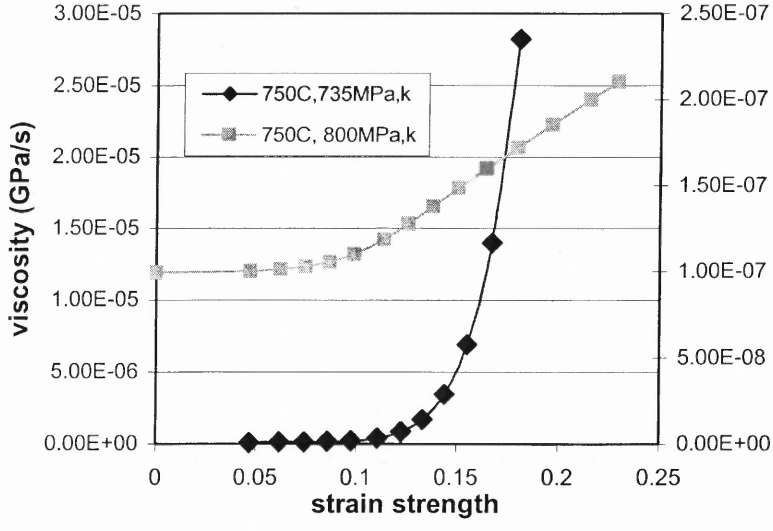

(b)

Figure 6.6 Directional viscosity versus strain strength at 750°C (a) viscosity component i and j (b) viscosity component k.

Figure 6.6 is the plot of directional viscosity change with strain strength at 750°C. Clearly, relationship between viscosity components and strain strength is much complicated than at high temperatures. Components *i* and *j* are no longer linear (Figure 6.6a), which implies that the mechanism of the deformation is not the same as high temperature, as described by Svoboda and Lukas (1997). At the same time, the viscosity components are sensitive to the stress which is different from the high temperature range. At either 735 MPa or 800 MPa, with an increase in strain strength, the viscosity decreases, although the extent of decrease is different. It seems at lower stress levels the viscosity decreases faster than at higher stress levels. Plot (b) depicts the change of the viscosity component *k* with strain intensity. At both stress levels, the viscosity component *k* increases with strain intensity; however the increase is not linear.

As stated above, viscosity characterizes the resistance of a material to change in shape and the strain strength represents the distortion of the material. For one dimensional deformation, it is easy to understand that as the material deforms, it becomes stiffer. This will lead to an increase in the viscosity. For three-dimensional deformations with anisotropic material properties, considering the deformation compatibility, the viscosity dependence on strain strength becomes much more complicated.

At high and low temperatures, the tendency of *i, j, k* changes with strain strength very differently. Comparison at high temperatures indicates that, viscosity components *i/j* and *k* have a similar tendency; at low temperatures, viscosity components *i/j* and *k* have significantly different behavior. This difference is a result of material anisotropy and can be explained by metallurgy theory. At low temperatures dislocation movements are strictly limited to fixed directions according to the corresponding maximum resolved shear stress. Diffusion plays no role at these temperatures. While at high temperatures,

more slip systems can be activated thus leading to more directions along which the dislocation can move. This reduces anisotropy in the deformation. More importantly, at high temperature atom vibrations become faster and with larger amplitude, these active the diffusion mechanism. This random diffusion can also reduce the deformation anisotropy.

6.3.2 Dependence of Directional Viscosity with Strain Strength in Other Directions

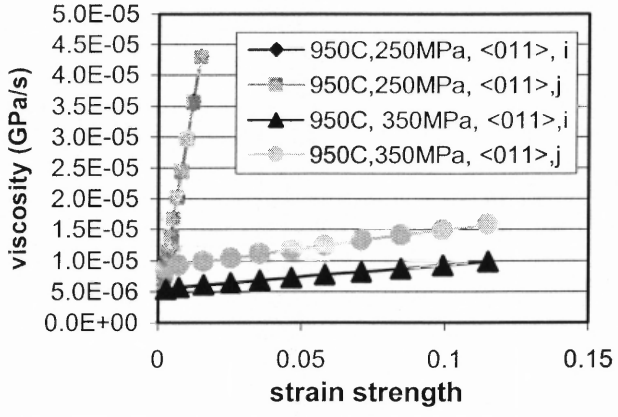

(a)

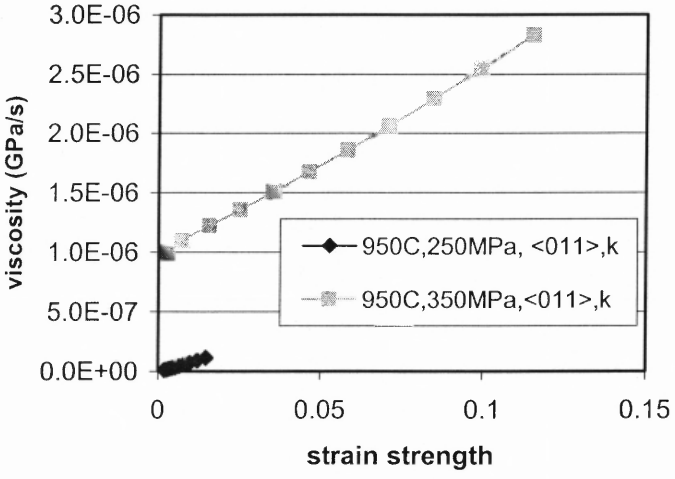

(b)

Figure 6.7 Directional viscosity versus strain strength at 950°, <011> orientation (a) viscosity component *i* and *j* (b) viscosity component *k*.

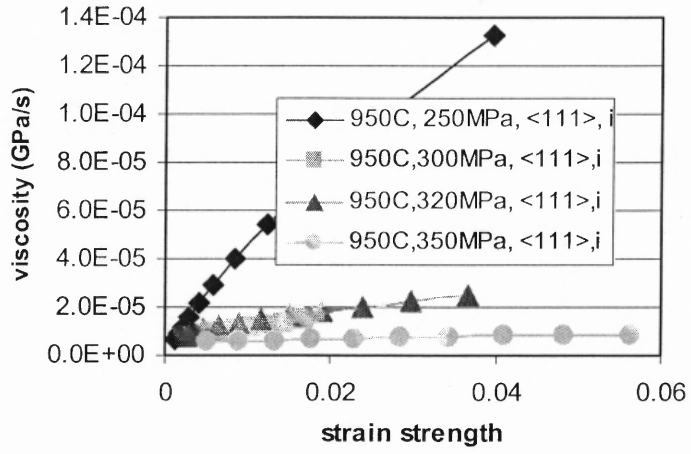

(a)

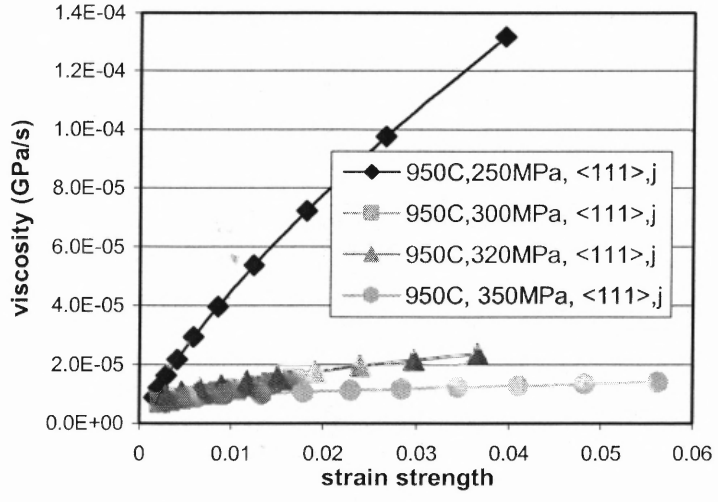

(b)

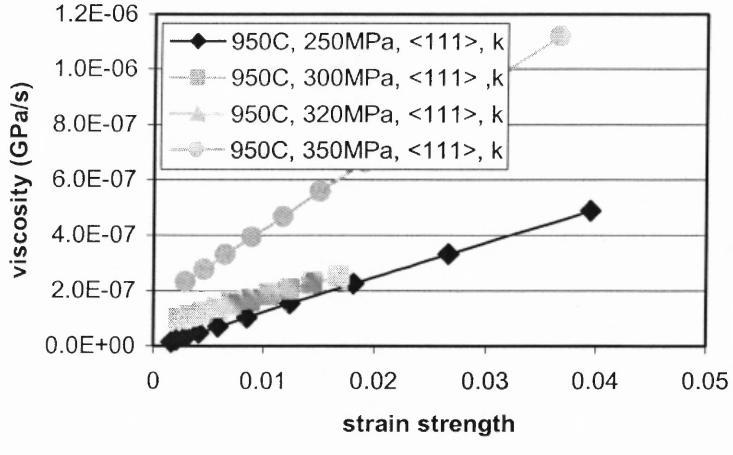

(c)

Figure 6.8 Directional viscosity versus strain strength at 950°C, <111> orientation (a) viscosity component i, (b) viscosity component j, (c) viscosity component k.

Figure 6.7 and Figure 6.8 show the dependence of directional viscosity on strain strength along <011> and <111> directions. It is clear that at any direction and stress level, the viscosity components increase linearly with strain strength and have the same tendency.

In the high temperature regime, the viscosity components change linearly with the nominal strain strength in any directions and stress levels. While at lower temperature (750°C) the behavior is different. This change reflects two main aspects: viscosity change with nominal strain is nonlinear; stress has a more significant influence at higher temperatures.

6.4 Strain Strength and Strain Rate

Strain rate has significant effects on material properties. Generally, very high strain rate ($100s^{-1}$~$1000s^{-1}$) will lead to sudden failure of materials and structures, such as in an impact event. At low strain rate level of $10^{-1}s^{-1}$~$10^{-3}s^{-1}$, especially for creep, very few literatures are available.

6.4. 1 The <001> direction

In the <001> orientation, strain rate increases with strain strength in the high temperature regime. But the tendency is not the same for 950°C and 1000°C. At 950°C (Figure 6.9) strain rate changes with strain strength linearly; while at 982°C and 1000°C (Figure 6.10 and Figure 6.11), the trend is nonlinearly. One of the important reasons is that at higher temperature (982°C and 1000°C) the total strain is much bigger than that at lower temperatures.

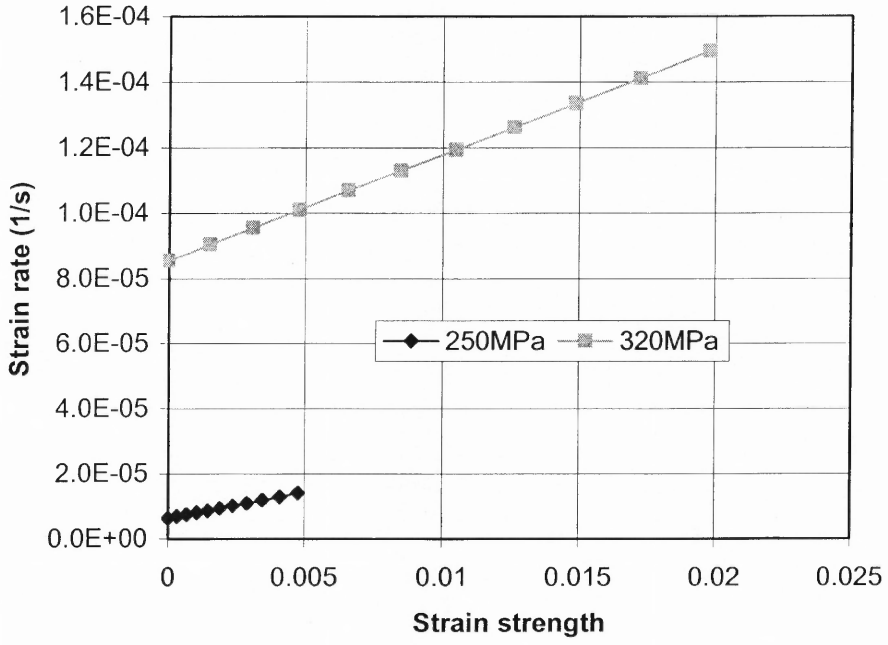

Figure 6.9 Strain strength with strain rate at 950°C, <001> orientation.

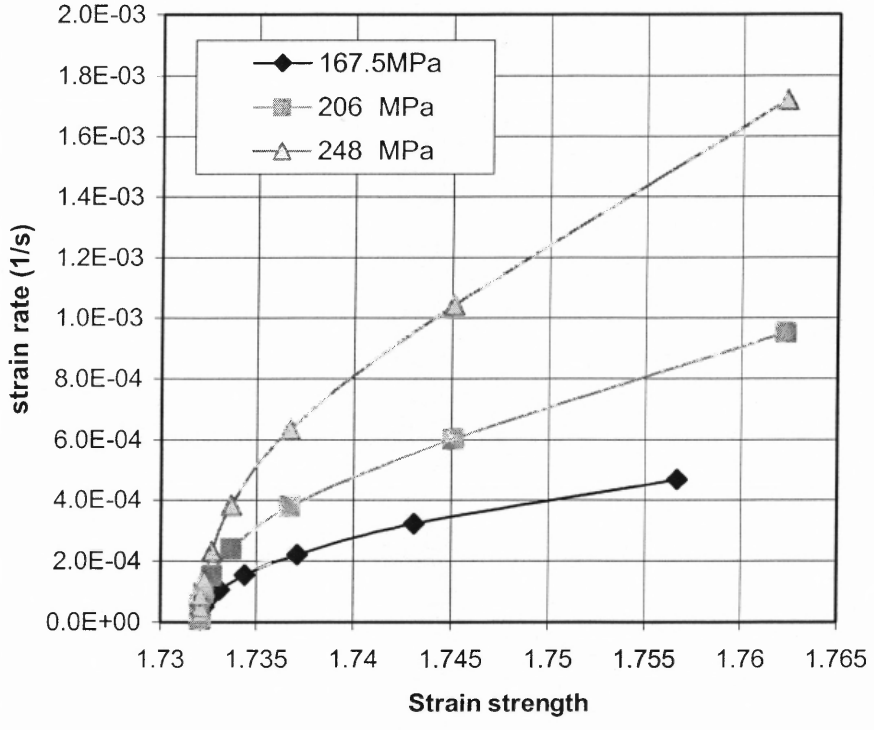

Figure 6.10 Strain strength with strain rate at 982°C, <001> orientation.

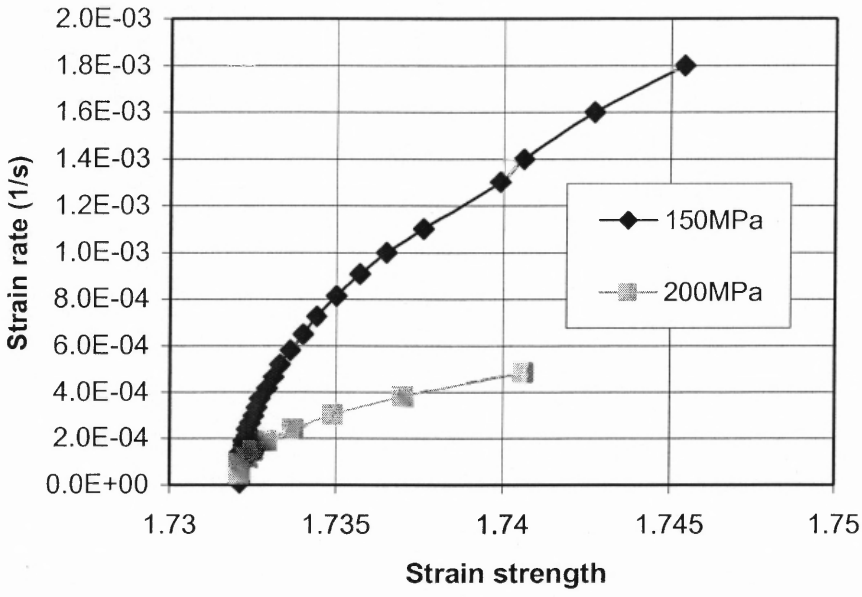

Figure 6.11 Strain strength with strain rate at 1000°C, <001> orientation.

6.4.2 In Other Directions

At 950°C, <011> and <111> directions, the stain strength is linear with strain rate as shown in Figure 6.12 and 6.13.

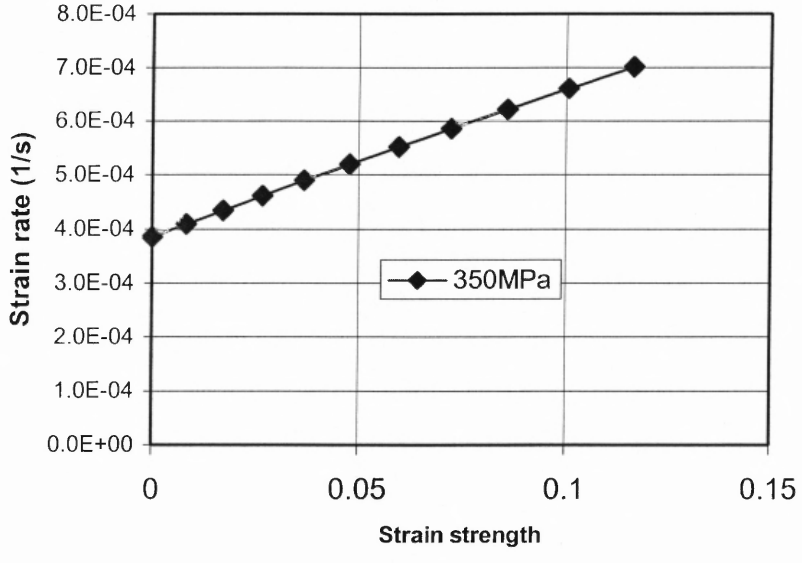

Figure 6.12 Strain strength with strain rate at 950°C, <011> orientation.

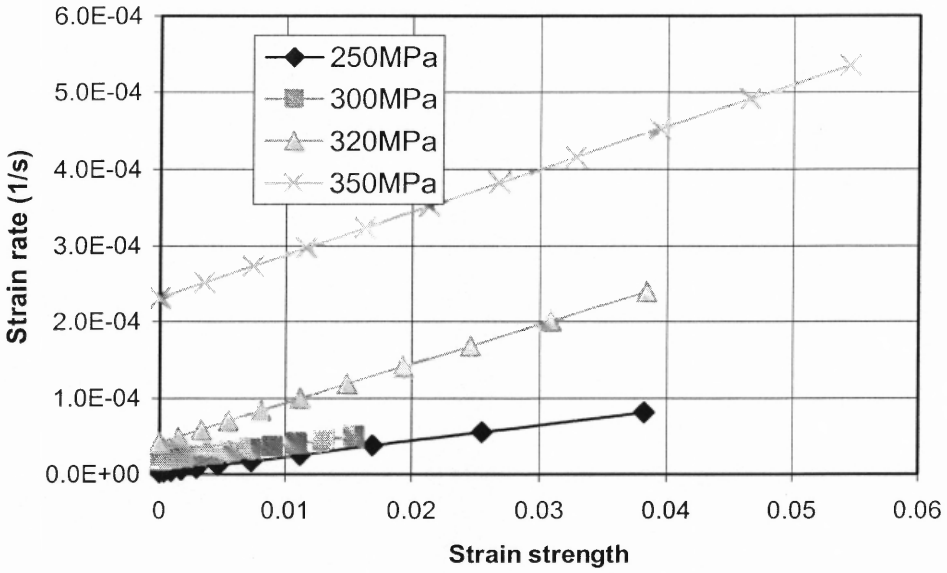

Figure 6.13 Strain strength with strain rate at 950°C, <111> orientation.

6.5 Nature of the Strain and Strain Rate

As described before, viscosity is a function of stress and strain; this captures the macroscopic characteristics of the viscosity property, as it varies with creep. In fact, this relation also reflects the underlying microscopic change that influences creep deformation.

In the following subsection a detailed description is given on the relationship between the viscosity and microscopic aspect of creep deformation.

Strain is the accumulation of deformation and includes elastic and inelastic strains. Elastic strain can be recovered when the load is released while inelastic deformation can't be recovered even after the load is released. The inelastic strain is caused by the movement of dislocations, which has a close relationship with inelastic

strain rate. It is well known that strain rate can be obtained by differentiating strain (as long as strain is small). In other words strain can be transformed to strain rate easily. The relationship between strain rate and the movement of dislocations is given by the Orowan equation (1954)

$$\dot{\varepsilon} = \rho b v \tag{6.13}$$

where $\dot{\varepsilon}$, ρ, b and v are strain rate, dislocation density, Burger's vector and average dislocation movement rate. Burger's vector describes the displacement direction or slip direction characterizing a particular dislocation. For an edge dislocation moving along its slip direction, the Burger's vector is usually one lattice spacing (Honeycombe, 1984), although this may change for dislocation climbing. Burger's vector can still be expressed by a lattice constant. For simplification, a constant Burger's vector is selected and attention is paid to the dislocation density and velocity.

Strain rate is a critical factor in the inelastic deformation. Usually two competitive processes take place during the inelastic deformation: hardening and softening. The hardening is caused by an increase in the internal energy of the metal/alloy due to the production of dislocation lines, and softening is attributed mainly to the thermally activated relaxation processes. Since the latter is time dependent, the effect of strain rate is such that the deformation processes at low strain rates experience more of it and thus metals/alloys are expected to go through softening. According to the different strain rates, the deformation mechanism change. For higher strain rates there is almost no softening taking place. While at lower strain rate process, (such as creep), the hardening is not significant. The reason behind it is that the deformation mechanisms are different at low

and high strain rates and the strain rate is related to the dislocation density and dislocation velocity by Orowan's equation, which describes the deformation from the microscopic point of view. Furthermore, according to the Orowan's equation, using known values of the material parameters, the dislocation density can be predicted using the model provided.

Burger's vector is the unit of the dislocation. Usually it is determined by the crystal lattice constants. If crystals are oriented in an orderly way, a strong plastic anisotropy can develop in the material. If crystals are oriented randomly one would expect the effect of the difference in the Burger's vector to superpose, so that an effectively constant Burger's vector can be obtained and no anisotropy occurs. Ashby and Verrall suggest a mean burger's vector of 6 Å according to the burger's vectors at different glide planes, b=5.98 Å at [001] plane, b=4.76 Å at [100] plane, b=10.2 Å at [010] plane.

While for FCC material, such as Nickel based single crystal Superalloys, the crystal lattice constants are all the same, a=0.358 Å, in the three crystal directions, say, [001], [010], and [100]. However the Burger's vectors can have different values, either the lattice constant or half of the lattice constant, depending on which slip system is active. Similarly with Ashby and Verrall (1978), the burger's vector for CMSX-4 material can be around 0.179 Å.

Another factor that should be considered is the dislocation velocity. It is clear that during the creep deformation, the velocity of dislocation will change over time. Von Grossmann and his coworkers (Von Grossmann, et al. 2000) proposed a range of velocities of the dislocation according to the experimental data, which can be from 10^{-9}~10^{-3} m/s.

The following are some predictions of the dislocation density change with strain (Figure 6.14 and Figure 6.15). At high temperature along <001> direction, dislocation density increases with the increase of strain. However at same strain the dislocation density saturates. This is the expected behavior.

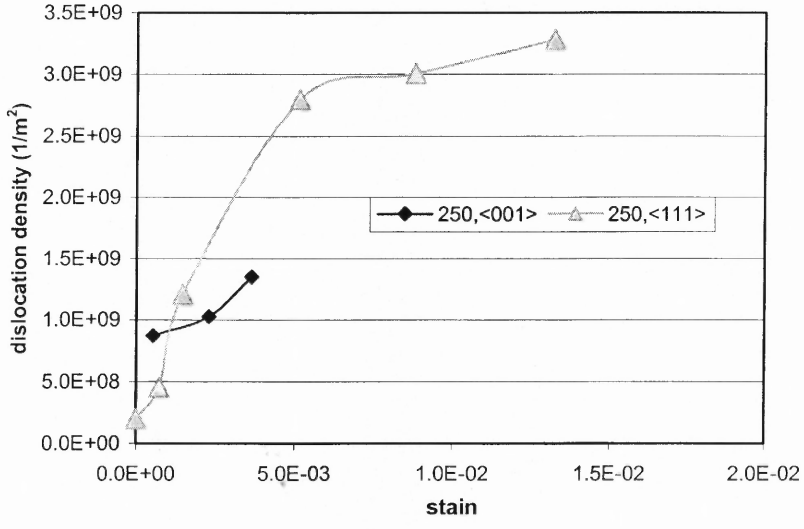

Figure 6.14 Prediction of dislocation density change with strain at 250 MPa.

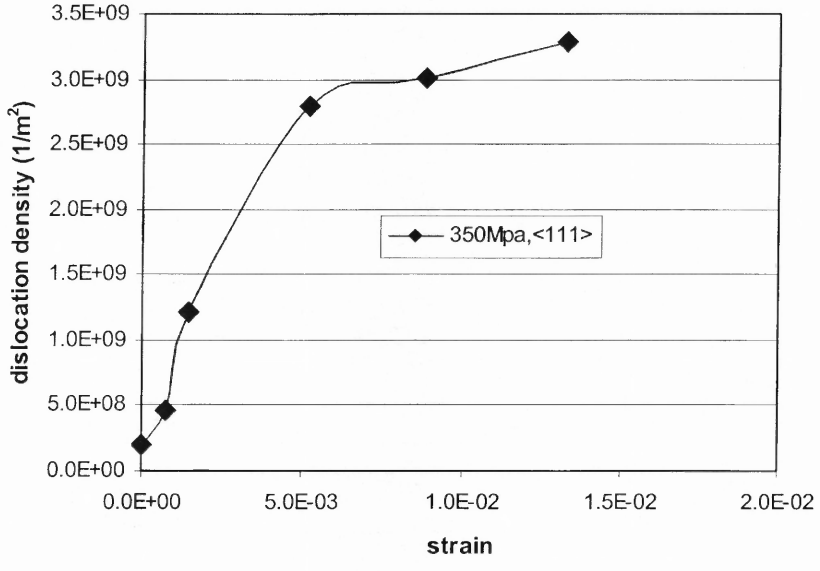

Figure 6.15 Prediction of dislocation density change with strain at 350 MPa.

6.6 Simulation and Predictions

Using the parametric study results to validate the experimental data, strain vs. strain rate curves are shown in Figures 6.16 to 6.19. It is clear that the simulation results have a good agreement with the experiment data. Figure 6.20 is the prediction of the creep curves for different stress/orientation and temperature. It is clear that the simulation results agree reasonably well with the experimental data. At the same time it shows the correct behavior, with an increase in stress, the creep life decreases, as described in Chapter 1.

Agreement between the analytical and experimental results for a wide range of time tends to support the representation of the model.

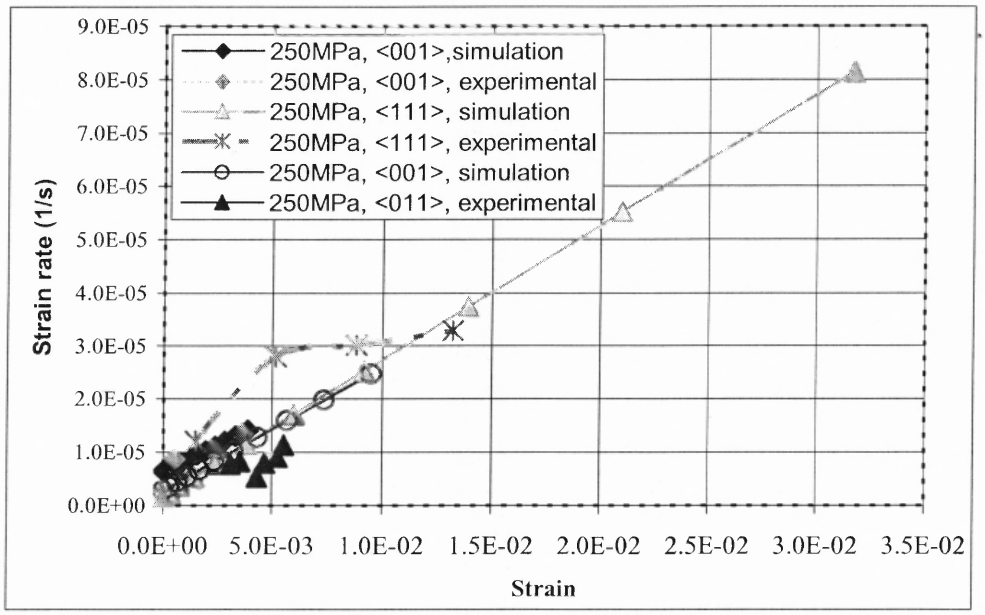

Figure 6.16 Strain versus strain rate at 950°C, 250 MPa, at <001>, <111> and <011> directions (Experimental data from Duncan et al. 2001).

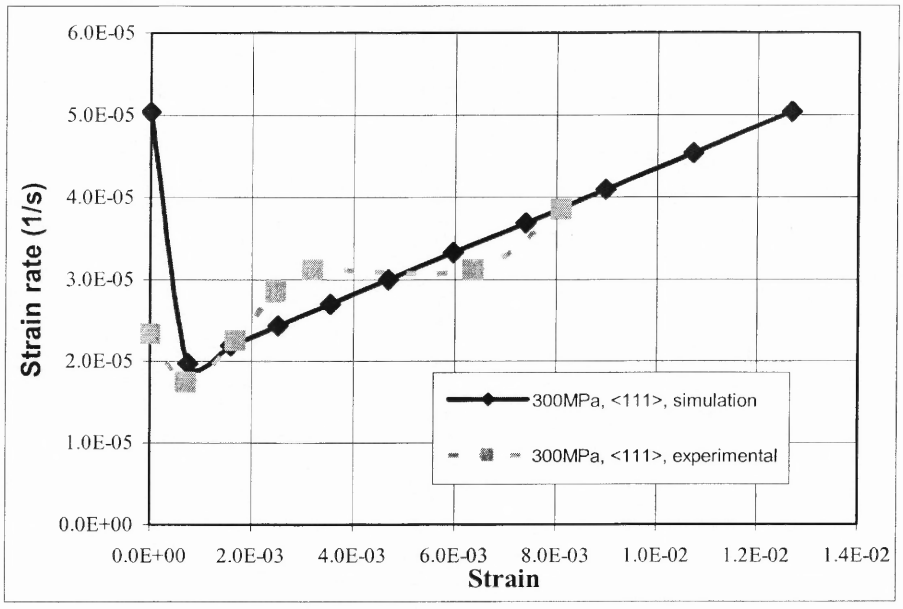

Figure 6.17 Strain versus strain rate at 950°C, 300MPa, at <111> direction (Experimental data from Duncan et al. 2001).

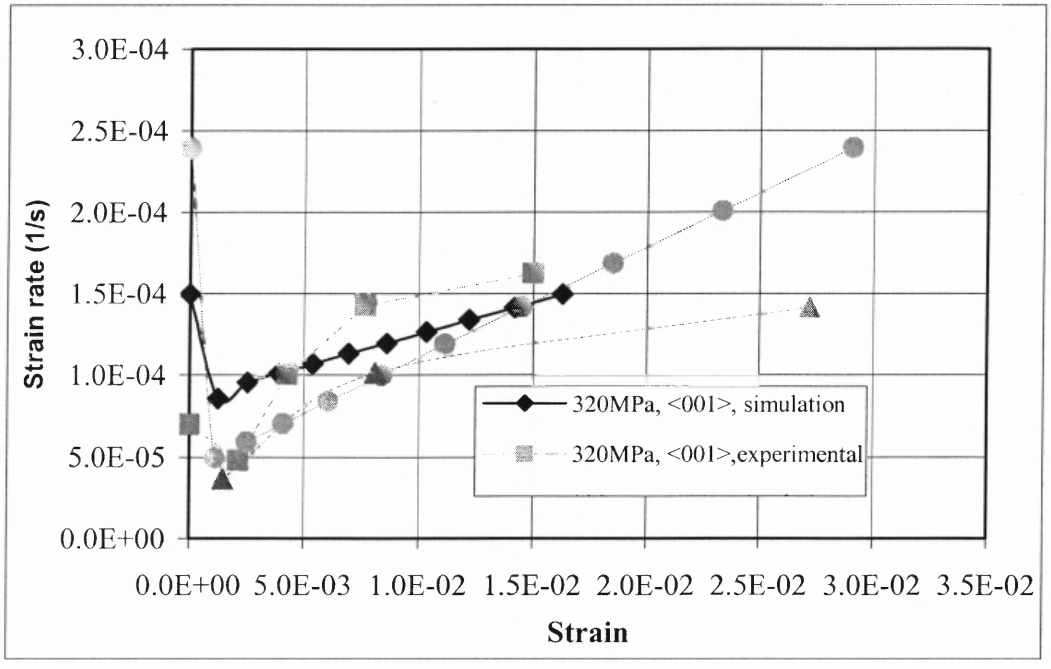

Figure 6.18 Strain versus strain rate at 950°C, 320MPa, at <001> and <111> directions (Experimental data from Duncan et al. 2001).

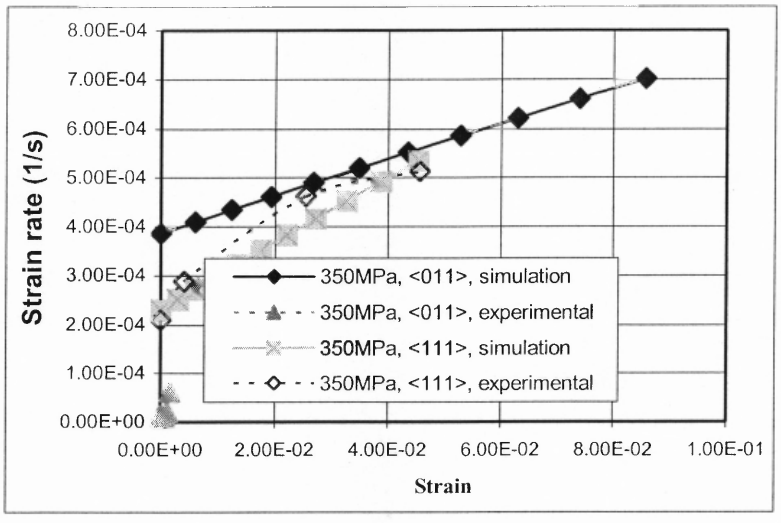

Figure 6.19 Strain versus strain rate at 950°C, 350Mpa, at <001> and <111> directions (Experimental data from Duncan et al. 2001).

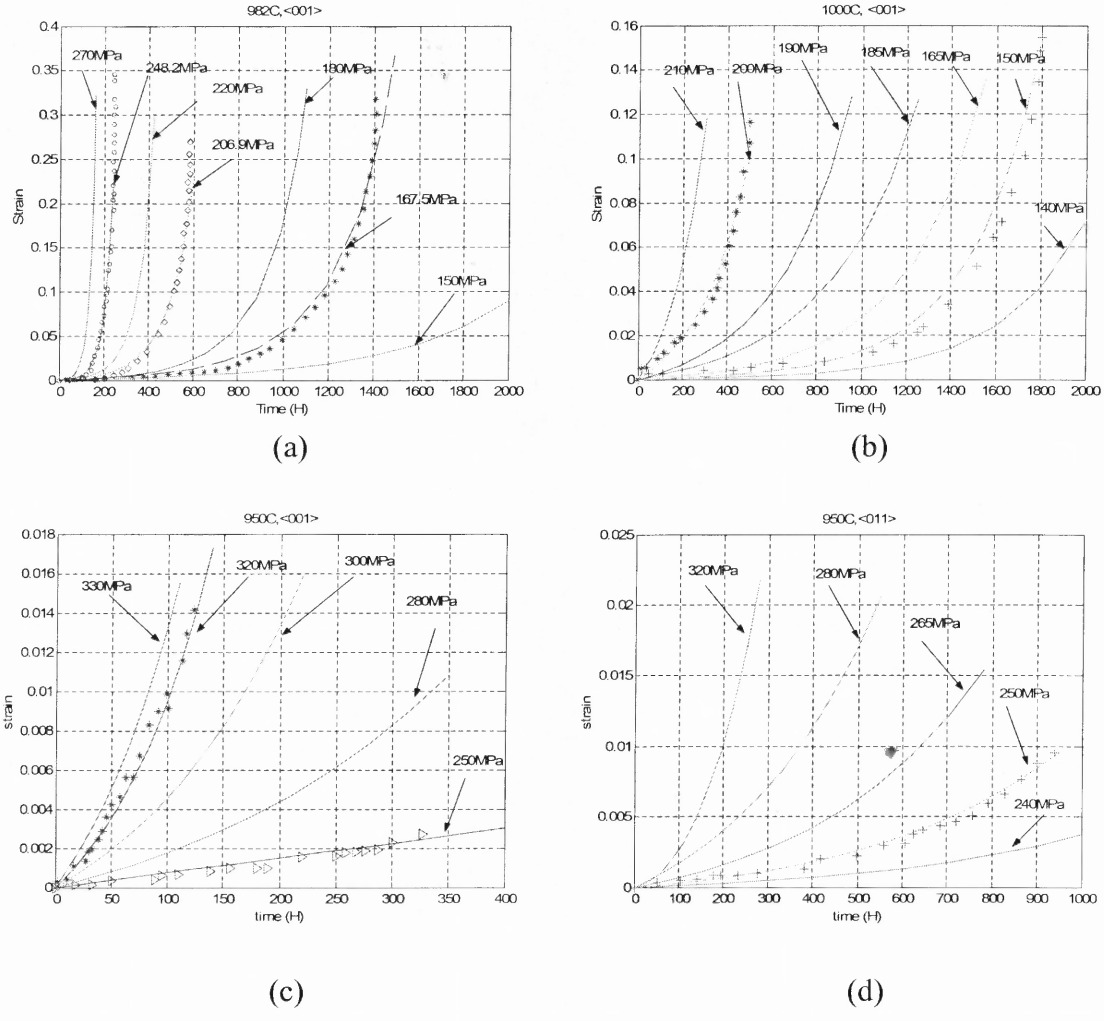

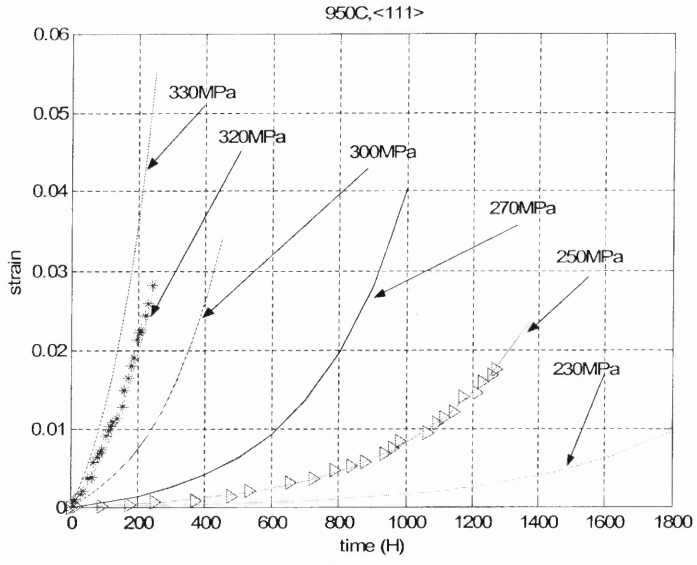

(e)

Figure 6.20 Prediction of creep life at different temperatures (a) 980°C at <001> direction; (b) 1000°C at <001> direction; (c) 950°C at <001> direction; (d) 950°C at <011> direction; (e) 950°C at <111> direction (Experimental data of 950°C from Duncan et al. 2001; Experimental data of 980°C and 1000°C from Henderson, et al. 1997).

Material parameters used in the simulation are listed in Table 6.1 and Table 6.2

Table 6.1 Material Constant for Creep at High Temperature

	Material constant for high temperature
α_1	1.1687E+007
α_2	-4.012
α_3	7.9939E-008
α_4	0.8103
γ_1	5.5337E-10
γ_2	1.8228
γ_3	2.0421e-41
γ_4	13.623

Table 6.2 Material Constant for Creep at Low Temperature of 750°C

	Material constant for low temperature	
	735MPa	800MPa
i_1	3.0E-2	1.8E-1
i_2	-3.23E-2	-3.23E-2
i_3	1.6	1.6
i_4	5.89E-6	2.4E-2
j_1	2.9996E-2	1.7997E-1
j_2	-3.23E-2	-3.23E-2
j_3	1.6	1.6
j_4	2.27E-6	2.16E-5

6.7 Conclusions

Directional viscosity is a key factor which will affect the creep life. In this chapter the representation of the directional viscosity is given. It is a real-time parameter which changes with strain strength and stress.

Directional viscosity is a function of the strain and stress invariants in this dissertation. This is based on the theory of continuum mechanics and modified for the model purposed here. The expressions of the components for the directional viscosity are deduced and are given in this chapter for both high and low temperature at different orientations. Material constants are calibrated from the experiments.

The relationship among directional viscosity, strain strength, strain rate are plotted. Prediction of the creep is also plotted. This model can give a good prediction at different temperature and orientation under consideration.

CHAPTER 7

FINITE-ELEMENT METHOD AND SIMULATION RESULTS

7.1 Introduction

The finite element method is a numerical procedure for analyzing structures and continua. Usually the problem addressed is too complicated to be solved satisfactorily by classical analytical methods.

In this chapter, the finite element implementation of the previously developed anisotropic constitutive model is discussed. The general procedure to integrate the inelastic rate equation is first reviewed. Two main algorithms, i.e., the forward Euler and backward Euler integration methods are explained. The procedure to implementation material constitutive model into a commercial finite element program ABAQUS/STANDARD is discussed. To verify the constitutive model, strain-time curves are plotted and compared with experimental for 2-D creep.

A finite element approach based on writing a user subroutine UMAT (Viscous) in ABAQUS to evaluate the material constitutive model developed in the previous chapters. This subroutine makes it possible to define any constitutive model of arbitrary complexity. And the developed model can be used with any ABAQUS structural element type. The user subroutine is based on a FORTRAN program.

Finite element is not the topic of this dissertation but it is a very important part relating the implementation of the constitutive equation into ABAQUS. A brief introduction of the fundamental concepts of the method is described here.

7.2 Finite Element Formulation

Conservation of linear momentum can be described either in the spatial coordinate system or a local coordinate system. For the solid material studied here, the local coordinate system is preferred.

The basis for the development of a displacement-interpolation finite element model begins with the introduction of some locally based spatial approximation to parts of the solution.

The exact solution of such a problem requires that both force and moment equilibrium be maintained at all times over any arbitrary volume of the body. The displacement finite element method is based on approximating this equilibrium requirement by replacing it with a weaker requirement, that equilibrium must be maintained in an average sense over a finite number of divisions of the volume of the body

To develop such an approximation, we begin by replacing the three equilibrium equations represented by an equivalent "weak form"—a single scalar equation over the entire body, which is obtained by multiplying the pointwise differential equations by an arbitrary, vector-valued "test function," defined, with suitable continuity, over the entire volume, and integrating.

7.2.1 Weak Form of Linear Momentum

In deriving equation for weak form of linear momentum, a volume occupied by a part of the body in the current configuration is denoted by V, and S is the surface bounding this volume. Furthermore, the surface traction at any point on S is assumed to be force $\boldsymbol{t}$ per unit of current area, and the body force at any point within the volume of material under

consideration is $\boldsymbol{f}$ per unit of current volume. Letting Ω_t denote a known configuration the constitutive equations is linearized about this known configuration.

The momentum equation cannot be discretized directly by the finite element method. In order to discretize this equation, a weak form is needed. The weak form is obtained by taking the product of the momentum equation with the test function and integrating over the domain. Here the weak form is formulated over the reference configuration and then transform to the current configuration. This gives

$$\Gamma(\boldsymbol{U},\boldsymbol{\delta}_0) = \int_{\Omega_0} (\rho_0 \dot{\boldsymbol{v}} - \rho_0 \boldsymbol{B} - Div(\boldsymbol{P}^T)\cdot\boldsymbol{\delta}_0 dV \tag{7.1}$$

The test function $\boldsymbol{\delta}_0$ has to satisfy the condition $\boldsymbol{\delta}_0 = \boldsymbol{0}$ on $\partial\Omega_U$. Combing the boundary conditions,

$$\boldsymbol{U} = \tilde{\boldsymbol{u}}, \text{ on } \partial\Omega_U \text{ and } \boldsymbol{t} = \boldsymbol{T}\boldsymbol{n} = \boldsymbol{t}_0 \text{ on } \partial\Omega_T \tag{7.2}$$

the weak form can be written as

$$\Gamma(\boldsymbol{U},\boldsymbol{\delta}_0) = \int_{\Omega_0} \boldsymbol{P}\cdot\boldsymbol{Grad}\boldsymbol{\delta}_0 \, dV - \int_{\Omega_0} \rho_0 \boldsymbol{B}\cdot\boldsymbol{\delta}_0 \, dV - \int_{\partial\Omega_0} \boldsymbol{t}_0\cdot\boldsymbol{\delta}_0 \, dA \tag{7.3}$$

where $\boldsymbol{U}$ is the displacement, $\boldsymbol{\delta}_0$ is the weight function at local coordinate system, $\boldsymbol{P}$ is the first Piola stress, $\boldsymbol{B}$ is the body force and $\boldsymbol{t}_0$ is the surface traction at the local coordinate system.

Given a nonlinear function $\Gamma(\boldsymbol{U},\boldsymbol{\delta}_0)$ and a known configuration x^* in the direction $\boldsymbol{u}$ about a particular configuration the following can be obtained,

$$\Gamma(\boldsymbol{U},\boldsymbol{\delta}_0)=\Gamma(x^*,\boldsymbol{\delta}_0)+D\Gamma(\boldsymbol{U},\boldsymbol{\delta}_0)|\boldsymbol{u}|+o(\boldsymbol{u}) \tag{7.4}$$

Where

$$D\Gamma(\boldsymbol{U},\boldsymbol{\delta}_0)|\boldsymbol{u}|=\frac{d}{d\theta}\left[\Gamma(x^*+\theta\boldsymbol{u},\boldsymbol{\delta}_0)\right]_{\theta=0} \tag{7.5}$$

Neglecting the higher order term (**o** (**u**)), and setting $\Gamma(\boldsymbol{U},\boldsymbol{\delta}_0)=0$, the following equation is obtained,

$$D\Gamma(\boldsymbol{U},\boldsymbol{\delta}_0)=-\Gamma(x^*,\boldsymbol{\delta}_0) \tag{7.6}$$

Using definition of equation (7.8) into each item in equation (7.5) and simplifying the equation, the following can be obtained:

$$D\Gamma(\underset{\sim}{\bar{x}},\boldsymbol{\delta}_0)=-\int_{\Omega_0}\boldsymbol{G}\mathrm{rad}\,\boldsymbol{\delta}_0\cdot\mathbb{N}\boldsymbol{G}\mathrm{rad}\,\boldsymbol{v}\,dV-\int_{\Omega_0}\rho_0\dot{\boldsymbol{B}}\cdot\boldsymbol{\delta}_0\,dV-\int_{\partial\Omega_0}\dot{\boldsymbol{t}}_0\cdot\boldsymbol{\delta}_0\,dA \tag{7.7}$$

where $\mathbb{N}=\dfrac{\partial\boldsymbol{P}}{\partial\boldsymbol{F}}$ is called stiffness matrix, $\boldsymbol{P}$ is the first Piola stress.

The test function can be imagined to be a "virtual" velocity field, $\boldsymbol{\delta}_v$, which is completely arbitrary except that it must obey any prescribed kinematical constraints and

have sufficient continuity: the dot product of this test function with the equilibrium force field then represents the "virtual" work rate.

Substituting $\boldsymbol{\delta_0}$ by $\boldsymbol{\delta u}$, the above equation is the so-called virtual work equation whose physical meaning can be expressed as following:

$$\begin{aligned} \delta W^{ext} &= \int_{\Omega_0} \rho_0 \dot{\boldsymbol{B}} \cdot \boldsymbol{\delta u}\, dV - \int_{\partial\Omega_0} \dot{\boldsymbol{t}}_0 \cdot \boldsymbol{\delta u}\, dA \\ \delta W^{int} &= \int_{\Omega_0} \boldsymbol{G}\mathrm{rad}\,\boldsymbol{\delta u} \cdot \mathbb{N}\boldsymbol{G}\mathrm{rad}\,\boldsymbol{v}\, dV \end{aligned} \tag{7.8}$$

The above δW^{ext} and δW^{int} are called external virtual work and internal virtual work, respectively.

The first Piola stress $\boldsymbol{P}$ is replaced by Kirchhoff stress $\boldsymbol{\tau}$, which is defined as $\boldsymbol{\tau} = J\boldsymbol{F}$. As usual, $\boldsymbol{F}$ is the deformation gradient and $J=det\boldsymbol{F}$. Set $\mathbb{S}_t = \int_{\Omega_0} \boldsymbol{P} \cdot \boldsymbol{Grad}\boldsymbol{\delta}_0\, dV$, then

$$\mathbb{DS}_t = \int_{\Omega_0} \dot{\boldsymbol{P}} \cdot \boldsymbol{Grad}\boldsymbol{\delta}_0\, dV \tag{7.9}$$

Using $Grad\boldsymbol{\delta}_0 = grad\boldsymbol{\delta}_0 \cdot \boldsymbol{F}$, $\boldsymbol{P} = \boldsymbol{\tau F}$ and $\dot{\boldsymbol{F}}^{-T} = -\boldsymbol{L}^T\boldsymbol{F}^{-T}$,and simplify equation (1.10) becomes

$$\mathbb{DS}_t = \int_{\Omega} \frac{1}{J}(\dot{\boldsymbol{\tau}} - \boldsymbol{\tau L}^T) \cdot grad\boldsymbol{\delta}_0\, dv \tag{7.10}$$

Further the rate of Kirchhoff stress is replaced by a frame-invariant rate, the Jauman rate, which is defined as:

$$\boldsymbol{\tau}^{J} = \dot{\boldsymbol{\tau}} - \boldsymbol{w}\boldsymbol{\tau} - \boldsymbol{\tau}\boldsymbol{w}^{T} \tag{7.11}$$

Then equation (7.10) can be written as

$$\mathbb{D}\mathbb{S}_{t} = \int_{\Omega} \frac{1}{J}(\boldsymbol{\tau}^{J} + \boldsymbol{w}\boldsymbol{\tau} - \boldsymbol{\tau}\boldsymbol{w}) \cdot grad\boldsymbol{\delta}_{0}\, dv \tag{7.12}$$

Thus the constitutive equation can be re-cast in the Jaumann rate as

$$\boldsymbol{\tau} = \mathbb{N}\boldsymbol{D} \tag{7.13}$$

where $\mathbb{N}$ is the stiffness matrix.

7.2.2 Integration Schemes

Based on the discretized rate equation, the next step is integrating the equations. Three major integration methods can be used, namely the forward, backward and midpoint Euler integration methods, which is summarized in this section.

Due to the nonlinear nature of the governing differential equations; an incremental solution procedure is usually required. Letting $\Delta(\bullet) = (\bullet)^{n+1} - (\bullet)^{n}$ denote an increment over a time interval $[t^{n}, t^{n+1}]$, the differential equations can be incrementally solved to obtain $\{T^{n+1}, \varepsilon^{n+1}, \varepsilon_{in}^{n+1}, V^{n+1}\}$ by using different integration schemes, if $\{T^{n}, \varepsilon^{n},$

ε_{in}^{n}, $V^{n}\}$ and the total strain increment $\Delta\varepsilon$ are known. The most popular integration schemes are forward integration and backward integration.

The rate equations are first discretized in the time domain, and the current incremental changes in the inelastic strain are approximated as $\Delta\varepsilon_{in} \approx \dot{\varepsilon}_{in}^{n}\Delta t$, with the current time increment $\Delta t = t^{n+1} - t^{n}$. It should be noticed that the rates at the beginning of the increment are used.

This numerical scheme is explicit in nature and, in particular, is suitable for very small time steps. In other words, the Forward Euler solution is conditionally convergent. In contrast to the Forward integration scheme, backwards Euler method has unconditional stability and the time steps are limited only by the accuracy. The numerical quantities are calculated from rates at the end of the current increment. That is $\Delta\varepsilon_{in} = \dot{\varepsilon}_{in}^{n+1}\Delta t$.

The advantage of the Backward Euler scheme over other midpoint schemes is that the solution is sought by using the normal at the final stress state. By implicitly assuming that such a stress state exists, the Backward Euler scheme is guaranteed to provide a solution, despite the size of the strain step. The Backward Euler algorithm is only accurate to the first order.

The explicit algorithm (Forward Euler) is based on using the starting point in the stress and internal variable space for finding all the relevant derivatives and variables.

It should be noted that the explicit algorithm performs only one step of the computation and does not check on the convergence of the provided solutions. This usually results in the slow drift of the stress-internal variable point from the yield surface for monotonic loading. It also results in spurious plastic deformations during elastic unloading, during cycles of loading-unloading.

The central difference method is always among the most popular in computational mechanics and physics. The time of the simulation, t, ($0 \le t \le t_E$), is subdivided into time steps $\Delta t^n, n = 1, n_{Ts}$, where n_{Ts} is the number of time steps and t_E is the simulation end. The superscript indicates the time step: t^n *and* $d^n \equiv d(t^n)$ over the time and displacement at time step n respectively.

$$\Delta t^{n+1/2} = t^{n+1} - t^n, \Delta t^{n+1/2} = \frac{1}{2}(t^{n+1} + t^n), \Delta t^n = t^{n+1/2} - t^{n-1/2}$$
$$\dot{d}^{n+1/2} \equiv v^{n+1/2} = \frac{d^{n+1} - d^n}{t^{n+1} - t^n} = \frac{d^{n+1} - d^n}{\Delta t^{n+1/2}} \tag{7.14}$$

This differential formula can be converted to an integration formula by rearranging the terms as following:

$$d^{n+1} = d^n + \Delta t^{n+1/2} v^{n+1/2} \tag{7.15}$$

In the remaining of this section, the central different integration method will be used to get the rate equation of stress. This begins with a rewriting of the stored energy.

Substituting equation (3.11) into equation (5.16), the stored energy in terms of $\boldsymbol{C}_e$ is,

$$\psi = \frac{1}{4}(\boldsymbol{C}_e - \boldsymbol{I}) \cdot \mathbb{C}(\boldsymbol{C}_e - \boldsymbol{I}) \tag{7.16}$$

Similarly, by introducing equation (7.16) into equation (4.29), the stress is given by

$$\boldsymbol{T} = 2\rho \boldsymbol{F}_e \mathbb{C} \boldsymbol{E}_e \boldsymbol{F}_e^T \tag{7.17}$$

For an inelastic deformation, the total strain can be written as the sum of the elastic strain and inelastic strain. In other words, the elastic strain can be written as follows,

$$\boldsymbol{E}_e = \boldsymbol{E} - \boldsymbol{E}_{in} \tag{7.18}$$

Substituting equation (7.18) into equation (7.17), and then using the time derivative, it yields,

$$\dot{\boldsymbol{T}} = 2\rho \mathbb{C} (\dot{\boldsymbol{E}} - \dot{\boldsymbol{E}}_{in}) \tag{7.19}$$

Since

$$\dot{\boldsymbol{E}}_{in} = \boldsymbol{D}_{in} = \mathbb{k}^{-1} \left[\boldsymbol{A}_{sys} - \frac{tr(\mathbb{k}^{-1} \boldsymbol{A}_{sys})}{tr(\mathbb{k}^{-1} \boldsymbol{I})} \boldsymbol{I} \right] \tag{7.20}$$

and using the definition of $\mathbb{C}$, equation (5.17), and $\mathbb{k}$, equation (5.27), the stress rate is obtained,

$$\dot{\boldsymbol{T}} = 2\rho \begin{bmatrix} a\dot{E}_{11} + b(\dot{E}_{22} + \dot{E}_{33}) - \frac{1}{3}(a-b)(i-j)(2T_{11} - T_{22} - T_{33}) \\ a\dot{E}_{11} + b(\dot{E}_{22} + \dot{E}_{33}) - \frac{1}{3}(a-b)(i-j)(2T_{22} - T_{11} - T_{33}) \\ a\dot{E}_{11} + b(\dot{E}_{22} + \dot{E}_{33}) - \frac{1}{3}(a-b)(i-j)(2T_{33} - T_{22} - T_{11}) \\ c\dot{E}_{12} - ckT_{12} \\ c\dot{E}_{13} - ckT_{13} \\ c\dot{E}_{23} - ckT_{23} \end{bmatrix} = \begin{bmatrix} \dot{T}_{11} \\ \dot{T}_{22} \\ \dot{T}_{33} \\ \dot{T}_{12} \\ \dot{T}_{13} \\ \dot{T}_{23} \end{bmatrix} \tag{7.21}$$

Now using the simple, stable central difference integration operator for equation (7.21), the stress increment for the main stress, ΔT_{xx}, and shear stress, ΔT_{xy}, are obtained as in equation (7.22) and equation (7.23). Stress increments of other components can be obtained, and they have similar forms.

$$\Delta T_{xx} = \frac{2}{3q-1}\{[(q-1)a + 2qb]\Delta\varepsilon_{xx} + [(2q-1)b + qa]\Delta\varepsilon_{yy} + [(2q-1)a + qa]\Delta\varepsilon_{zz} - q(3T_{xx} - T_v)\} \tag{7.22}$$

and

$$\Delta T_{xy} = \frac{2c}{1 + ck\Delta t}(\Delta\dot{\varepsilon}_{xy} - k\Delta t T_{xy}) \tag{7.23}$$

where

$$q = \frac{\rho\Delta t}{6}(i-j)(a-b) \tag{7.24}$$

7.2.3 Tangent Stiffness

It appears that Simo and Taylor in (1985) and Runesson and Samuelsson (1985) were the first to derive the consistent tangent stiffness tensor. Other interesting articles on the subject can be found in Simo and Taylor (1986), Simo and Govindjee (1988), Koiter, (1953), Braudel, Abouaf, and Chenot (1986), Crisfield (1987). As a consequence of consistency, the use of the consistent tangent stiffness tensor significantly improves the convergence characteristics of the overall equilibrium iterations, if a Newton - Raphson scheme is used for the latter. Use of the consistent tangent stiffness tensor yields a quadratic convergence rate of Newton - Raphson equilibrium iterations.

The final goal in deriving the Backward Euler scheme for integration of elasto-plastic constitutive equations is to use that scheme in finite element computations. If the Newton - Raphson iterative scheme is used at the global equilibrium level then the use of the so called traditional tangent stiffness tensor destroys the quadratic rate of asymptotic convergence of the iterative scheme. In order to preserve such a quadratic rate, a consistent, also called algorithmic, tangent stiffness tensor is derived. The consistent tangent stiffness tensor makes use of derivatives of direction normal to the potential function, and they are derived at the final of each iteration. This is in contrast to the traditional forward scheme where a constant derivative is evaluated at the intersection point.

Thus the Jacobian matrix has the terms:

$$\frac{\Delta T_{xx}}{\Delta \varepsilon_{xx}} = \frac{2\rho}{4q^2 + 5q + 1}[(3q+1)a - 2bq] \tag{7.25}$$

$$\frac{\Delta T_{xx}}{\Delta \varepsilon_{yy}} = \frac{2\rho}{4q^2 + 5q + 1}[(3q+1)b - q(a+b)] \tag{7.26}$$

and

$$\frac{\Delta T_{xx}}{\Delta \varepsilon_{xy}} = \frac{2\rho c}{2\text{-}ck\Delta t} \tag{7.27}$$

7.3 UMAT Development and Solution Techniques

7.3.1 UMAT Development

The commercial FE software ABAQUS provides a powerful tool by allowing user to implement their own constitutive models through a user subroutine UMAT. This subroutine is called at every integration point, hence it needs to be accurate, robust and yet computationally efficient.

The data passed into a UMAT include the stress, strain and internal variables from the last converged increment, and the current total strain increment that is computed from the node displacement after solving the global equilibrium equations. The output of a UMAT is stress, internal variables and consistent tangent stiffness matrix for implicit finite element program.

Employing the constitutive equation developed in the preceding chapters, and the Jacobian derived in this chapter, the equations for a user material (UMAT) subroutine for implementation in the ABAQUS finite element code is presented in this section.

A finite element approach is based on writing a user subroutine in ABAQUS to evaluate the constitutive equation under given loads. Two dimensional 4-node solid elements are used (Figure 7.1). The user subroutine is based on the FORTRAN90

programming Language and the corresponding flow chart for writing UMAT is listed in Appendix B.

7.3.2 Boundary and Load Conditions

Due to the uniform distribution of the stress in the specimen for this case, only one element will be enough to model the problem. A 4-node solid element will be used in the simulation. The sketches of the finite element model for both <001> and <011> orientations are shown in Figure 7.1, and loading curve is shown in Figure 7.2.

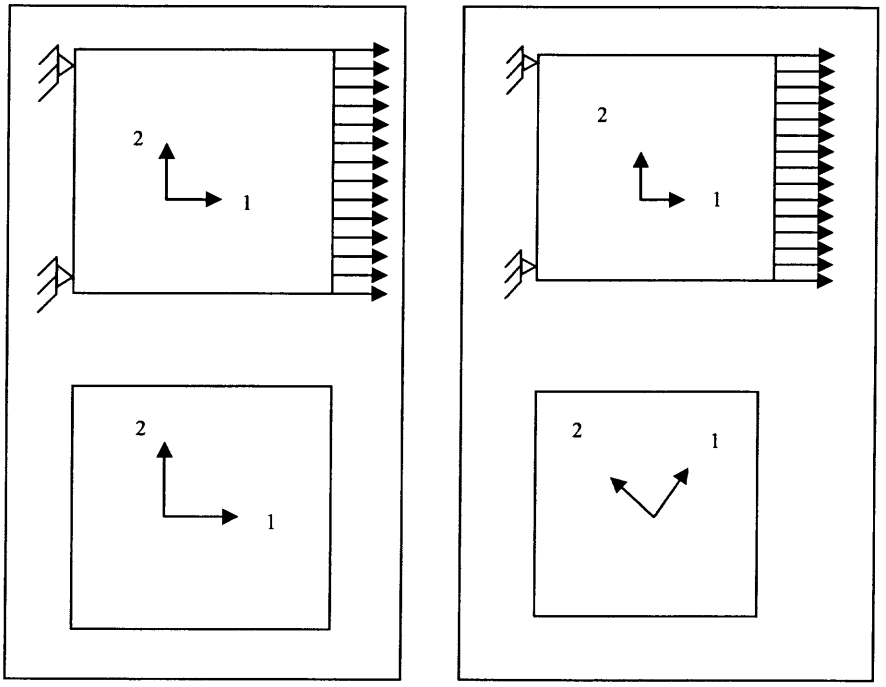

Figure 7.1 Finite element model for <001> and <011> orientations.

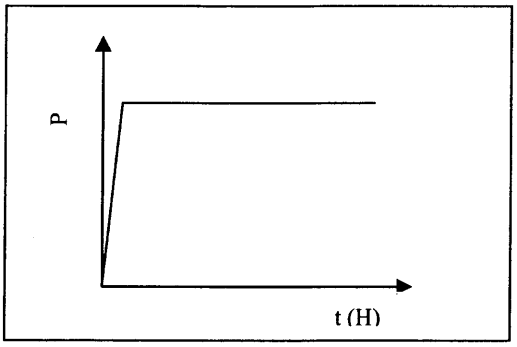

Figure 7.2 Schematic plot of loading curve.

7.3.3 Element Technology

The objective of element technology is to develop elements with better performance, particularly for large-scale calculations and for incompressible materials. Low-order elements when applied to incompressible materials tend to lock volumetrically. Although incompressible materials are quite rare in linear stress analysis, many materials behave in a nearly incompressible manner in the nonlinear regime. The ability to treat incompressible materials effectively is important in nonlinear finite element. Understanding this shortcoming and picking the right elements are crucial in the selection of elements for nonlinear analysis.

In selecting elements, the ease of mesh generation for a particular element should be borne in mind. Triangular and tetrahedral elements are very attractive because they are the easiest to mesh. Therefore, they are preferable when all other performance characteristics are comparable for the problem at hand.

The most frequently used low-order elements in two dimensions are the 3-node triangle and 4-node quadrilateral. The corresponding three dimensional elements are the 4-node tetrahedron and the 8-node hexahedron, respectively.

In order to avoid the severe volumetric locking, 3-node triangle element in 2-D and 4-node tetrahedron element in 3-D should not be considered. At the same time, for the sake of large-scale calculation, the element selected for the simulation is 4-node quad element in two dimension, and 8-node hexahedron elements are the best choice. Considering the geometry used here, in this dissertation we pick 4-node rectangular element.

7.4 Finite Element Results

Finite element results will be given in this chapter which includes creep results, maximum strain distribution and energy ratio.

7.4.1 Material Parameters and Constants

In table 7.1 a summary of all the material parameters and constants used in this simulation are provided. The following are the physical interpretation of these parameters and constants.

Elastic constant $\mathbb{C}$: The elastic constants for CMSX-4 Nickel based single crystal Superalloy is available in the literature (Li, 1997) and are listed in Table 7.2. This set of material constants are tested at a temperature of 950°C. The elastic modulus depended on temperature and this simulation is run at different temperatures, 750°C and 1000°C different from Li (1997). In general, the effect of temperature should be accounted for. However, in this case it will modify the behavior only in the initial elastic region. Hence, without any loss in generality, we assume a single set of modulus independent of temperature for our simulation.

Elastic stored energy ψ_e: The elastic stored energy is defined as in equation (5.1).

Nominal strain strength ε_r: Nominal strain strength is calculated using equation (6.7). It is accounted for the inelastic strain accumulation and determines the viscosity at real-time during the creep deformation.

Stress invariance tr ($\boldsymbol{T}$): It is the first stress invariance and is a factor which affects the creep deformation.

Table 7.1 List of material parameters and constants

No.	Parameter	Depends on	Remarks
1	$\mathbb{C}$	constant	Elastic constants
2	ψ_e	constant	Elastic stored energy
3	ε_r	strain	Strain strength
4	tr($\boldsymbol{T}$)	stress	Stress invariant
5	i	strain and stress	Dynamic viscosity component
6	j	strain and stress	Dynamic viscosity component
7	k	strain and stress	Dynamic viscosity component

Table 7.2 Elastic Material Constants

a= 1.162E-5N/m^2, b=-4.51E-6N/m^2, c= 1.162E-5N/m^2

Directional viscosity: The anisotropic nature of material properties is captured through the three-dimensional directional viscosity tensor, which in turn depends on three components, *i, j* and *k* consistent with cubic symmetry. The directional viscosity is determined by the stress and strain strength in real-time and can be calculated by equations (6.11 and 6.12).

7.4.2 Simulation Results

Figures 7.3 and 7.4 are the simulation results at different orientations and stresses. The finite element results are reasonably fit to the experimental results.

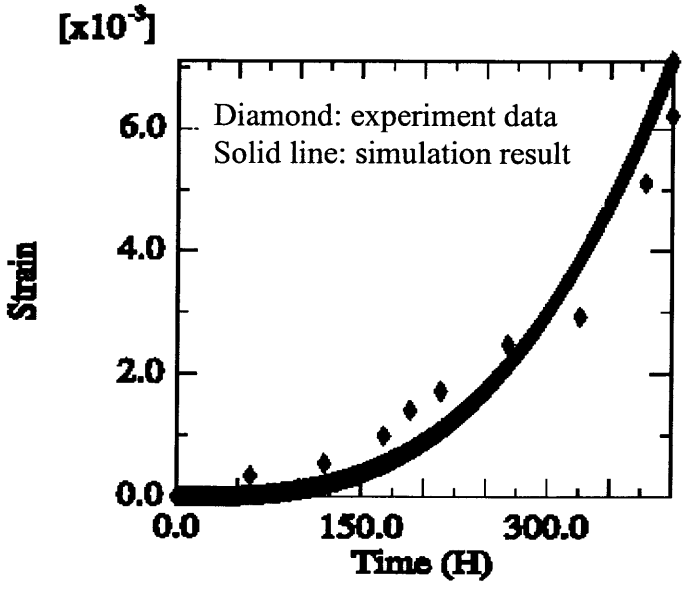

(a)

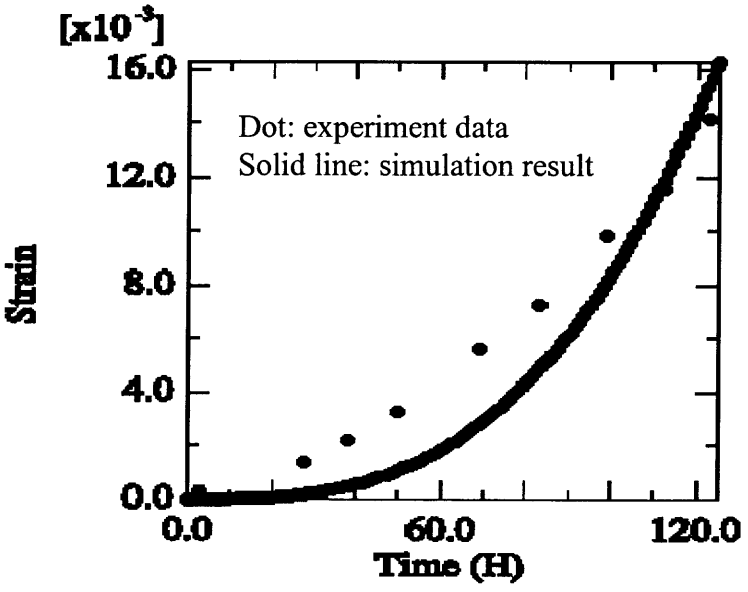

(b)

Figure 7.3 Simulation curve at <001> 950°C (a) 250MPa, (b) 320MPa (Experimental data from Duncan et al. 2001).

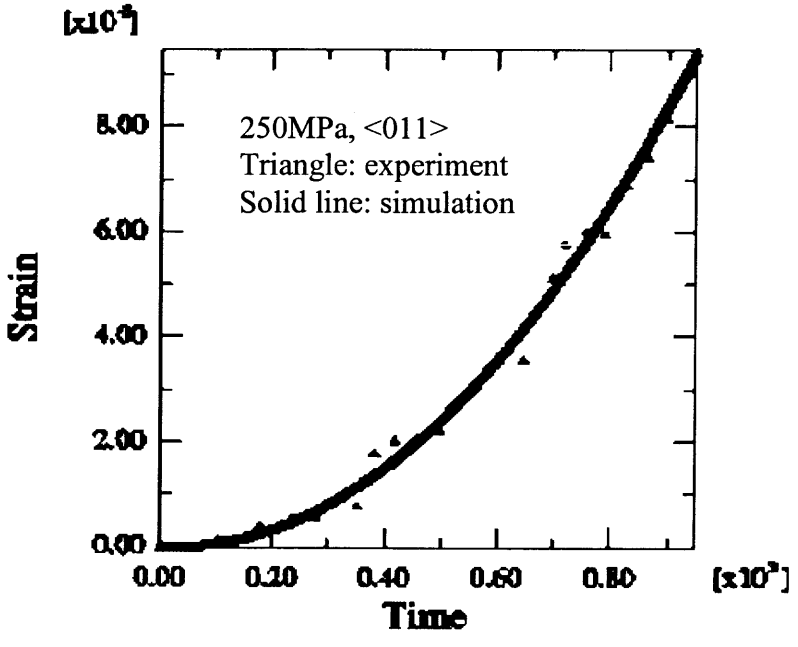

(a)

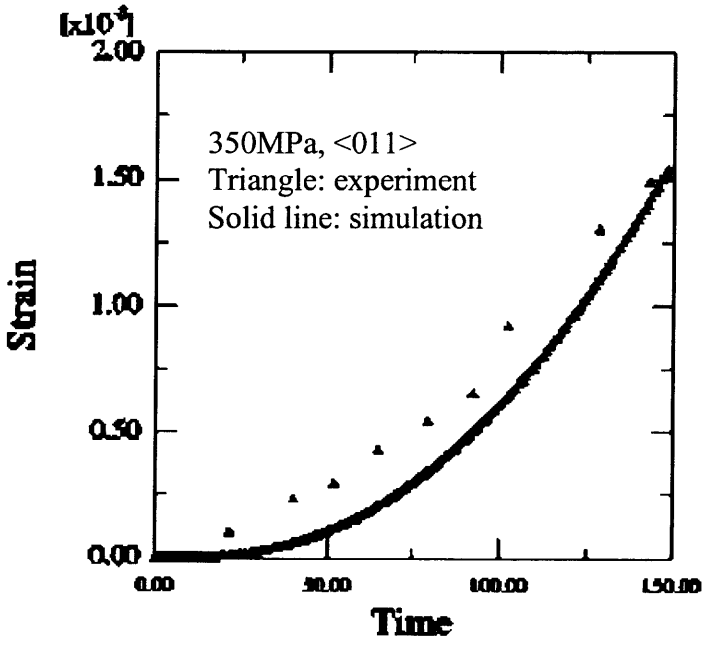

(b)

Figure 7.4 Simulation results for <011> direction, (a) 250MPa, (b) 350MPa (Experimental data from Duncan et al. 2001).

7.4.3 Two-dimensional Strain Analysis

In order to test the developed model, 2D multiple elements specimens will be used and paths are set to further investigate the anisotropic deformation.

A multiple element 2D problem (Figure 7.5) is used to conduct the strain analysis. Five paths are distinguished to determine the strain distribution. The path on the left is fixed while the path on the right is the loading side. The load is a uniformly distributed stress. Path on the top is stress free. The paths middle and middlev are the symmetric lines running through the center in the horizontal and vertical directions, respectively. The distance here is the normalized distance and the strain refers to the maximum principal strain which can be calculated by equation (7.28) for a two-dimensional problem,

$$E_{\max} = \frac{E_x + E_y}{2} + \sqrt{(\frac{E_x - E_y}{2})^2 + E_{xy}^2} \tag{7.28}$$

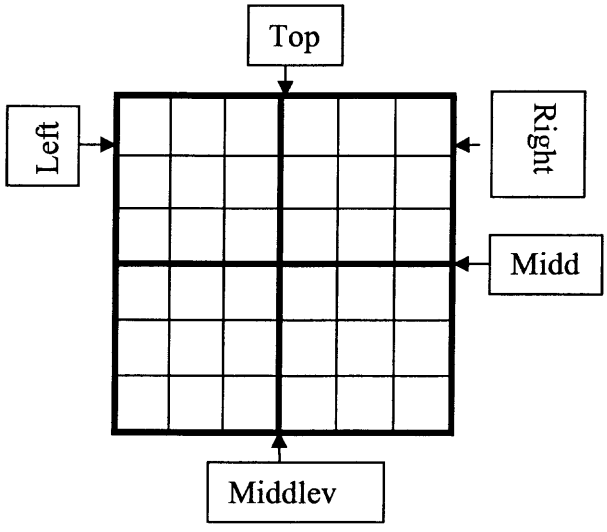

Figure 7.5 Schematic definition of path.

Four cases are plotted in the Figures 7.6 to 7.7 for the comparison of the strain distribution for 250 MPa at <001> and <011> orientations along different paths. It is clear that for all the cases maximum strain at <011> material orientation is larger than that for the <001> orientation. Another significant difference is the maximum strain distribution along path middlev and path right for <001> and <011> material orientations. At the <001> orientation along path middlev, strain distribution is almost a constant while <011> isn't. These differences resulted from the anisotropic property of material and its deformation.

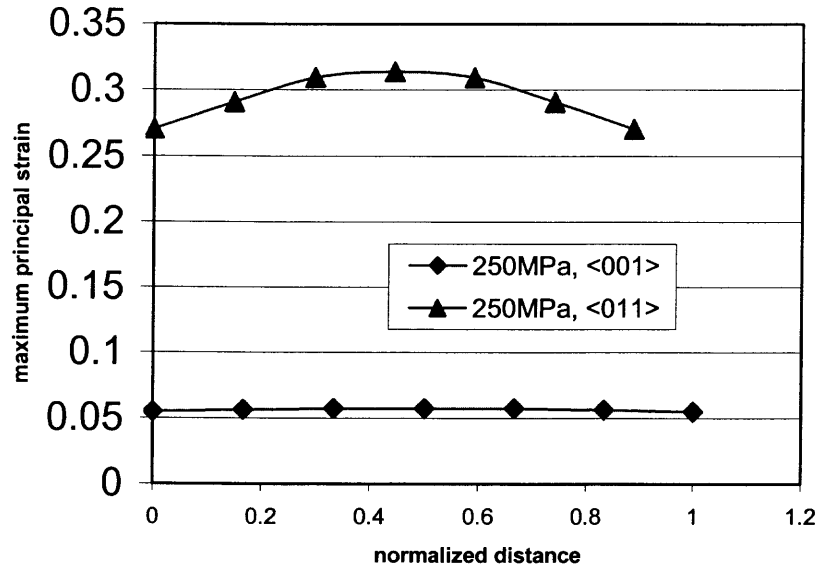

(a)

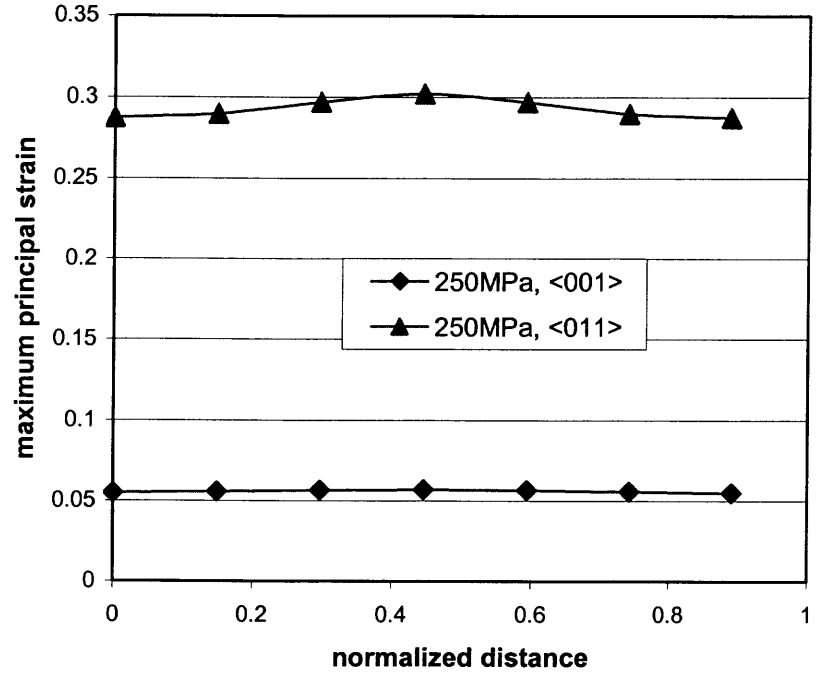

(b)

Figure 7.6 Maximum principal strains for the vertical paths (a) path middlev and (b) path right.

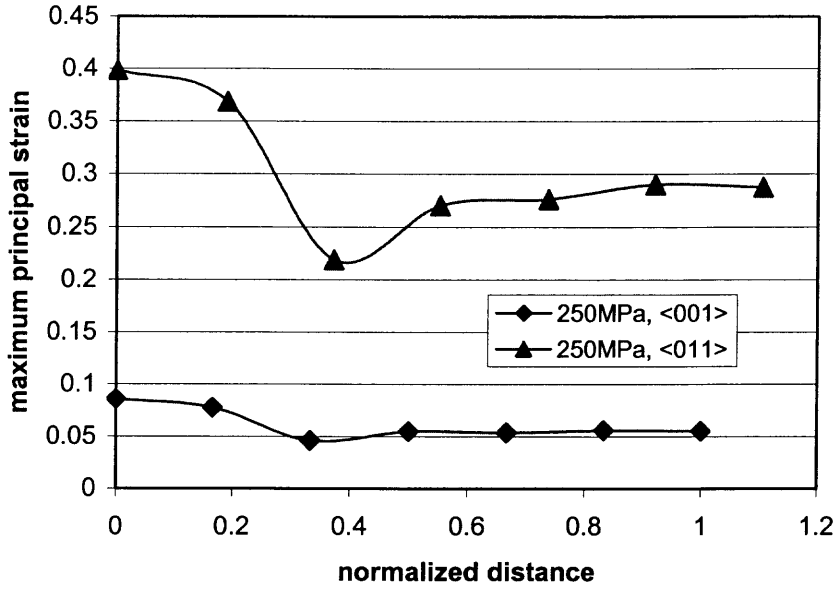

(a)

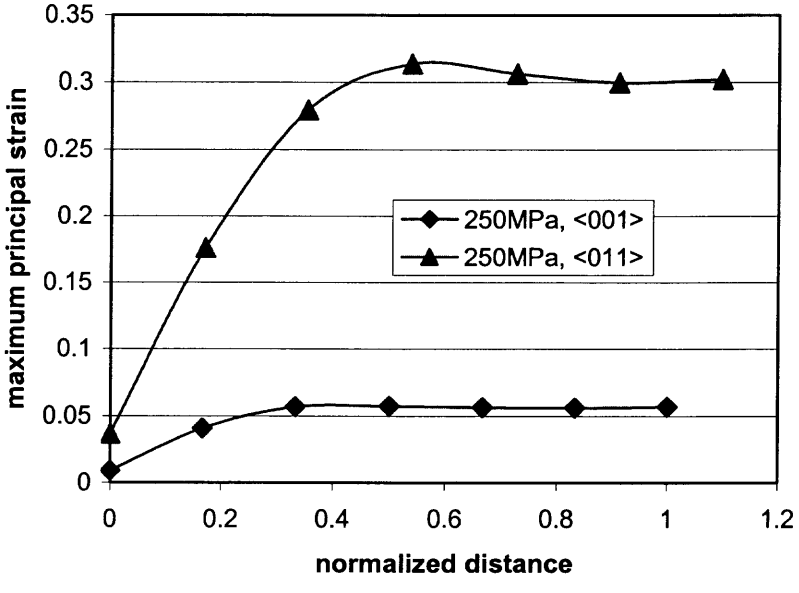

(b)

Figure 7.7 Maximum strains for the horizontal paths (a) path top and (b) path middle.

A direct view of strain distribution can also be seen from the contours in Figure 7.8 to Figure 7.10, which indicate the different strain distribution at <001> and <011> orientations.

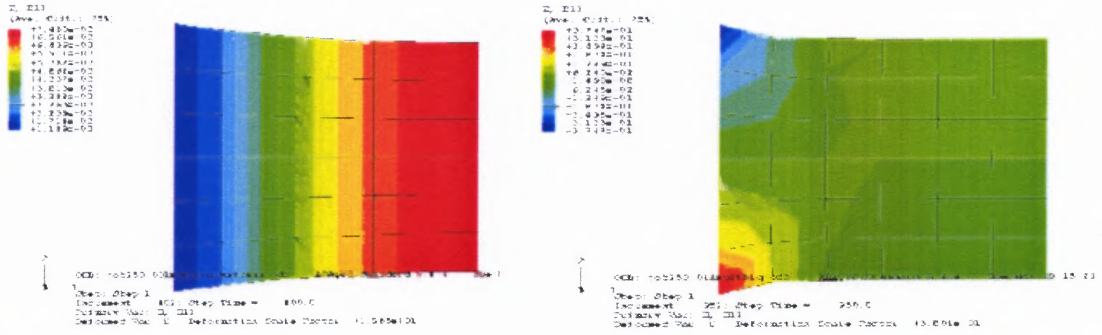

(a) (b)

Figure 7.8 Contour plot of stress E_{11} at 250 MPa, along different orientations (a) <001>, (b) <011>.

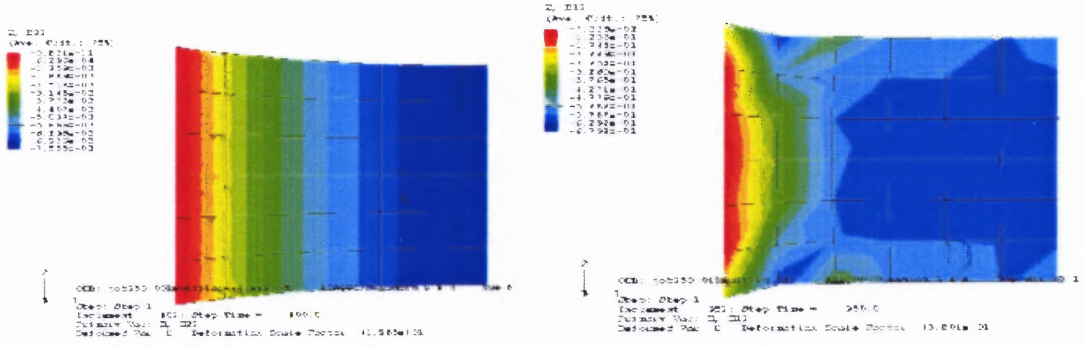

(a) (b)

Figure 7.9 Contour plot of stress E_{22} at 250 MPa, along different orientations (a) <001>, (b) <011>.

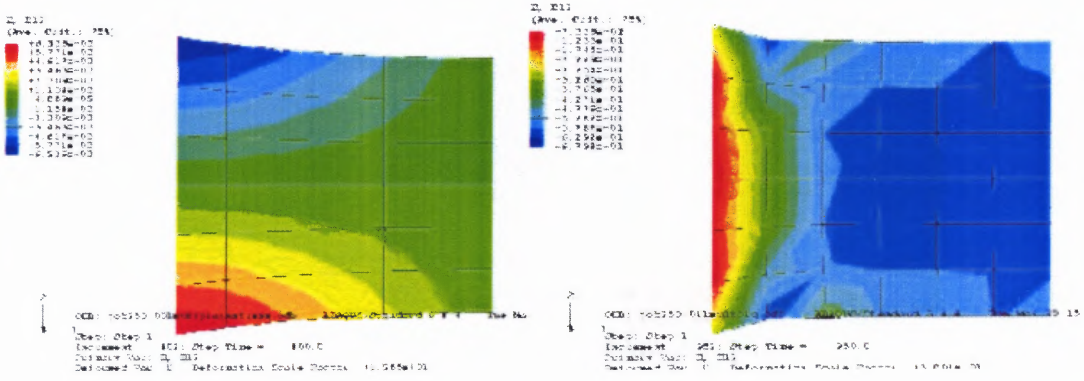

(a) (b)

Figure7.10 Contour plot of stress E_{12} at 250 MPa, along different orientations (a) <001>, (b) <011>.

7.5 Conclusions

The aim of this chapter is to incorporate the developed constitutive equations into the finite element method simulate creep in complex geometries. The tangent stiffness matrix and integration schemes were introduced. Methods are described to derive the material tangent stiffness and to integrate the constitutive equation.

Implicit backwards Euler's method was used in integration and for writing the UMAT. The motivation for this choice as a numerical technique for solving the nonlinear equilibrium equations is primarily the convergence rate obtained by using Newton's method compared to the convergence rates exhibited by alternate methods (usually modified Newton or quasi-Newton methods) for the types of nonlinear problems most often studied with ABAQUS.

Two dimensional elements were used to test the <001> and <011> directions and the comparison with the experimental results are given. 2D strain analysis were also studied which proved that the model developed in this dissertation can capture the anisotropic behavior.

CHAPTER 8

CONCLUSIONS AND FUTURE WORK

With the increasing of the entry temperature the turbine efficiency also increases which can reduce the energy consumption. New materials, including nickel based single crystal Superalloys, are developed continuously to meet this requirement. To validate or test the creep life for these materials at different working conditions, such as temperature, stress, orientations, etc, a huge number of creep tests should be performed in order to get the creep data. Since the creep tests need a specific setup and the tests last a long time, the whole procedure is time and money consuming. In addition, a change in the working condition will also affect the creep life. The reasonable way to solve this problem is to develop a practical model, based on the fundamental creep data from the same material. This model can then be used to predict the creep life at various working conditions.

So far two kinds of model are available in the literature, crystallographic model and phenomenological model. Due to the limitations of these models, a new model was developed here based on the framework of multiple natural configurations. This framework has been used to develop constitutive models for a variety of materials.

The theory of multiple natural of configuration was used in this dissertation; to develop a new creep model for Nickel based single crystal Superalloys CMSX-4. The model was evaluated for several temperatures/stresses and orientations. The parameters and constants in the model were evaluated according to the procedure introduced in Chapter7. This model was implemented into a commercial program ABAQUS 6.4 as a User Define Material subroutine. A finite element simulation of the alloy under constant

stress load was conducted and compared with the experimental results. A 2-D element type simulation was conducted. The results have fair agreement with the experiments.

The contributions of this dissertation are summarized into the following aspects:

1. A new creep model has been proposed by using the framework of multiple natural configurations.
2. A directional viscosity tensor was introduced into the model to capture the anisotropic material and deformation characteristics. The directional viscosity dependence of stress and strain was mathematically expressed.
3. This was a rather general model which can be used to simulate the creep behavior at high temperature. The model has been tested for three temperatures ranges, and its predictions are in agreement with the experimental data.
4. This model was also used to test the creep behavior at different orientations at isothermal conditions; the predications are in good agreement with the experimental data.
5. Implementation of the constitutive equation by writing a User Defined Material subroutine which can capture the anisotropic material property and deformation.

This was the first attempt to simulate creep deformation based on the multiple natural configurations. Thus there are several ways in which this work could be extended in the future. Some important and promising directions include:

- Low temperature range, especially at temperature of 750°C and below. At present, the turbine entry temperature was the main concern and hence the research focused on the upper end range of the temperature of about 950°C. But in practice, due to the

efficient cooling system the core of the blade was at the temperature range of 750°C. Thus the creep behavior at this temperature is also of vital importance in determining the overall performance of the blade. Thus a detailed model for low temperatures can be extended from this work.

- This model was developed for primary and secondary creep, which implies that this creep model does not include the tertiary creep stage, in which voids and cracks begin to form. Further study is needed to predict the total creep behavior for a single crystal material including yielding criterion and damage mechanisms.
- This model was developed on the assumption that the creep takes place at an isothermal condition. In practice creep can occur at either constant temperature or changing temperature condition, such as the turbine and blades experienced at the take off of an airplane. There is still a room for extending this model to non-isothermal condition.
- Application of the model to realistic turbine blade geometries, to predict creep in a real turbine blade.

APPENDIX A

COORDINATE SYSTEM TRANSFORMATION

This Appendix contains the matrix ***A*** and ***B*** which are used to transform the coordinate systems.

A and ***B*** are fourth order tensors for the transformation and can be calculated from the direction cosine with respect to the two coordinate systems as follow,

$$\beta_1 = l^2 + m^2 + n^2$$
$$\beta_2 = m^2 + n^2$$

where l, m, n represent the direction of the coordinates in the crystallographic coordinate system.

$$\mathbf{A} = \frac{1}{\beta_1\beta_2}\begin{bmatrix} \beta_2^2 & 0 & l^2\beta_2^2 & 0 & 2l\beta_2\sqrt{\beta_2} & 0 \\ m^2l^2 & n^2\beta_1 & m^2\beta_2 & 2mn\sqrt{\beta_1\beta_2} & -2m^2l\sqrt{\beta_2} & -2lmn\sqrt{\beta_1} \\ l^2n^2 & m^2\beta_1 & n^2\beta_2 & -2mn\sqrt{\beta_1\beta_2} & -2ln^2\sqrt{\beta_2} & 2lmn\sqrt{\beta_1} \\ l^2mn & -mn\beta_1 & mn\beta_2 & (n^2-m^2)\sqrt{\beta_1\beta_2} & -2lmn\sqrt{\beta_2} & l(m^2-n^2)\sqrt{\beta_1} \\ -ln\beta_2 & 0 & ln\beta_2 & -lm\sqrt{\beta_1\beta_2} & (\beta_2-l^2)n\sqrt{\beta_2} & -m\beta_2\sqrt{\beta_1} \\ -lm\beta_2 & 0 & lm\beta_2 & ln\sqrt{\beta_1\beta_2} & (\beta_2-l^2)m\sqrt{\beta_2} & n\beta_2\sqrt{\beta_1} \end{bmatrix}$$

$$\mathbf{B} = \frac{1}{\beta_1\beta_2}\begin{bmatrix} \beta_2^2 & 0 & l^2\beta_2^2 & 0 & l\beta_2\sqrt{\beta_2} & 0 \\ m^2l^2 & n^2\beta_1 & m^2\beta_2 & mn\sqrt{\beta_1\beta_2} & -m^2l\sqrt{\beta_2} & -lmn\sqrt{\beta_1} \\ l^2n^2 & m^2\beta_1 & n^2\beta_2 & -mn\sqrt{\beta_1\beta_2} & -ln^2\sqrt{\beta_2} & lmn\sqrt{\beta_1} \\ 2l^2mn & -2mn\beta_1 & 2\,mn\beta_2 & (n^2-m^2)\sqrt{\beta_1\beta_2} & -2lmn\sqrt{\beta_2} & l(m^2-n^2)\sqrt{\beta_1} \\ -2\,ln\beta_2 & 0 & 2ln\beta_2 & -lm\sqrt{\beta_1\beta_2} & (\beta_2-l^2)n\sqrt{\beta_2} & -m\beta_2\sqrt{\beta_1} \\ -2lm\beta_2 & 0 & 2lm\beta_2 & ln\sqrt{\beta_1\beta_2} & (\beta_2-l^2)m\sqrt{\beta_2} & n\beta_2\sqrt{\beta_1} \end{bmatrix}$$

APPENDIX B

FLOW CHART FOR UMAT

This Appendix describes the flow chart for UMAT

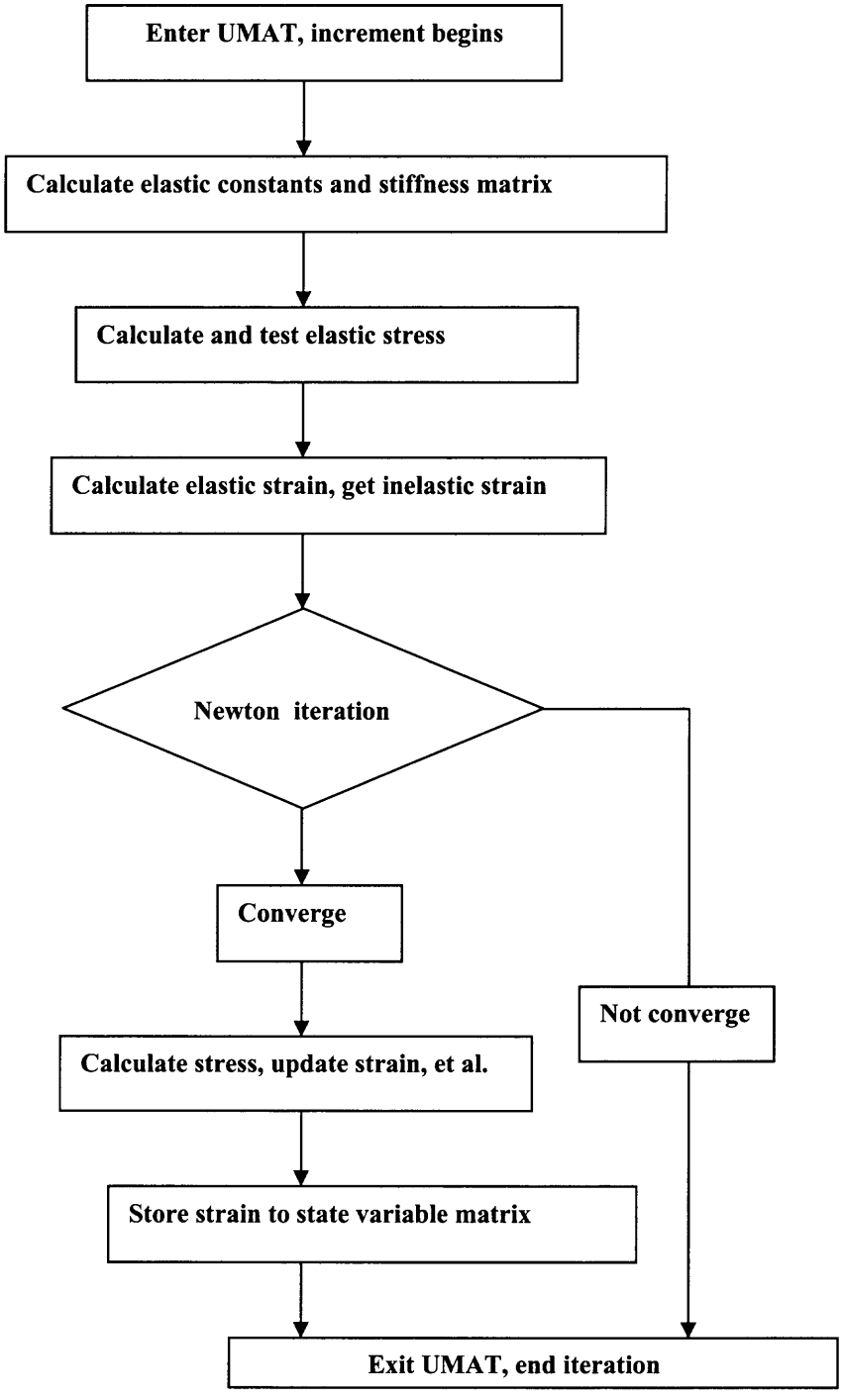

REFERENCES

Arrell, D. J. and Valle's, J. L., 1994, "Interfacial dislocation based criterion for the prediction of rafting behavior in superalloys", *Scripta Metal. Mater.*, 30(2), p.149.

Ashby, M.F. and Verall, R.A., 1978, "Micromechanisms of flow and fracture, and their relevance to the rheology of the upper mantle", *Philosophical Transactions of the Royal Society of London* 288, p.59-95.

Bertram A. and Olschewski, J., 1996, "Anisotropic creep modeling of the single crystal superalloy SRR99", *Computational Materiasl Science*, 5, p.12.

Betteridge, W., 1982, "Nickel and its Alloys," Ellis Horwood Ltd.

Bettge, D. and Esterle, O. W., 1999, "In microstructure and mechanical properties of metallic, high-temperature materials", *DFG-Report,* ed. H. Mughrabi, et al., Wiley-VCH, Weinheim, p.370.

Braudel, H. J., Abouaf, M., and Chenot, J. L., 1986, "An implicit and incremental formulation for the solution of elastoplastic problems, by the finite element method", *Computers and Structures*, 22(5), p.801-814.

Buffiere, J. Y. and Ignat, M., 1995, "Dislocation based criterion for the raft formation in nickel-based superalloys single crystals", *Acta Metall. Mater.*, 43(5), p.1791.

Caron, P., Ohta, Y., Nakagawa, Y.G., Khan, T., 1988, "Superalloys," AIME Publishing, Warrendale, PA, USA.

Chaboche, J. L., 1989, "Constitutive equations for cyclic plasticity and viscoplasticity", *Int. J. Plast.*, 5, p.247-302.

Chest, T. S. and Willian, C. H., 1972, "The Superalloys", John Wiley & Sons, New York.

Chest, T. S., Norman, S. S. and Willian, C. H., 1987, "Superalloys II", John Wiley & Sons, New York.

Choi, S. H. and Krempl, E., 1989, "Viscoplasticity theory based on overstress applied to the modeling of cubic single crystals", *European J. of Mechanism and Solid*, 8, p.219-233.

Crisfield, M. A., 1987, "Consistent schemes for plasticity computation with the Newton Raphson method", *Computational Plasticity Models, Software, and Applications*, 1, p.136-160.

Dame, L.T. and Stouffer, D.C., 1988, "A crystallographic model for nickel based single crystal alloys", J. *Applied Mechanics*, 55, p.325-331.

Dlouhy, A., Schaublin, R. and Eggeler, G., 1998, "Transmission electron microscopy contrast simulation of <100> superdislocation in the LL_2 ordered structure", Scripta *Materialia*, 39, p.1325–1332.

Duncan W. MacLachan, Lawrence W. Wright, Satish Gunturi and David M. Knowles, 2001, "Constitutive modeling of anisotropic creep deformation in single crystal blade alloys srr99 and cmsx-4", Int. *J. of Plasticity*, 17, p.441-467.

Durand-Charre M., 1997, "The Microstructure of Superalloys", London, Gordon and Breach Science Publishers.

Endre SÜli and David Mayers, 2003, "An Introduction to Numerical Analysis", University Press, Cambridge, United Kingdom.

Feller-Kniepmeier, M., Link, T., Poschmann, I., Scheunemann-Frerker, G., Schulze, C., 1996, "Temperature dependence of deformation mechanism in a single crystal nickel based alloy with high volume fraction of γ' phase", *Acta Materialia,* 44, p.2397-2407.

Fleury, G., Schubert, F. abd Nickel, H., 1996, "Modeling of the thermo-mechancial behavior of the single crystal superalloy cmsx-4', *Computational Materials Scicence*, 7, p.187.

Gell, M., Duhl, D.N. and Giamei, A. F., 1980, "Processing of the Fourth International Symposium on Superalloys", *ASM*, Metals Park, OH, p.205.

Gilman, J. J., 1969, "Micromechanics of Flow in Solids," McGraw-Hill, New York.

Halmos, 1958, "Finite Dimensional Vector Spaces", 2nd ed. Van Nostrand, Princeton, Toronto, and London, p.83.

Hackett, R. M., and Bennett, J. G., 1999, ''An implicit finite element material model for energetic particulate composite materials'', Technical Report, LAUR-99-3139, Los Alamos National Laboratory, Los Alamos, NM.

Han, S. L., Li, S. X. and Smith, D.J., 2001, "Comparison of phenomenological and crystallographic models for single crystal nickel base superalloys. I. Analytical identification", *Mechanics of Materials*, 33, p.251-266.

Han, S. L., Li, S. X. and Smith, D. J., 2001, " Comparison of phenomenological and crystallographic models for single crystal nickel base superalloys. II. Numerical simulations", *Mechanics of Materials*, 33, p.267-282.

Haupt P., 2000, "Continuum Mechanics and Theory of Materials", Springer, Berlin, Germany.

Henderson, P. J. and Lindblom, J., 1997, "High temperature creep in a <001> single crystal nickel-base superalloy", *Scripta Materialia*, 37(4), p.491-496.

Henderson, P. J. and K Omenda, J., 1998, International Gas Turbine and Aero Engine Congress, Stockholm, Sweden, ASME 98-GT-488.

Henderson, P. J., Berglin, L. Jansson, C., 1999, "On rafting in a single crystal nickel based superalloy after high and low temperature creep", *Scripta Materialia*, 40, p.229-234.

Hillier, 1984, Ph.D dissertation, University of Cambridge.

Honeycombe, R., W. K., 1984, "The Plastic Deformation of Metals", 2nd edition, Edward Arnold Ltd.

Javier Bonet and Richard D. Wood, 1997, "Nonlinear continuum mechanics for finite element analysis", University Press, Cambridge, United Kingdom.

Jeremic, B., and Sture, S., "Implicit integrations in elasto-plastic geotechnics", 1997, *International Journal of Mechanics of Cohesive-Frictional Materials*, 2, p.165-183.

Jordan, E. H. and Walker, K. P., 1992, "A viscoplastic model for single crystal", *J. Eng. Mater. Technol.*, 114, p.19-26.

Kachanov, L. M., 1971, "Foundations of the Theory of Plasticity", North-Holland Company, Amsterdam.

Kear, B.H. and Piearcey, B.J., 1967, Trans.TMS-AIME 239, p.1209.

Koiter, W. T., 1953, "Stress - strain relations, uniqueness and variational theorems for elastic - plastic materials with singular yield surface", *Quarterly of Applied Mathematics*, 2, p.350-354.

Klaus-JÜRGEN Bathe and Edward L. Wilson, 1976, "Numerical Methods in Finite Element Analysis", Prentice-Hall, Inc., Englewood Cliffs, NJ, USA.

Kolbe, M., Dlouhy, A., Eggeler, G., 1998, "Dislocation reactions at γ/γ'-interfaces during shear creep deformation in the macroscopic crystallographic shear system (001) [110] of CMSX6 superalloy single crystals at 1025°C", *Materials Science and Engineering*, A246, p.133-142.

Lall, C., Chin, S. and Pope, D.P., 1979, "The orientation and temperature dependence of yield stress of Ni_3(Al, Nb) single crystal", *Metall Trans. A*, 10A (6), p.1323-1332.

Leverant G. R, Kear B. H, and Oblak J. M., 1971, "Influence of matrix stacking fault energy on creep deformation modes in gamma' precipitation-hardened nickel-base alloys", *Met Trans*, 2(8), p.2305.

Leverant G. R, Kear B. H, and Oblak J. M., 1973, "Creep of precipitation-hardened nickel-base alloy single crystals at high temperatures", *Metallurgical Transactions*, 4 (1), p.355-362.

Leverant G.R. and Kear B.H., 1970, "Mechanism of creep in gamma prime precipitation-hardened nickel- base alloys at intermediate temperatures", *Met Trans*, 1(2), p. 491-498.

Li, S. X. and Smith, D. J., 1995, "Temperature and orientation dependence of elastic and yield properties of single crystal nickel-base superalloys", *Mat. Sci. Tech*, 11(7), p.1253-1260.

Li, Jiang, 1999, "Experimental Investigations in Nonlinear Viscous Behavior of Subgrade Soils under Traffic-Induced Loading", Report.

Li, S. X. and Smith, D. J., 1997, "Development of an anisotropic constitutive model for single-crystal superalloy for combined fatigue and creep loading", *Int. J. Mech. Sci.*, 40, p.937-948.

Lothar Collatz, 1960, "The Numerical Treatment of Differential Equations", 3rd, Springer, Berlin, Germany.

Louchet, F. and Hazotte, A., 1997, "A model for low stress cross-diffusional creep and directional coarsening of superalloys", *Sripta Materialia*, 37, p.589-597.

Lukas, P., Cadek, J., Sustek, V., and Kunz, L., 1996, "Creep of CMSX-4 single crystals of different orientations in tension and compression", *Materials Science and Engineering*, A208, p.149-157.

MacKay, R.A. and Maier, R.D., 1982, "The influence of orientation on stress ruptures of nickel based single crystal superalloy", *Metallurgy Transactions*, 13A, p.1747.

Maldini, M., Harada, H., Koizumi, Y., Kobayashi, T., and Lupinc, V., 2000, "Tertiary creep behavior of a new single crystal superalloy at 900°C", Scripta *Materialia*, 43, p.637-644.

Malvern, L. E., 1969, "Introduction To The Mechanics Of A Continuous Medium", Prentice-Hall, Englewood Cliffs, NJ.

Marisky J, 1995, "An Introduction to Linear Algebra", Oxford, Clarendon Press, p.263.

Matan, N., Cox, D.C., Carter, P., Rist, M.A., Rae, C.M.F., and Reed, R.C., 1999, "Creep of cmsx-4 superalloy single crystal: effects of misorientation and temperature", *Acta Materialia* , 47, p.1549-1563.

Mayr, C., Eggeler, G., Webster, G.A., and Peter, G., 1995, "Double shear creep testing of superalloy single crystals at temperatures above 1000°C", *Materials Science and Engineering*, A199, p.121-130.

Mayr, C., Eggeler, G., and Dlouhy, A., 1996, " Analysis of dislocation structures after double shear creep deformation of CMSX-6 superalloy single crystals at temperatures above 1000°C", *Materials Science & Engineering*, A207, p.51-63.

Miehe, C., 1996, "Numerical computation of algorithmic tangent moduli in large-strain computational inelasticity", *Computer Methods on Applied Mechanics And Engineering*, 6(134), P. 223-240.

Mkamaraj, 2003, "Rafting in single crystal nickel-base superalloys – An overview", *Sādhanā* , 28, p.115-128.

Mollica, F., Rajagopal, K. R. and Srinivasa, A. R., 2001, "The inelastic behavior of metals subject to loading reveral", *International Journal of Plasticity*, 17, p.1119.

Nabarro, F. R. N., 1994, "The superiority of superalloys", *Mater. Sci. Eng.*, A184, p. 167-171.

Nabarro, F. R. N. and De Villers, H. L., 1995, "The physics of creep: creep and creep-resistant alloys", Taylor & Francis, London.

Nabarro, F. R. N., 1996, "Rafting in superalloys", Meta. *Mater. Trans.*, 27(A), p.513-530.

Nitz, A. and Nembach, E., 1997, "Anisotropy of the critical resolved shear stress of a γ' (47 volume%)-hardened nickel-base superalloy and its constituent γ-and γ'-single-phases", *Materials Science and Engineering*, A234, p.684.

Nouailhas, D., 1990, "Anisotropic constitutive equations for cyclic viscoplasticity applications to the case of materials with cubic symmetry", *Researches Aerospatiales*, 3, p.11-28.

Nouailhas, D., Culie, J. P., Cailletaud, G. and MeRic, L., 1995, "Finite element analysis of the stress-strain behavior of single-crystal tubes", *J. of Mech.A/Solid*, 14, p.137-154.

Oddy, A. S., Reed, R. C. and McDill, J. M. J., 2000, "Three-dimensional, finite deformation, rate-dependent plasticity in single-crystal nickel alloys at elevated temperatures", *Computers and Structures*, 77, p.583-593.

Ogorodnikov V. A.,Sadovyi, A., Tyun'kinE.,S., 1995, "Viscosity of aluminum and lead in shock-wave experiments", *J. App. Mech. Tech .Phys.*,36(1), p.4-9.

Orowan, E.,1954, "Dislocation in Metals", Ed. Cohen, M.,Warrendale, PA, 152.

Osterle, W., Bettge, R. C., McMdill, J. M. I., 2000, "Modeling the orientation and direction dependence of the critical resolved shear stress of nickel based superalloy single crystals", *Acta Materialia*, 48, p.689-700.

Pavel Strunz, Ralph Gilles, Debashis Mukherji, Albrecht Wiedenmann, Rajeshwar P. Wahi and Jozef Zrník, 1999, "Microstructural characterization of single-crystal nickel-base superalloys by small-angle neutron scattering", *Materials Structure*, 6(2), p.91-95.

Pollock, T. M. and Argon, A. S., 1992, "Creep resistance of cmsx-3 nickel base superalloy single crystals", *Acta Matell. Mater.*, 40(1), 1-30.

Probst-Hein, M., Dlouhy, A., Eggeler, G., 1999, "Interface dislocations in superalloy single crystals", *Acta Materialia*, 47, p.2497-2510.

Qi, W., Brocks, W. and Bertram, A., 2000, "An FE-analysis of anisotropic creep damage and deformation in the single crystal srr99 under multiaxial loads", *Computational Materials Science*, 19, p.292-297.

Rajagopal, K. R. and Srinvasa, A. R., 1998A, "Mechanics of the inelastic behavior of materials, part 1, theoretical underpinnings", *Int. J. of Plasticity*, 14, p. 945-967.

Rajagopal, K. R. and Srinvasa, A. R., 1998B, "Mechanics of the inelastic behavior of materials, part 2, inelastic response", *Int. J. of Plasticity*, 14, p. 969-995.

Rajagopal, K. R. and Srinvasa, A. R., 2000, "A thermodynamic framework for rate type fluid models", *J. Non-Newtonian Fluid Mechanics*, 88, p. 207-227.

Ramm, E., and Matzenmiller, A., 1988, "Consistent linearization in elasto - plastic shell analysis", Engineering *Computations*, 5, p.289-299.

Rao, I. J. and Rajapopal, K. R. 2000, "A phenomenological modeling of crystallization in polymers using the notion of multiple nature configurations", *Interfaces and Free Boundaries*, 2, p.73-94.

Rao, I. J. and Rajapopal, K. R. 2001, "A study of strain induced crystallization in polymer", Int. *J. of Solids and Structures*, 38, p.1149-1167.

Rao, I. J. and Rajagopal, K. R., 2002,"A thermodynamic framework to study crystallization in polymers", *ZAMP*, 53, p.365-406.

Reed, R.C., Matan, N., Cox, D., C., Rist, M., A., and Rae, C. M. F., 1999, "Creep of CMSX-4 superalloy single crystals: effects of rafting at high temperature", *Acta Materialia*, 47, p.3367-3381.

Rist, M.A., Oddy, A.S. and Reed, R. C., 2000, "Three-dimensional simulation of inhomogeneous tertiary creep in single-crystal superalloy test pieces", *Scripta Materialia*, 43, p.719-725.

Runesson, K., and Samuelsson, A., 1985, "Aspects on numerical techniques in small deformation plasticity", *Proceedings of NUMETA '85, Numerical Methods in Engineering, Theory and Applications,* Middleton, J. and Pande, G.N. (Eds), Balkema, Amsterdam, p.337-347.

Sass, V., Glatzel, U., and Feller-Kniepmeier, M., 1996, "Anisotropic creep properties of the nickel based superalloy CMSX-4", *Acta Materialia*, 44(5), p.1967-1977.

Sass, V., Feller-Kniepmeier, M., 1998, "Orientation dependence of dislocation structures and deformation mechanism in creep deformed CMSX-4 single crystals", *Materials Science and Engineering*, A245, p.19-28.

Schmid, E., Diegele, G., 1931, I Eletrachew. 37, p.447.

Simo, J. C., and Taylor, R. L., 1985, "Consistent tangent operators for rate-independent elastoplasticity", *Computer Methods in Applied Mechanics and Engineering*, 48, p.101-118.

Simo, J. C., and Taylor, R. L., 1985, "A returning mapping algorithm for plane stress elastoplasticity", *International Journal for Numerical Methods in Engineering,* 22, p.649-670.

Simo, J. C., and Govindjee, S., 1988, "Exact closed - form solution of the return mapping algorithms in plane stress elasto – viscoplasticity", *Engineering Computations,* 5, p.254-258.

Srinivasan, R., Eggeler, G.F., and Mills, M.J., 2000, "γ'-cutting as rate-controlling recovery process during high-temperature and low-stress creep of Superalloy single crystals", *Acta Materialia*, 48, p.4867-4878.

Stoloff, Norman S., 1988, "Alloying of Nickel", Alloying. Ed. Walter, M.R. Jackson, C. T. Sims. ASM International: Metals Park, Ohio, p.371.

Svoboda, J., and Lukas, P., 1997, "Modeling of recovery controlled creep in nickel based superalloy single crystals", *Acta Materialia*, 45, p.125-135.

Svoboda, J., and Lukas, P., 1998, "Model of creep in <001>-oriented superalloy single crystals", *Acta Materialia*, 46, p.3421-3431.

Takeuchi, S. and Kuramoto, E., 1973, "Temperature and orientation dependence of yield stress in Ni_3Ga single crystal", *Acta Metall*, 21(3), p.425-425.

Truesdell, C. and Noll, W., 1965, "The Non-linear Field Theories of Mechanics", 2nd ed., Springer, Berlin.

Veron, M., Brechet, Y., and Louchet, F., 1996, "Strain induced directional coarsing in Ni-based superalloys", *Scripta Mater.*, 34, p.1883-1886.

Victor N. Kaliakin, 2002, "Introduction to Approximate Solution Techniques, Numerical Modeling, and Finite Element Methods", Marcel Dekker, Inc., NY, USA.

Voelkl, Rainer, Glatzel, Uwe, Feller-Kniepmeier and Monika, 1998, "Measurement of the unconstrained misfit in the nickel-base superalloy CMSX-4 with CBED", *Scripta Materialia*, 38(6), p.893-900.

Volkl,R., Glatzel, U., Feller-Kniepmeier, M et al, 1998, "Measurement of the lattice misfit in the single crystal nickel based superalloys CMSX-4, SRR99 and SC16 by convergent beam electron diffraction", *Acta Mater.*,46(12), p.4395-4404.

William Weaver,Jr. and Paul R. Johnston, 1984, "Finite Elements for Structure Analysis", Prentice-Hall, Inc., Englewood Cliffs, NJ, USA.

Yue, Z.F. and Zheng, C. Q., 1993, "The study of the tension/compression yield behavior of single crystal blade superalloys", *Acta Aeronautical et astronautica Sinica*, 14(12A), p.556-559.

Yue, Z.F., Lu, Z. Z. and Zheng, C. Q., 1995, "The creep damage constitutive life predictive model for nickel base single crystal superalloys", *Metal. Mater. Trans. A*, A26, p.1815-1821.

Veron, M., Brechet, Y. and Louchet, F., 1996, "Strain induced directional coarsening in Ni-based superalloys," *Scripta Materialia,* 34(12), p. 1883-1886.

Von Grossmann, B., Biermann, H. and Mughrabi, H., 2000, "Measurement of service-induced internal elastic strains in a single-crystal nickel-based turbine blade with convergent-beam electron diffraction", *Philosophical Magazine A*, 80(8), p.1743-1757.